FLOW ANALYSIS WITH FIBER PREFORM DEFORMATION DURING COMPRESSION RESIN TRANSFER MOLDING

by

Justin Merotte

A thesis submitted to the Faculty of the University of Delaware in partial fulfillment of the requirements for the degree of Master of Science in Mechanical Engineering

Winter 2010

Copyright 2010 Justin Merotte
All Rights Reserved

FLOW ANALYSIS WITH FIBER PREFORM DEFORMATION DURING COMPRESSION RESIN TRANSFER MOLDING

by
Justin Merotte

Approved: _____
Suresh G. Advani, Ph.D.
Professor in charge of thesis on behalf of the Advisory Committee

Approved: _____
Pavel Šimáček, Ph.D.
Professor in charge of thesis on behalf of the Advisory Committee

Approved: _____
Anette M. Karlsson, Ph.D.
Chair of the Department of Mechanical Engineering

Approved: _____
Michael J. Chajes, Ph.D.
Dean of the College Engineering

Approved: _____
Debra Hess Norris, M.S.
Vice Provost for Graduate and Professional Education

ACKNOWLEDGMENTS

I wish to express my deepest gratitude to my Advisor, Prof. Suresh Advani, for his guidance and his priceless advice to help me through my research here at the University of Delaware. He taught me basic thinking as well as he improved my explanation and presentation skills.

I also would like to thank Dr. Pavel Simacek for his help concerning the process modeling and the numerical simulation and his precious advice to write my papers.

I am also very happy to thank Dr. Victor Kaliakin and Dr. James Glancey who accepted to be my committee members and gave me priceless suggestions.

I am very grateful to Prof. Christophe Binetruy, Dr. Mylene Deleglise and the Polymer and Composite department of the Ecole des Mines de Douai for their support and encouragements to do my master's degree at the University of Delaware.

I also would like to thank my fellow students from the department of mechanical engineering Mehmet Temel, Melissa Lugo, Vasan Chandrasekaran, Justin Alms, Kenneth Okonkwo, Srikanth Arisetty and many others for helping me through my research and classes. Thanks for their cheerfulness and friendship. I would like to thank Steve Beard, Machinist at the Mechanical Engineering department for his precious advice concerning experiments but also for our long conversations!

On a personal note, my best thoughts go to the "French connection", Jean-Remy, Jean-Christophe, Julien and Erwan and all the other friends I have met during those two and a half years. They made Newark my new home.

Finally, I owe all the thanks in the world to my parents and family for their support while I was away from home. They were always present and helped me to go through some dark times. Without them, I would certainly not be where I am now…

TABLE OF CONTENTS

LIST OF TABLES

LIST OF FIGURES

ABSTRACT

Compression resin transfer molding (CRTM) is an alternative solution to conventional resin transfer molding processes. It offers the capability to produce net shape composites with fast cycle times making it conducive for high volume production. The resin flow during this process can be separated into three phases; (i) metered amount of resin injection into a partially closed mold containing dry fiber preform, (ii) closure of the mold until it is in contact with the fiber preform displacing all the resin into the preform and (iii) further mold closure to the desired thickness of the part compacting the preform and redistributing the resin. Understanding the flow behavior in every phase is imperative for predictive process modeling that guarantees full preform saturation within a given time and under specified force constraints.

In this thesis, the CRTM flow is modeled as a two dimensional flow in a gradually deformed porous medium during all three phases. The governing equations are formulated and coupled with the constitutive equations that describe the deformation and permeability behavior. Due to the non-linear nature of coupled system of equations, a numerical solution is developed that describes the flow front progression and the preform deformation during the process. A non dimensional analysis is conducted in which the applied force and initial gap size emerge as the important process variables that influence the process cycle time. Limiting cases are identified which reduce the flow to one dimensional flow for which a simplified solution is developed. The results are verified using an experimental setup which

applies a constant force to the preform in a transparent mold allowing one to track the flow front.

This study quantifies the effect of preform deformation due to the fluid pressure and should prove useful in applications that involve fluid impregnation in deforming porous media.

Chapter 1

INTRODUCTION

An advanced polymer composite consists of a polymer matrix and continuous fiber strands. The fibers are mainly responsible for the mechanical properties while the polymer matrix transfers the load to the fibers and protects them from environmental damage. The interface between fibers and matrix is as important as the fibers and the matrix. Hence manufacturing, which combines the fibers and resin together, plays a key role in determination of the composite physical and mechanical properties. In the early days of composites, the resin was applied to the fabric by hand, which formed air bubbles and poor interface resulting in deterioration of properties. Many processes emerged to address this issue along with the ability to automate the process and reduce the labor required to make a composite part. Among them, liquid composite molding (LCM) processes have been preferred for net shape part manufacturing as they allow for complexity of part geometry and have the ability to produce parts with desired mechanical properties and good surface finish. In LCM, the preform is placed in a mold or on a tool surface and resin is transferred to cover the spaces between the fibers to make a composite.

Before the mid nineties, most of the improvements in LCM were done by "trial and error" methodology and experience of the process engineer. However, as composite parts are being considered for replacing metal parts in many application areas such as automotive, sports, marine or aerospace, there is a need to develop a prototype in a relative short time period without numerous trials. Hence, the tools of

process analysis and simulation developed over the last decade are being used to mitigate the risk of failure to manufacture and to speed up the prototype development cycle. In some cases one can use these tools to optimize and even control the variability in part manufacturing.

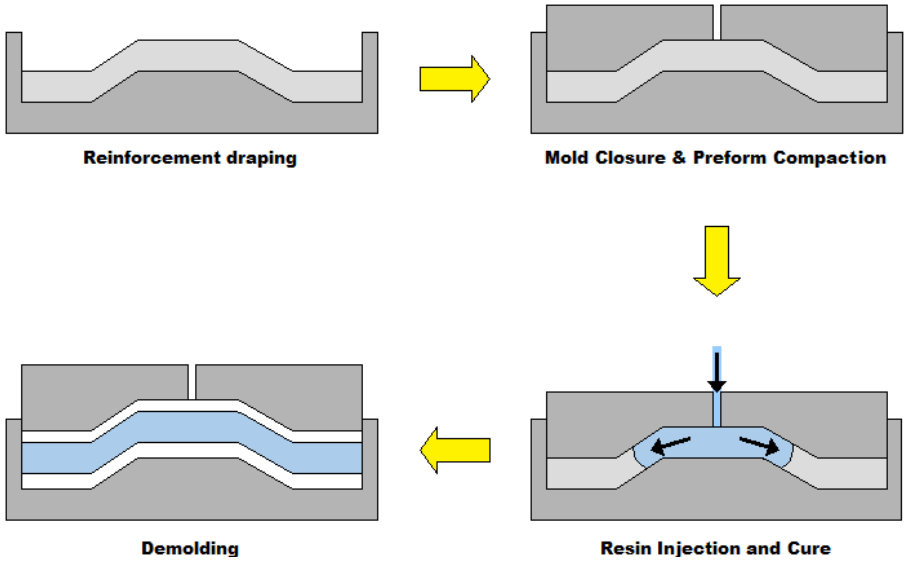

Figure 1-1 Schematic of the resin transfer molding process

The most common LCM manufacturing process used to make parts of the order of one meter is called resin transfer molding (RTM) and consists of injecting resin into the stationary fiber reinforcement compacted inside a mold. It can be described in steps which are fiber reinforcement cutting and draping, fiber compaction,

resin injection, cure and final part demolding (see Figure 1-1). The advantages of RTM include manufacturing speed (compared to hand layup) and the potential to manufacture void free net shape parts at high fiber content with class A surface finish. However the RTM process is limited for certain applications as the cost of the mold and the injection equipment increases rapidly with part size.

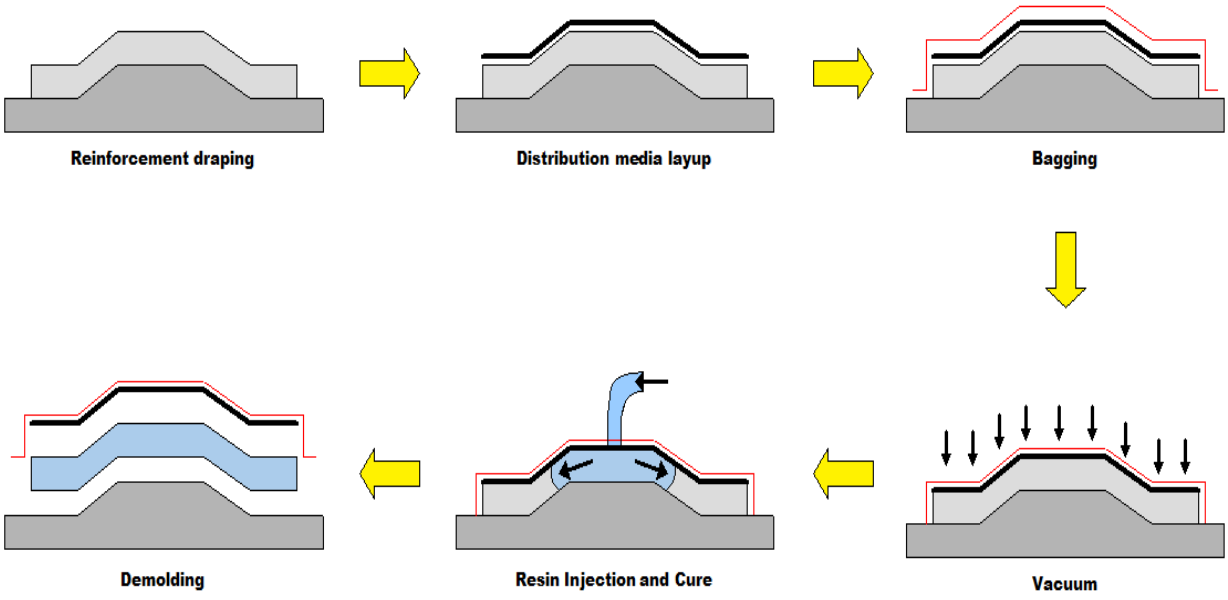

Figure 1-2 Schematic of the vacuum assisted resin transfer molding process

An alternative to this process that is cost effective for large structures is called vacuum assisted resin transfer molding (VARTM). The reinforcing fiber preform is draped on a bottom mold and a plastic film is placed on top of it, playing

the role of the upper side of the mold. The whole setup is sealed and a vacuum is applied to pull the resin from a resin reservoir at atmospheric pressure. In this process the preform is compacted, the compaction pressure being created by the vacuum (see Figure 1-2). A major improvement in filling time of this process was invented by Seemann where they place a very high permeability layer called distribution media on top of the reinforcement. This process is called Seemann's Corporation Resin Infusion Molding Process (SCRIMP) [1-3]. This facilitates the distribution of the fluid over the fiber preform surface and has for consequence to increase the speed of the impregnation as the resin has to travel only in the thickness direction (see Figure 1-3). This process is preferred to RTM for manufacturing large structures at lower costs. However, this process encounters several disadvantages such as a very poor surface finish on the bagging side, manufacturing limited to only nearly flat structures, a long time for material preparation (involving high labor cost) and a lack of automation in addition to removal of the distribution media from the part after the resin has cured. Hence this process is not very suitable for large scale production.

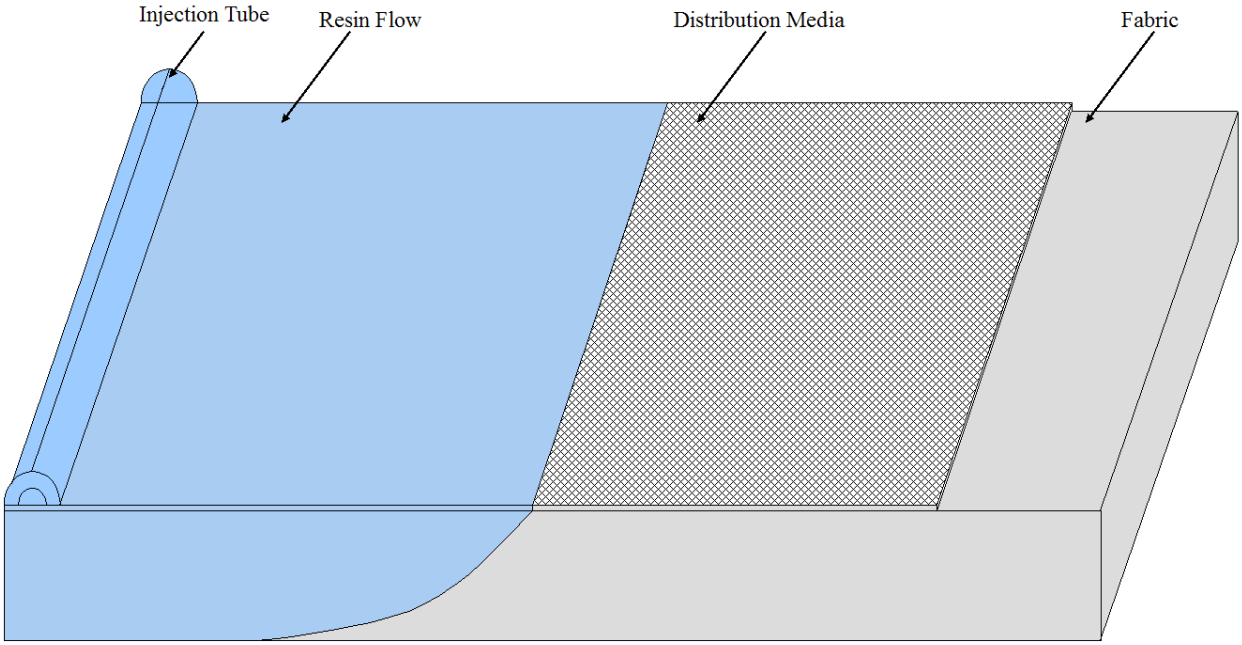

Figure 1-3 Schematic of the SCRIMP process

A new process that emerged in the last few years is called Compression Resin Transfer Molding (CRTM). This process can be used for high volume production and does have the potential to make large scale structures that can be filled at a much faster rate than RTM.

1.1 CRTM process

The CRTM process can be described in three phases. In the first phase, the resin amount necessary to obtain the desired amount of fiber volume fraction for a part of known dimensions is injected into a gap created on purpose between the plate and the preform. The resin will fill the gap quickly due to very low resistance to flow in the

gap over the surface of the preform and may also slightly penetrate the preform as depicted in Figure 1-4. This flow can be modeled as a flow during the SCRIMP process, the gap playing the role of the distribution media. The permeability of this "distribution media" will vary with the thickness of the gap. Since the operator can inject the resin at any pressure, the preform may undergo some deformation during this stage.

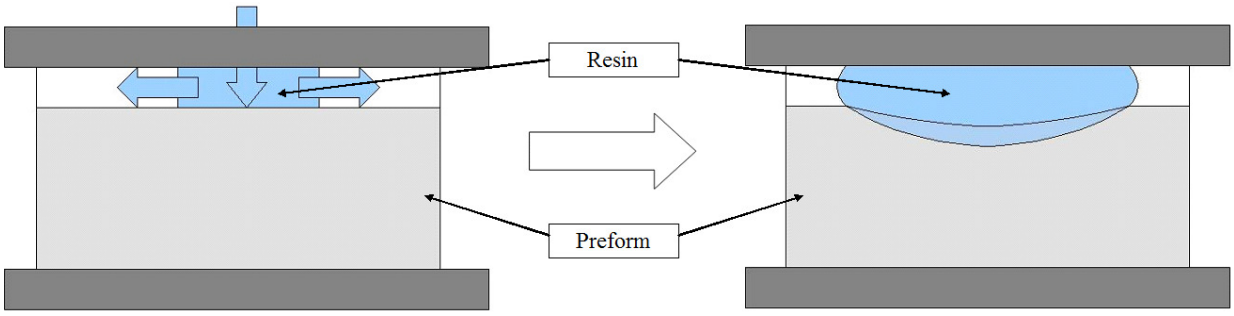

Figure 1-4 Schematic of the Configuration at the Beginning and the end of phase 1

In the second phase (Figure 1-5), the mold is subjected to a prescribed load and starts to close, reducing the gap size and squeezing the resin into the preform. This phase is assumed to be complete when the mold comes in contact with the preform. During this phase, as the resin pressure is much higher due to the prescribed load on the mold, the preform will deform further due to the pressure gradients, even

though there is no mold/preform contact. As the gap size reduces during this phase, the permeability of the gap also decreases. During this phase, the compaction force transmitted to the reinforcement affects both the dry and saturated parts of the fiber preform. However, it has been experimentally observed that the compaction stress influences principally the wet part of the preform.

The closing motion of the mold may be kinematically or force driven. In this thesis, the focus will be on the force driven case with the use of a compaction force. This is in line with manufacturing presses which are hydraulic and use constant pressure to create a force on the platen of the mold.

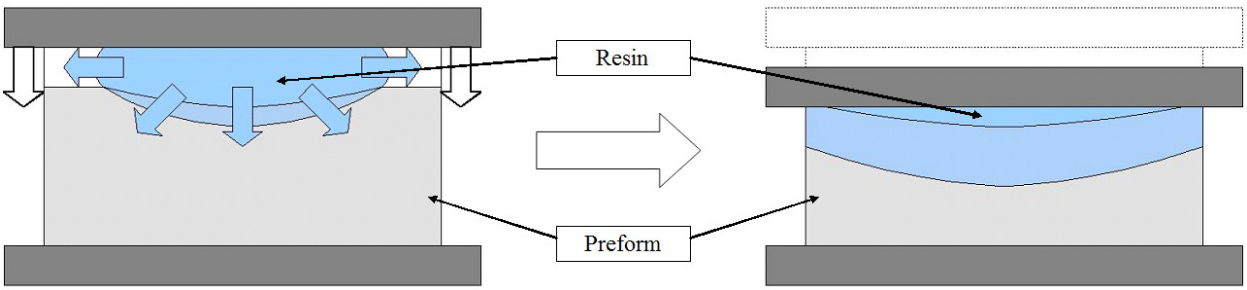

Figure 1-5 Schematic of the Configuration at the Beginning and the end of phase 2

During the third phase (Figure 1-6), the mold continues to close the gap while compressing the preform in contact with the tool. Once the entire surface of the tool is in contact with the reinforcement, the upper platen continues to move down

until the final thickness of the part is achieved. During this phase the resin redistributes from saturated regions which are being compressed into regions that are devoid of resin. In this phase, until the entire tool surface comes in contact with the preform, it is difficult to describe the compaction as both the tool force and fluid pressure have non uniform and spatially varying magnitudes which act on the preform. After the mold in is physical contact with the entire preform, the compaction corresponds to the plate motion. When the mold is kinematically driven, the boundary displacement is directly given by the mold displacement. When the compaction method is a prescribed force, one has to relate the displacement through strain to the stress in the preform to predict the compaction.

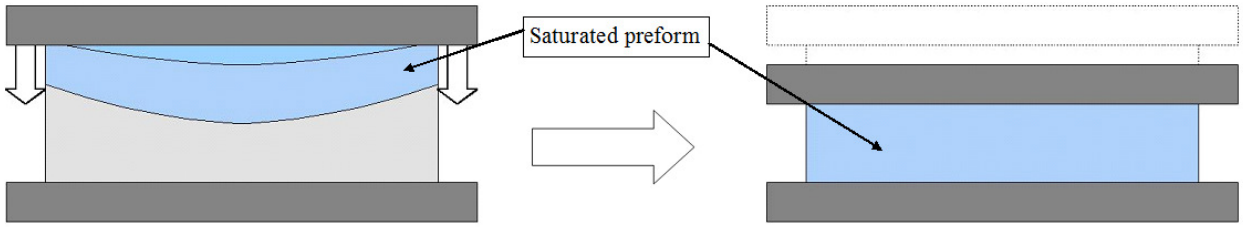

Figure 1-6 Schematic of the Configuration at the Beginning and the end of phase 3

As the final part is enclosed between two plates with high surface finish guarantees a final part with class A surface finish. Due to the high pressures needed,

the main reason preventing this process to be more widely used is the tooling cost. Moreover, despite the recent studies on the process, very little is known concerning all the physics involved and hence the need for the process analysis.

There has been some work in this area in which the process and its challenges have been described [4] using several assumptions but an accurate simulation which accounts for the key physics involved (flow in a progressively deforming media) and identification of important material and process parameters still needs to be established. Bhat et. al developed a simulation tool of the three phases assuming that the deformation only happens when there is contact between the tool and the preform [5, 6]. Shojaei [7-9], Kang [10] and Pillai [11, 12] also developed a simulation tool for complex parts. However, the deformation due to the fluid was neglected. Many studies have investigated the phenomenon related to some phases of the process. Bickerton [13, 14] and Pham [15] modeled the compaction behavior of the preform and the flow front progression when the tool compacts the preform (phase III). Bickerton also studied the tooling force necessary to compact a partially saturated fabric [16, 17]. Finally, most of the studies previously cited do not incorporate an open gap inside the mold during the injection. The mold is already in contact with the uncompressed preform. The CRTM process is then composed of an injection phase (RTM in a low fiber volume fraction media) followed directly by preform compaction. Many geometric, material and process parameters influence the filling time. For instance, the choice of gate location and number of gates, the closing speed of the mold platen and the material properties such as preform permeability and part aspect ratio will influence the flow [18]. Thus, an analysis to understand the role of such parameters has to be conducted to optimize the process.

1.2 Scope of this thesis

The objective of this thesis is to predict the compression of the fabric and the impregnation of the resin into the preform during the CRTM process. This thesis will account for the fact that the preform is non uniformly deformed by the fluid pressure gradient as well as the elastic stress even when the preform is not in contact with the tool. This study will also include simplifications that can be made to the process simulation and derive and discuss their detailed solutions. The thesis has been organized as follows. Chapter 2 presents the formulation of the governing equations that couple the deformation to the resulting flow through the preform. Chapter 3 provides the constitutive equations to describe preform compression and preform permeability for the materials used in this study and the experimental methodology to characterize the material properties. The important process parameters are determined in chapter 4. Chapter 5 details the two dimensional numerical simulation of the process. Discretization method, numerical algorithms used and finally the numerical validation of the simulation is presented. A parametric study is conducted in chapter 6, it explores the influence of key parameters such as gap size and compaction force on the flow geometry and on preform deformation. Chapter 7 derives and investigates two simplified cases that shed light on important dimensionless variables and their influence on filling and deformation. The results of simplified cases are validated with experiments designed and conducted for that purpose. Chapter 8 summarizes the contributions and proposes future work for improvement of the modeling and simulation and technique in CRTM.

Chapter 2

THEORY AND FORMULATION OF GOVERNING EQUATIONS

Previous researchers have modeled various stages of the CRTM process using simplifying assumptions. Shojaei [7-9], Bhat [5, 6] and Pillai [11, 12] assumed that during phase 2 the preform does not deform if it is not in contact with the mold. This allowed them to decouple the fluid flow from deforming porous media which made the solution much less complex. To test the validity of these assumptions, we designed and carried out experiments to specifically monitor the compression of the preform during phase 2 of the process (Figure 2-1). The experimental setup is detailed in section 7.1.6. We used a fabric that is not necessarily very compliant (24 oz. E-glass woven fabric). Our experiments clearly demonstrated that the deformation during phase 2 cannot be neglected. The results in Figure 2-2 show that the preform compacted on the order of 15% over the phase 2 confirming that the flow analysis during this phase has to address the deformation of the preform thus introducing a non-linear coupling between flow and fiber deformation.

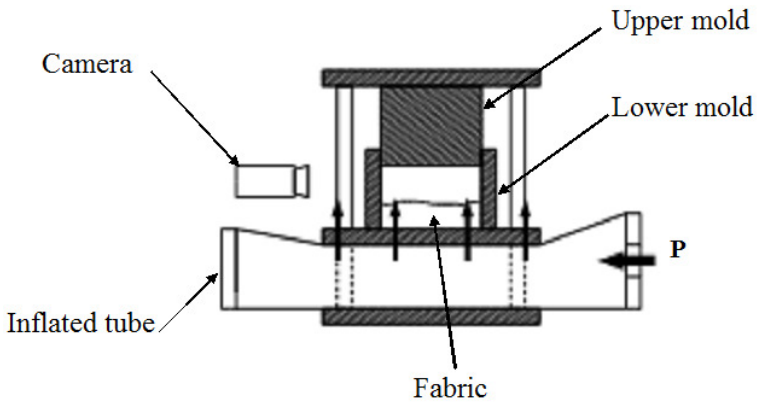

Figure 2-1 Experimental setup used to monitor the deformation of the preform during the process

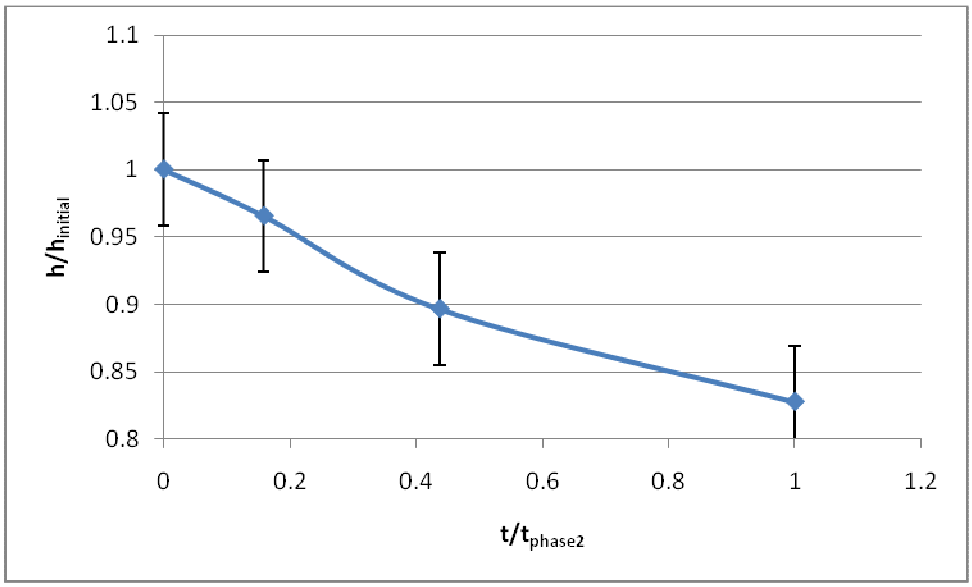

Figure 2-2 Preform thicknesses during second phase of CRTM

The goal of this thesis is to develop and formulate a model that will address the preform compaction during all the phases. All process models have neglected preform compaction during phase 1 and 2. The model will still follow Darcy's law to describe the resin impregnation into a deforming preform and we will assume that quasi steady assumption at each time step still applies. This assumption has been justified and validated [19].

The process model will be addressed by analyzing different regions during the phases of the CRTM process as showed in Figure 2-3. In this study, the model will describe the filling process of a rectangular part of length L and thickness H. A total of five governing equations will be used to model the CRTM process (Figure 2-3). Two governing equations will control the progression of the resin flow through the gap and the preform. Two equations will govern the distribution of the fluid pressures in the gap as well as in the preform. Finally, a last equation will relate the fluid pressure to the compressive stress experienced by the fabric.

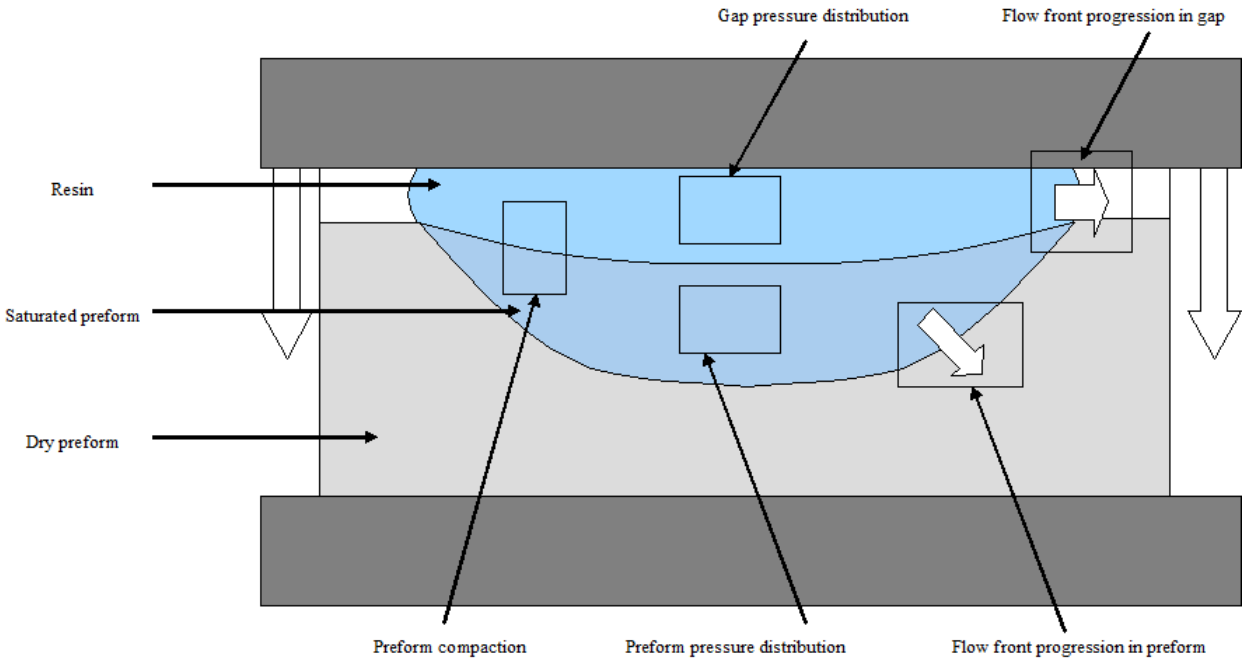

Figure 2-3 Development of governing equations in different regions during the CRTM process

Only one injection gate will be used and it will be located in the middle of the part. One can take advantage of symmetry along the vertical axis that passes through the injection gate location to simplify the problem. A numerical solution will be used to solve the system of partial differential equations which is presented in chapter 5. The horizontal origin of the system is located at the injection point and the vertical origin corresponds to the preform top. A schematic of the problem is given in Figure 2-4.

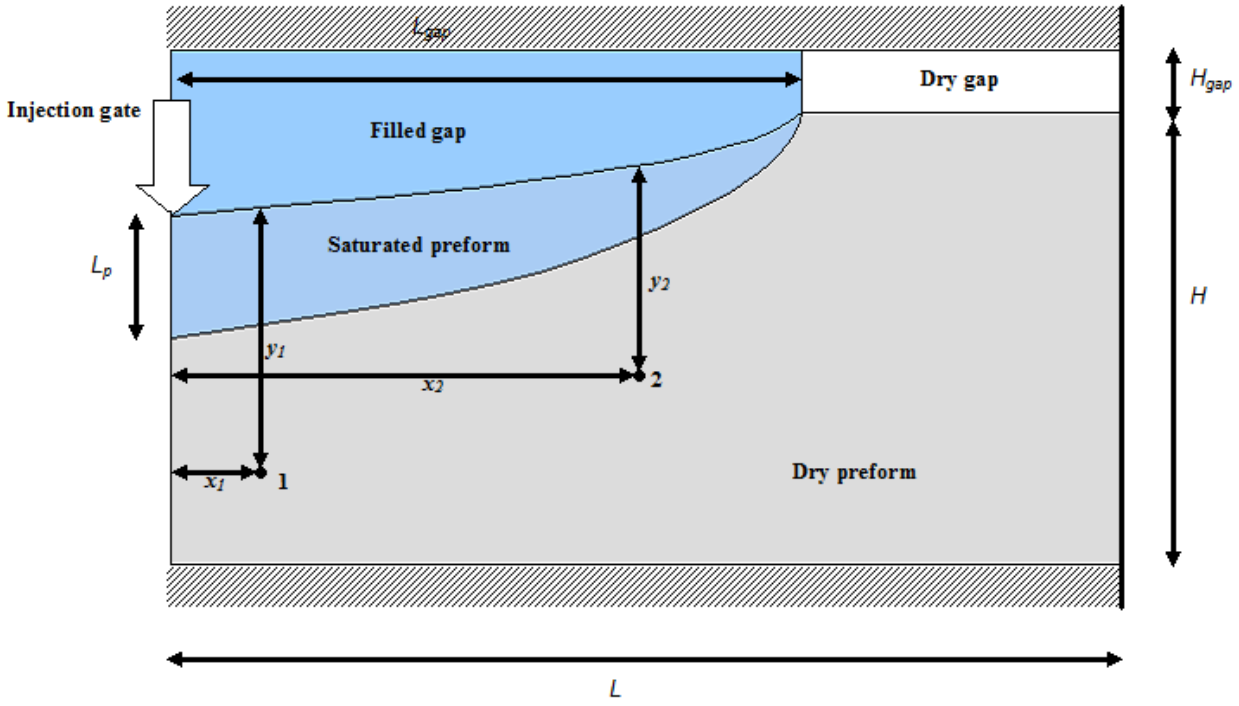

Figure 2-4 Schematic of the problem. Note that as the preform compresses under fluid pressure (exaggerated in the figure), the gap between the preform and the mold plate can be non-uniform

2.1 Flow progression

2.1.1 Flow progression in the gap

As the resin enters the gap, the gap is much smaller than the length or the width direction; one can treat the movement of the resin in the gap as a lubrication flow. This, in turn, can be described as flow through porous media of equivalent permeability and porosity of 1. Thus one can use Darcy's law [19-21] to describe the

flow in the gap in the average sense. The general form of Darcy's equation can be written as,

$$\langle v \rangle = -\frac{\mathbf{K}}{\eta}.\nabla p \tag{2.1}$$

Where $\langle v \rangle$ is the volume averaged velocity, K the permeability tensor, η the fluid viscosity and p is the fluid pressure. Applying one dimensional form of Eq. (2.1) in the x direction in the gap and the preform (Figure 2-4),

$$\frac{\partial L_{gap}}{\partial t} = -\frac{K_{gap}\left(x = L_{gap}\right)}{\eta}\left(\frac{\partial p}{\partial \mathrm{x}}\right)_{x=L_{gap}} \tag{2.2}$$

here L_{gap} is the flow front position moving along the x axis starting from the center (x=0 in Figure 2-4), K_{gap} is the in plane permeability of the gap. The in-plane permeability of the gap can be calculated using the gap thickness H_{gap} as follows,

$$K_{gap}\left(x\right) = \frac{H_{gap}\left(x\right)^2}{12} \tag{2.3}$$

2.1.3 Flow progression in the preform

The resin in the preform flows in the plane as well as through the thickness direction (Figure 2-5). If L_p is the depth to which the resin penetrates into the preform (Figure 2-4) one can write a differential equation to describe this depth of penetration along the x direction.

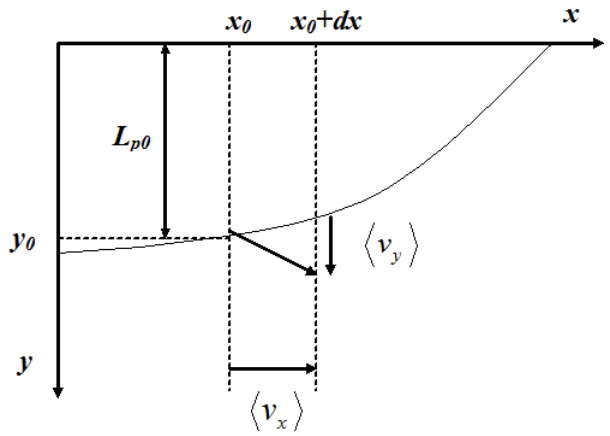

Figure 2-5 Flow front progression in the preform

The position of a fluid particle at time $t=t_0$ is (x_0,y_0). Its position at a time $t=t_0+dt$ is (x_0+dx,y_0+dy). Where,

$$dx = \frac{\langle v_x \rangle}{\phi} dt \tag{2.4}$$

And

$$dy = \frac{\langle v_y \rangle}{\phi} dt \tag{2.5}$$

$\langle v_x \rangle$ and $\langle v_y \rangle$ are the averaged velocities and ϕ is the preform porosity. The depth of penetration L_p is a function of x and t. At time $t=t_0$, one has,

$$L_p(x_0, t_0) = L_{p0} \tag{2.6}$$

At time $t=t_0+dt$, the depth of penetration at $x=x(t_0+dt)=x+dx$ is,

$$L_p(x_0 + dx, t_0 + dt) = L_{p0} + \frac{\langle v_y \rangle}{\phi} dt \tag{2.7}$$

Then, $L_p(x_0,t+dt)$ becomes,

$$L_p\left(x_0,t_0+dt\right)=L_p\left(x_0+dx,t_0+dt\right)-dx\left(\frac{\partial L_p}{\partial x}\right)_{x_0} \tag{2.8}$$

Substituting Eqs. (2.4), (2.5) and (2.7) in Eq. (2.8) and rearranging results in,

$$\frac{L_p\left(x_0,t_0+dt\right)-L_{p0}}{dt}=\frac{\left\langle v_y\right\rangle}{\phi}-\left(\frac{\partial L_p}{\partial x}\right)_{x_0}\frac{\left\langle v_x\right\rangle}{\phi} \tag{2.9}$$

taking the limits as dx→0, dt→0 results in,

$$\left(\frac{\partial L_p}{\partial t}\right)_x=-\left(\frac{\partial L_p}{\partial x}\right)_x\frac{\langle v_x\left(x\right)\rangle}{\phi\left(x,y=L_p\right)}+\frac{\langle v_y\left(x\right)\rangle}{\phi\left(x,y=L_p\right)} \tag{2.10}$$

Using Darcy's law to find the averaged velocities in x and y directions, one can write a differential equation for how the depth of penetration varies with x and the fluid pressure p,

$$\left(\frac{\partial L_p}{\partial t}\right)_x=\left(\frac{\partial L_p}{\partial x}\right)_x\frac{K_{xx}\left(x,y=L_p\right)}{\eta\phi\left(x,y=L_p\right)}\left(\frac{\partial p}{\partial x}\right)_{x,y=L_p}-\frac{K_{yy}\left(x,y=L_p\right)}{\eta\phi\left(x,y=L_p\right)}\left(\frac{\partial p}{\partial y}\right)_{x,y=L_p} \tag{2.11}$$

2.2 Pressure distribution

2.2.1 Pressure distribution in the gap

In our model, the pressure within the gap are assumed to vary only with x and not the y direction hence this will also be the pressure experienced by the surface of the preform in contact with the resin in the gap and will serve as the boundary condition when one does the force balance for the preform. To perform a mass balance of the resin in the gap, we need to include the preform boundary as some of the resin

from the gap will be exiting into the preform as shown in a control volume selected for mass balance in Figure 2-6.

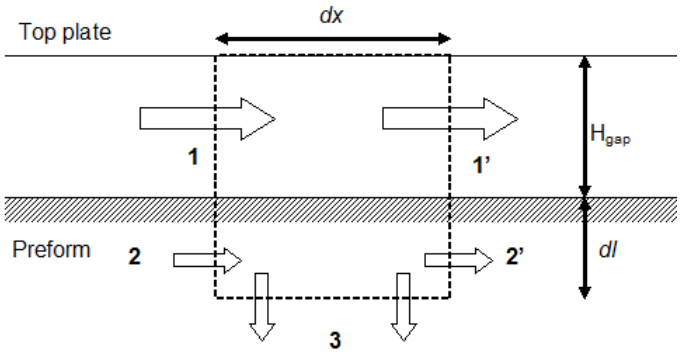

Figure 2-6 Mass balance for a control volume in the gap that includes the resin that impregnates the preform in touch with the resin in the gap

In the gap, the injected resin travels along the gap and also penetrates the preform. The resin pressure in the gap is responsible for the fabric deformation due to the pressure load, which is accounted for in the part of the control volume in the preform. Thus a mass balance on a control volume located in the gap as depicted in Figure 2-6 can be written as,

$$\left(\frac{dH_{gap}}{dt}\right)_x dx+\left(\frac{d\varepsilon}{dt}\right)_{x,y=dl} dxdl = V_1(x)H_{gap}(x)-V_1(x)'H_{gap}(x)+V_2(x)dl-V_2(x)'dl-V_3(x)dx \quad (2.12)$$

with ε as the infinitesimal strain of deformation, dx as the infinitesimal length of the control volume, dl as the infinitesimal height of a control volume in the preform, H_{gap} is the gap thickness, V_1 and V_1' are the velocities of the resin entering and leaving the gap region of the control volume, V_2 and V_2' are the velocities of the resin entering and leaving the preform region of the control volume and V_3 is the velocity of the resin leaving the gap and entering the preform.

The volume of resin leaving the control volume only in the gap can be expressed as a function of the volume of resin entering the volume as follows,

$$V_1(x)'H_{gap}(x) = V_1(x)H_{gap}(x) + \left(\frac{\partial V_1}{\partial x}\right)_x dxH_{gap}(x) \tag{2.13}$$

Similarly, the volume of resin leaving the preform part of the control volume can be expressed as,

$$V_2(x)'dl = V_2(x)dl + \left(\frac{\partial V_2}{\partial x}\right)_x dxdl \tag{2.14}$$

Substituting Eq. (2.13) and (2.14) in (2.12),

$$\begin{aligned} &\left(\frac{dH_{gap}}{dt}\right)_x dx + \left(\frac{d\varepsilon}{dt}\right)_{x,y=dl} dxdl = \\ &-\left(\frac{\partial V_1}{\partial x}\right)_x dxH_{gap}(x) - \left(\frac{\partial V_2}{\partial x}\right)_x dxdl - V_3(x)dx \end{aligned} \tag{2.15}$$

Applying Darcy's law to the velocities and substituting them in the mass balance equation (7) and taking the limits of dx going to zero results in,

$$\begin{aligned} &\left(\frac{\partial \varepsilon}{\partial t}\right)_{x,y=dl} dl + \left(\frac{\partial H_{gap}}{\partial t}\right)_x = \frac{K_{yy}(x, y=dl)}{\eta}\left(\frac{\partial p}{\partial y}\right)_{x,y=dl} + \\ &\frac{\partial}{\partial x}\left(\frac{H_{gap}(x)^3}{12\eta}\left(\frac{\partial p}{\partial x}\right)_{x,y=dl}\right)_{x,y=dl} + \frac{\partial}{\partial x}\left(\frac{K_{xx}(x, y=dl)}{\eta}\left(\frac{\partial p}{\partial x}\right)_{x,y=dl}\right)_{x,y=dl} dl \end{aligned} \tag{2.16}$$

Here K_{yy} and K_{xx} represent the in plane and through the thickness permeabilities respectively of the preform, η the resin viscosity, p the fluid pressure, x and y are the spatial coordinates as shown in Figure 2-4.

2.2.2 Pressure distribution in the preform

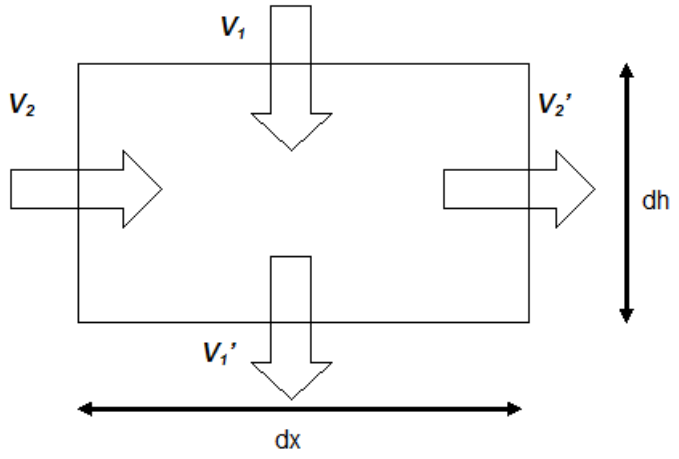

Figure 2-7 Resin flow through a control volume in the preform

In the preform, the resin enters the control volume in the vertical and horizontal direction. As the preform gets compacted, the control volume will reduce and act as a source of resin. In the schematic above *dx* is a constant value. However, the preform deforms vertically and *dy* is not constant. The thickness of the control

volume will then be called *dh* and will change with its location. A mass balance on the control volume depicted in Figure 2-7 results in,

$$\left(\frac{d\varepsilon}{dt}\right)_{x,y} dxdh(x,y) = V_2(x,y)dh(x,y) - V_2(x,y)'dh(x,y) + V_1(x,y)dx - V_1(x,y)'dx \tag{2.17}$$

Expressing the volume of resin leaving the control volume as a function as the volume entering it,

$$V_2(x,y)'dh(x,y) = V_2(x,y)dh(x,y) + \left(\frac{\partial V_2}{\partial x}\right)_{x,y} dxdh(x,y) \tag{2.18}$$

Substituting Eq (2.18) in Eq. (2.17) results in,

$$\left(\frac{d\varepsilon}{dt}\right)_{x,y} dxdh(x,y) = -\left(\frac{\partial V_2}{\partial x}\right)_{x,y} dxdh(x,y) - \left(\frac{\partial V_1}{\partial y}\right)_{x,y} dh(x,y)dx \tag{2.19}$$

The equation governing the pressures distribution can be formulated by combining Darcy's law in the x and y directions with Eq (2.19),

$$dh(x,y)\left(\frac{\partial \varepsilon}{\partial t}\right)_{x,y} = \frac{\partial}{\partial x}\left(\frac{dh(x,y)K_{xx}(x,y)}{\eta}\left(\frac{\partial p}{\partial x}\right)_{x,y}\right)_{x,y} + dh(x,y)\frac{\partial}{\partial y}\left(\frac{K_{yy}(x,y)}{\eta}\left(\frac{\partial p}{\partial y}\right)_{x,y}\right)_{x,y} \tag{2.20}$$

2.3 Preform Compaction

The compaction of each control volume of the preform is a function of a compressive stress p_{pref} related to the fluid pressure. The strain rate is then a function of p_{pref}, the constitutive equation relating p_{pref} and ε will be described in chapter 3. A relation between the fluid pressure and the compressive stress in a porous media has been highlighted by the Terzaghi's relation [22],

$$p_{pref} = p_{top} - p \tag{2.21}$$

Where p_{pref} is the compressive stress. If the preform is saturated, the compressive stress is a combination of the pressure on top of the preform p_{top} (pressure in the gap) and the fluid pressure in the preform p. When the preform is dry, $p = 0$ and on top of the preform, p_{pref}=0.

When all the equations governing the process are determined, one has to determine constitutive relationships in order to apply these equations to a specific material.

Chapter 3

MATERIAL CHARACTERIZATION

The governing equation formulated in chapter 2 are general expressions which can incorporate any constitutive equation one selects to describe the change in fiber stress p_{pref}, and preform permeability K_{xx}, as a function of v_f. This chapter will describe the characterization method used to find the material constants that constitutively describe the permeability and compaction behavior with fiber volume fraction.

3.1 Compaction behavior

The goal here is to record how much stress the fibers take as the preform is compressed from their unloaded state (initial fiber volume fraction) to a higher fiber volume fraction and then describe the relationship with a mathematical form for the range of fiber volume fraction explored.

3.1.1 Experimental Setup

To describe the stress-strain relationship of the preform, an Instron machine coupled to a load cell was used. The load cell records the force needed by the two circular steel plates to compact the fabric (see Figure 3-1). The samples were cut into circular discs and placed between the two plates. The two plates move toward each other at a constant speed and compact the preform. The data is recorded at constant time intervals (Δt=0.5 s). The use of perforated plate helps one to describe the

influence of lubrication on the behavior. To do so, the preform is soaked into a resin bath and placed between the discs. The perforations in the plates help to bleed the resin more easily, avoiding an increase in resin pressure thus making it possible to accurately measure the load exerted only on the fiber preform. Woven e-glass 24oz fabric was used as the perform material for characterization.

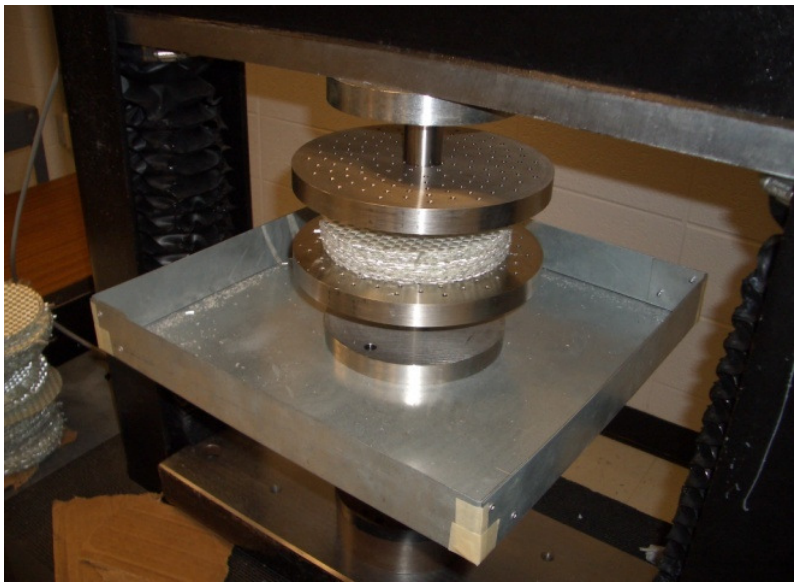

Figure 3-1 Experimental setup used to measure the compaction behavior

3.1.2 Experiment Analysis

The lubrication is known to help the compaction and therefore increase the final fiber volume fraction corresponding to a given applied stress. When the preform is only partially saturated through the thickness (existence of a flow front), the overall behavior is a combination of saturated and dry behavior. According to Terzaghi's relation (Eq. (2.21)), if the preform is saturated with resin, the compressive stress is the difference between the resin pressure at the preform surface and the resin pressure within the saturated preform. However, for the part of the preform that is dry, p_{top}=0 and therefore p_{pref}=p_{top} (Figure 3-2 schematically shows the distribution of stresses over the preform).

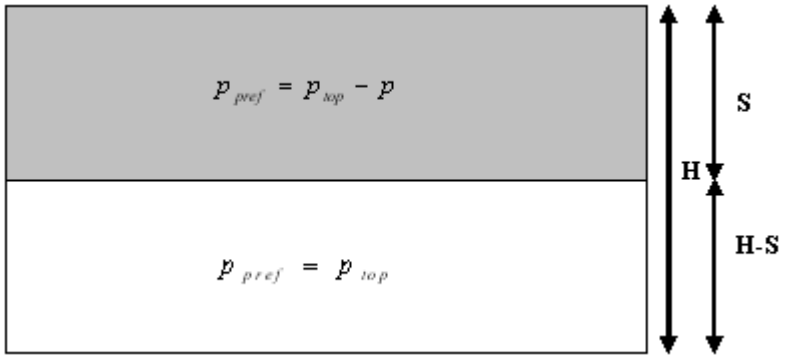

Figure 3-2 Compressive stresses distribution over a partially saturated preform

One can then formulate the global displacement of the perform top, λ, as an addition of the deformation experienced by the wet preform λ_{wet} and by the dry preform λ_{dry},

$$\lambda = \lambda_{wet} + \lambda_{dry} \tag{3.1}$$

Using Figure 3-2,

$$\lambda_{wet} = \int_0^S f\left(p_{top} - p\right) dy \tag{3.2}$$

And

$$\lambda_{dry} = \int_S^H g\left(p_{top}\right) dy \tag{3.3}$$

where *f* and *g* are functions relating the strain to the stress. In order to investigate the compaction behavior of the E-glass 24 oz. woven fabric, several experiments were conducted, varying different parameters such as lubrication, compaction speed, number of layer, etc. The study was performed by M. Gebauer from the Center for Composite Materials [5]. Figure 3-3 and Figure 3-4 show the stress-fiber volume fraction data collected for different compaction speeds (15 mm/s and 25mm/s) under wet and dry states of the fiber preform. The testing material was a 24 oz. E-glass woven fabric and each experiment has been conducted without pre-compaction.

From Figure 3-3 and Figure 3-4, one can assume that until a high compaction speed, the dry and saturated behaviors can be assumed to be the same, thus one can assume that the function *f* varies the same way as the function *g*.

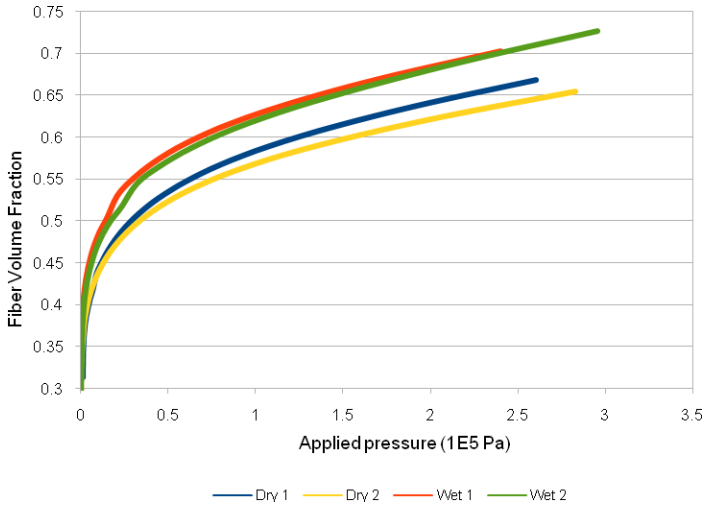

Figure 3-3 Stress-fiber volume fraction data for Instron speed of s=25mm/s

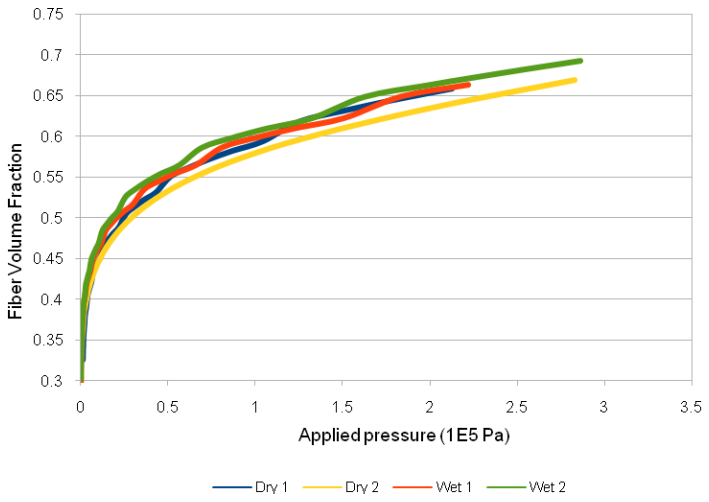

Figure 3-4 Stress-fiber volume fraction data for s=15mm/s

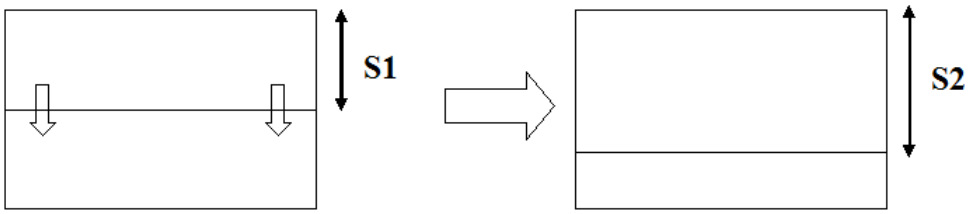

Figure 3-5 Evolution of resin penetration during the second phase of CRTM

By studying two different depth of penetration of the fluid S1 and S2, if the flow progresses ($S2 \rangle S1$ in Figure 3-5) and if $f = g$, the deformation λ_1 corresponding to a depth of penetration S1 is,

$$\lambda_1 = \int_0^{S1} f\left(p_{top} - p\right)dy + \int_{S1}^{H} f\left(p_{top}\right)dy \tag{3.4}$$

Similarly, the deformation λ_2 associated to a depth of penetration S2 is,

$$\lambda_2 = \int_0^{S2} f\left(p_{top} - p\right)dy + \int_{S2}^{H} f\left(p_{top}\right)dy \tag{3.5}$$

which leads to

$$\lambda_1 > \lambda_2 \tag{3.6}$$

According to eq.(3.6), if $f = g$, the deeper the flow goes the less compaction the preform will experience. This means that as soon as a compressive stress is applied on top of the preform, one should assist to a sudden deformation followed by a relaxation of the preform as the flow progresses through the thickness. From Figure 2-2, it is seen that for higher compaction speed (more than 30mm/min) the top of the preform keeps moving downward as the flow progresses. To accomodate this behavior, the dry preform has to be much stiffer than the saturated one. This could be explained by the

visco-elastic behavior of the preform. Robitaille [23, 24] has shown that the compaction speed has an influence on the stress-strain relation when the fabric is dry. When it is lubricated, for limited compaction speeds, it can be assumed that the speed does not really affect this relation. Further investigation would have to be done to explain the compaction behavior of a partially filled preform. To account of this property of CRTM, the dry preform will be assumed to be undeformable and only the saturated part will deform during the compression.

3.1.2 "Hyperbolic tangent" compaction model

A number of compaction models have been published through the years [17, 23-29]. The most commonly used is a power law model and takes the form,

$$p_{pref} = a.v_f^{\,b} \tag{3.7}$$

where v_f is the resulting fiber volume fraction and a and b are the material parameters. The power law model is simple, however it neither predicts the fiber volume fraction when the compaction stresses p_{pref} is zero nor does it reflect the true asymptotic behavior at high stress levels usually experienced in CRTM processing. As this behavior is important to describe and capture, in this work we use the following compaction model to characterize the materials [32, 43],

$$v_f = v_{f0} + \left(v_{fmax} - v_{f0}\right)\tanh^n\left(\frac{p_{pref}}{p_{pref\max}\, m}\right) \tag{3.8}$$

$P_{prefmax}$ is the minimum stress after which the fiber volume fraction will not increase with any additional stress on the fibers. The m and n are two curve fitting parameters. The compression behavior is captured by equation (3.8) at the price of evaluating additional constants. However, these constants can be found from the same

experiments and do not require any additional characterization. Table 3-1 lists the constants that gave us the best least squares fit with the experimental data depicted in Figure 3-3.

Table 3-1 Model parameters for compaction model described by Eq. (3.8)

E-glass woven (24 oz)	
n	0.45
m	0.86
v_{fmax}	0.62
v_{f0}	0.30
$p_{prefmax}$	$4.5.10^5$ Pa

To study the sensitivity of the two shape parameters *n* and *m*, their values were varied from 0.35 to 0.55 for *n* and from 0.75 to 0.95 for *m*. As one can notice from Figure 3-6, a slight change in the value of *m* and *n* does cause a significant change in the value of fiber volume fraction at the same force (stress) level. This ensures that the fit of the experimental data is very sensitive to the values of *m* and *n*. Thus for each material one can determine *m* and n with reasonable accuracy from the stress- fiber volume fraction curve.

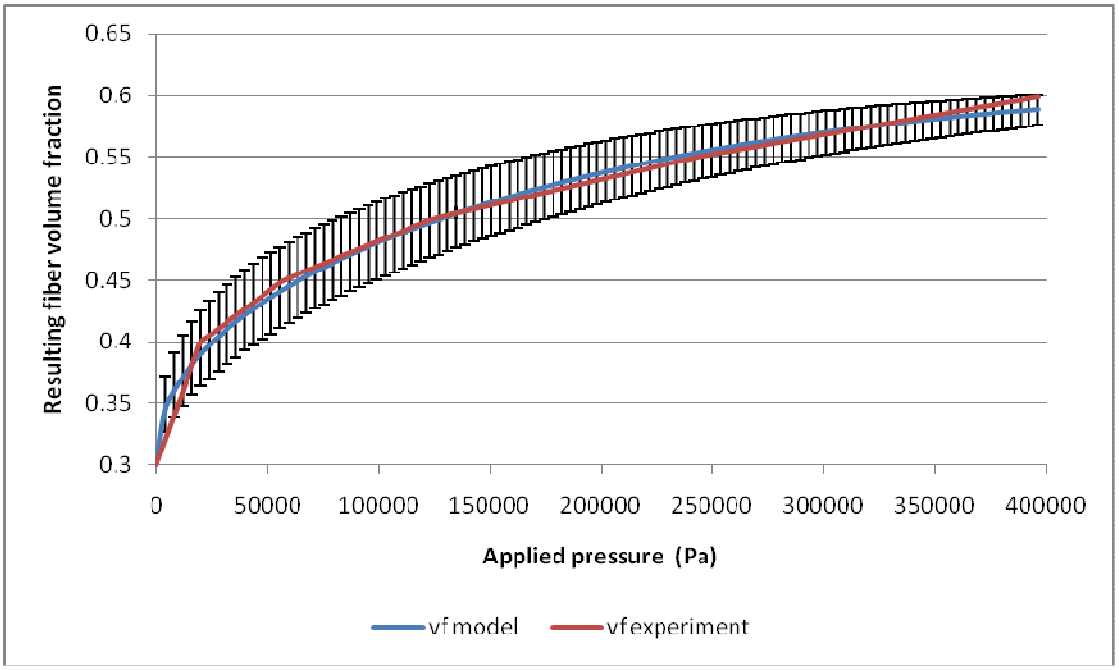

Figure 3-6 Range of resulting fiber volume fractions corresponding to a prescribed load (errors bars correspond to different values of m and n applied to the model)

The derivatives of this model will also be needed as zero compressive pressures are encountered at the top surface of the preform. When p_{pref}=0, $\frac{\partial v_f}{\partial p_{pref}} = \infty$, whereas $\frac{\partial v_f}{\partial p_{pref}}$ is finite experimentally. The experimental derivatives are calculated from the strain-stress relation as follows,

$$\left(\frac{dv_f}{dp_{pref}}\right)^i = \frac{v_f^{i+1} - v_f^{i-1}}{p_{pref}^{i+1} - p_{pref}^{i-1}} \tag{3.9}$$

i+1 and *i-1* represent the neighboring data points of point *i*. At $p_{pref}=0$, the model value of dv_f/dp_{pref} is infinite, however this derivative will not be used in the system as the only locations where compacting pressure is 0 lies on the boundary. There, p is set to P_{top} and $v_f=v_{f0}$. Figure 3-7 compares the model and experimental fiber volume fractions and their derivatives with respect to applied stress.

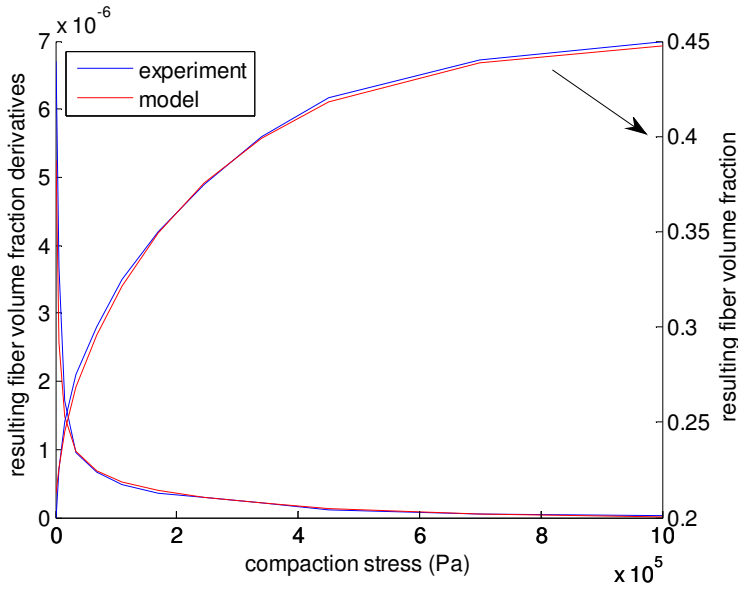

Figure 3-7 Change in fiber volume fraction and its derivative with respect to compaction pressure for E-glass woven fabric

3.1.3 Linear Stress strain relation

In order to model the two dimensional flow during the CRTM process, it has been assumed that the stress strain relationship is linear. This may not be a bad

assumption if the strains are small. This simplification allows us to model the compaction behavior by a linear model using a fabric Young's modulus E and describing the strain of each element as a function of stress due to the fluid p_{pref} and the stress due to the contact tool/preform p_{el},

$$\varepsilon = -\frac{p_{pref}}{E} - \frac{p_{el}}{E} \tag{3.10}$$

However, as one would calculate the strain spatially at all discretized locations as shown in Figure 2-3, a slight oscillatory behavior of one of them can have a dramatic impact on the entire system of equations. In order to attenuate these temporary oscillations, an exponential damping term is added to the computations of the deformation,

$$h_{t+1} = h_t + \left((1+\varepsilon)H - h_t\right)\left(1 - e^{-cdt}\right) \tag{3.11}$$

where H is the initial preform thickness, t is the last recorded time and c is a damping coefficient chosen arbitrarily.

3.2 Permeability

In CRTM, the resin flows along the preform in the in-plane direction as well as in the thickness direction which is the direction in which the upper platen moves to compress the preform. Therefore, one needs to characterize the permeability of the preform as a function of the fiber volume fraction across the thickness as well as in-plane.

3.2.1 Experimental setup

In order to measure the permeability of a preform as a function of the compaction, a RTM mold was used. Different combinations of spacers were used, it

provided different mold cavity thicknesses which led to different preform compactions and hence fiber volume fractions. Once the preform is placed in the mold and compacted to a selected thickness dictated by the spacer plate, the resin is injected at a selected constant pressure into the mold in a uniform way through a line gate creating a one dimensional flow in the plane. The location of the flow front is recorded. Using Darcy's law (Eq.(2.1)) and the movement of the one dimensional flow, one can calculate the in-plane permeability of the fabric at that fiber volume fraction. The experiment was repeated at different compactions thus recording permeability values at various fiber volume fractions.

To measure the permeability in the thickness direction, we applied the lead length concept to the RTM mold [32]. By placing a distribution media of higher permeability on top of the preform, the resin was allowed to flow preferentially through the high permeability layer and then to permeate through the thickness of the preform (Figure 3-8). The resin front advancement is recorded on top (where the distribution media is) and the bottom (Figure 3-9). The difference between the flow fronts during the experiments is called as the lead length and is a function of the fiber volume fraction and the permeability of the distribution media. A numerical three dimensional mold filling code LIMS was used to find the through the thickness permeability [33].

Once the data was measured at a few fiber volume fractions, one could use these results in constitutive models for permeability as a function of the fiber volume fraction.

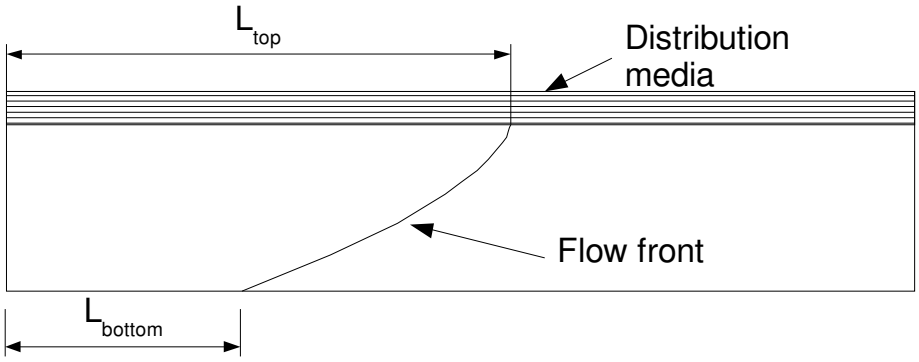

Figure 3-8 Lead length schematic

Figure 3-9 Experimental setup to measure through thickness permeability by recording the advancement of the flow front at the top and the bottom surface of the mold.

3.2.2 Kozeny-Carman model

One could use one of the many available models in the literature; we selected the Kozeny-Carman [19, 20, 30, 34] relation to describe this change which is given by,

$$K\left(v_f\right) = ko\frac{\left(1-v_f\right)^3}{v_f^2} \tag{3.12}$$

The fiber volume fraction can be expressed as a function of the initial fiber volume fraction v_{f0}, initial thickness H and actual thickness h,

$$v_f = \frac{v_{f0}H}{h} \tag{3.13}$$

One could easily substitute another expression to describe the change in permeability. As shown in Figure 3-10, a good fit with the in-plane experimental data was found at the higher values of fiber volume fractions using equation (3.12) when a value of 4.10^{-10}m^2 was used for k_o. The curve fit with the four last experiment data points (Figure 3-10) leads to the following results for the through plane (ko_{yy}) and in-plane (ko_{xx}) permeability coefficients,

$$ko_{yy} = 2.7.10^{-12}m^2 \tag{3.14}$$

And

$$ko_{xx} = 4.10^{-10}m^2 \tag{3.15}$$

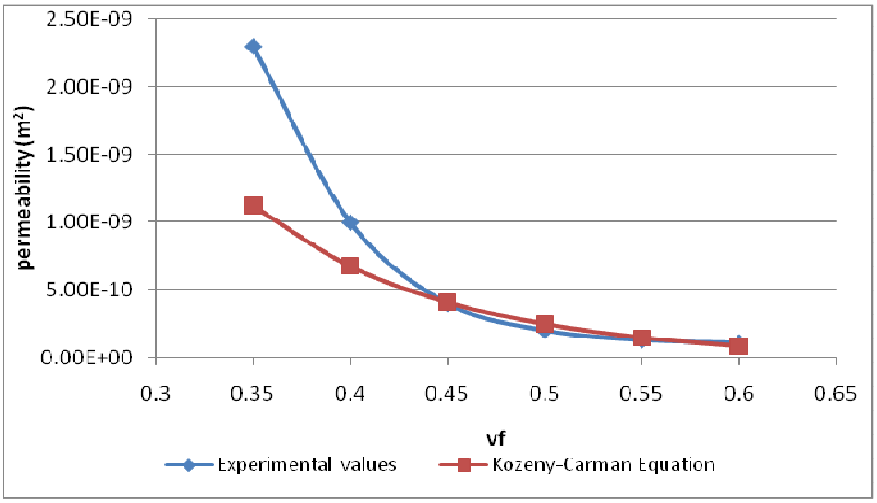

Figure 3-10 In plane permeability values for e-glass woven fabric and its fit with the Kozeny Carman equation at higher fiber volume fractions (R^2=0.99 for the last four data points)

Chapter 4

NON DIMENSIONAL ANALYSIS

In this chapter, a non dimensional analysis is conducted to identify the important process parameters. The governing equations derived in chapter 2 are as follows:

Flow progression in the gap,

$$\frac{\partial L_{gap}}{\partial t} = -\frac{K_{gap}\left(x = L_{gap}\right)}{\eta}\left(\frac{\partial p}{\partial \mathrm{x}}\right)_{x=L_{gap},dl} \tag{4.1}$$

Flow progression in the preform,

$$\left(\frac{\partial L_p}{\partial t}\right)_x = \left(\frac{\partial L_p}{\partial x}\right)_x \frac{K_{xx}\left(x, y = L_p\right)}{\eta\phi\left(x, y = L_p\right)}\left(\frac{\partial p}{\partial x}\right)_{x, y=L_p} - \frac{K_{yy}\left(x, y = L_p\right)}{\eta\phi\left(x, y = L_p\right)}\left(\frac{\partial p}{\partial y}\right)_{x, y=L_p} \tag{4.2}$$

Pressure distribution in the gap,

$$\begin{aligned}\left(\frac{\partial \varepsilon}{\partial t}\right)_{x, y=dl} dl + \left(\frac{\partial H_{gap}}{\partial t}\right)_x &= \frac{K_{yy}\left(x, y = dl\right)}{\eta}\left(\frac{\partial p}{\partial y}\right)_{x, y=dl} + \\ \frac{\partial}{\partial x}\left(\frac{H_{gap}\left(x\right)^3}{12\eta}\left(\frac{\partial p}{\partial x}\right)_{x, y=dl}\right)_{x, y=dl} &+ \frac{\partial}{\partial x}\left(\frac{K_{xx}(x, y = dl)}{\eta}\left(\frac{\partial p}{\partial x}\right)_{x, y=dl}\right)_{x, y=dl} dl\end{aligned} \tag{4.3}$$

Pressure distribution in the preform,

$$dh(x,y)\left(\frac{\partial \varepsilon}{\partial t}\right)_{x,y} = \frac{\partial}{\partial x}\left(\frac{dh(x,y)K_{xx}(x,y)}{\eta}\left(\frac{\partial p}{\partial x}\right)_{x,y}\right)_{x,y} + dh(x,y)\frac{\partial}{\partial y}\left(\frac{K_{yy}(x,y)}{\eta}\left(\frac{\partial p}{\partial y}\right)_{x,y}\right)_{x,y} \tag{4.4}$$

To non dimensionalize, independent and dependent variables were identified and non-dimensionalized with respect to characteristic values. When the characteristic values were not obvious, they were determined by normalizing the coefficients of the equation.

Dependent and independent variables have been non-dimesionalized and listed in Table 4-1,

For example, the in-plane permeability is non dimensionalized in the following way,

$$\hat{K}_{xx} = \frac{K_{xx}}{k_{oxx}} \tag{4.5}$$

Using the variables from Table 4-1, the governing equations listed in chapter 2 will be non-dimensionalized.

Table 4-1 Non dimensionalized variables with their characteristic value

Variable	Physical significance	characterized value with respective to which it is non-dimensionalized
x	Horizontal coordinate	L (length of the mold)
y	Vertical coordinate	H (thickness of the mold)
dh	Control volume thickness	H
h	Preform thickness	H
L_g	Flow position in the gap	L
L_p	Flow position in the preform	H
H_g	Gap size	H_{gap} (thickness of the gap)
K_{xx}	In plane permeability	k_{oxx} (in-plane permeability)
K_{yy}	Through plane permeability	k_{oyy} (through thickness permeability)
t	Time	t_c (characteristic time)
P_{el}	Stress due to contact preform/tool	P_{ap} (applied pressure on top of preform)
p	Fluid pressure	P_{ap}, P_{inj} (injection pressure)
A	Horizontal surface of the preform (unity depth in coordinate z)	L

4.1 Pressure distribution

The equation governing most of the process being the bulk equation (2.20) it will be the first one to be non-dimensionalized,

$$d\hat{h}(\hat{x},\hat{y})\left(\frac{\partial \varepsilon}{\partial \hat{t}}\right)_{\hat{x},\hat{y}} = \frac{ko_{xx}H^2}{ko_{yy}L^2}\frac{\partial}{\partial \hat{x}}\left(d\hat{h}(\hat{x},\hat{y})\hat{K}_{xx}(\hat{x},\hat{y})\left(\frac{\partial \hat{p}}{\partial \hat{x}}\right)_{\hat{x},\hat{y}}\right)_{\hat{x},\hat{y}} + d\hat{h}(\hat{x},\hat{y})\frac{\partial}{\partial \hat{y}}\left(\hat{K}_{yy}(\hat{x},\hat{y})\left(\frac{\partial \hat{p}}{\partial \hat{y}}\right)_{\hat{x},\hat{y}}\right)_{\hat{x},\hat{y}} \tag{4.6}$$

Where t_c is chosen as such,

$$t_c = \frac{H^2 \eta}{ko_{yy} P_{inj}} \tag{4.7}$$

for phase 1 and,

$$t_c = \frac{H^2 \eta}{ko_{yy} P_{ap}} \tag{4.8}$$

for phase 2 and 3. t_c represents twice the time to fill a cavity of length H of fabric of permeability ko_{yy} by a fluid of viscosity η at a pressure P_{ap}.

The infinitesimal strain rate of deformation can be expressed from Eq. (3.11) and non dimensionalized,

$$\begin{aligned} \left(\frac{\partial \varepsilon}{\partial \hat{t}}\right)_{\hat{x},\hat{y}} &= \frac{d\hat{y} - d\hat{h}^t(\hat{x},\hat{y})}{d\hat{h}^t(\hat{x},\hat{y})\, d\hat{t}}\left(1 - e^{-ct_c d\hat{t}}\right) - \\ &\frac{d\hat{y}}{d\hat{t} d\hat{h}^t(\hat{x},\hat{y})} \frac{P_{ap}}{E}\left(\hat{p}_{pref}(\hat{x},\hat{y}) - \hat{p}_{el}(\hat{x},\hat{y})\right)\left(1 - e^{-ct_c d\hat{t}}\right) \end{aligned} \tag{4.9}$$

Substituting Eq. (4.9) into (4.6), one finds for phase 1,

$$\begin{aligned} &\frac{ko_{xx} H^2}{ko_{yy} L^2} \frac{\partial}{\partial \hat{x}}\left(d\hat{h}(\hat{x},\hat{y})\, \hat{K}_{xx}(\hat{x},\hat{y})\left(\frac{\partial \hat{p}}{\partial \hat{x}}\right)_{\hat{x},\hat{y}}\right)_{\hat{x},\hat{y}} + \\ &d\hat{h}(\hat{x},\hat{y}) \frac{\partial}{\partial \hat{y}}\left(\hat{K}_{yy}(\hat{x},\hat{y})\left(\frac{\partial \hat{p}}{\partial \hat{y}}\right)_{\hat{x},\hat{y}}\right)_{\hat{x},\hat{y}} = \\ &d\hat{h}(\hat{x},\hat{y})\left(\frac{d\hat{y} - d\hat{h}^t(\hat{x},\hat{y})}{d\hat{h}^t(\hat{x},\hat{y})\, d\hat{t}}\left(1 - e^{-ct_c d\hat{t}}\right)\right) - \\ &d\hat{h}(\hat{x},\hat{y})\left(\frac{d\hat{y}}{d\hat{t} d\hat{h}^t(\hat{x},\hat{y})} \frac{P_{inj}}{E}\left(\hat{p}_{pref}(\hat{x},\hat{y}) - \hat{p}_{el}(\hat{x},\hat{y})\right)\left(1 - e^{-ct_c d\hat{t}}\right)\right) \end{aligned} \tag{4.10}$$

And for phase 2 and 3,

$$\frac{ko_{xx}H^2}{ko_{yy}L^2}\frac{\partial}{\partial\hat{x}}\left(d\hat{h}(\hat{x},\hat{y})\hat{K}_{xx}(\hat{x},\hat{y})\left(\frac{\partial\hat{p}}{\partial\hat{x}}\right)_{\hat{x},\hat{y}}\right)_{\hat{x},\hat{y}} + d\hat{h}(\hat{x},\hat{y})\frac{\partial}{\partial\hat{y}}\left(\hat{K}_{yy}(\hat{x},\hat{y})\left(\frac{\partial\hat{p}}{\partial\hat{y}}\right)_{\hat{x},\hat{y}}\right)_{\hat{x},\hat{y}} = d\hat{h}(\hat{x},\hat{y})\left(\frac{d\hat{y}-d\hat{h}^t(\hat{x},\hat{y})}{d\hat{h}^t(\hat{x},\hat{y})d\hat{t}}\left(1-e^{-ct_c d\hat{t}}\right)\right) - d\hat{h}(\hat{x},\hat{y})\left(\frac{d\hat{y}}{d\hat{t}d\hat{h}^t(\hat{x},\hat{y})}\frac{P_{ap}}{E}\left(\hat{p}_{pref}(\hat{x},\hat{y})-\hat{p}_{el}(\hat{x},\hat{y})\right)\left(1-e^{-ct_c d\hat{t}}\right)\right) \tag{4.11}$$

In Eq. (4.10) and (4.11) one can identify the ratio of in-plane versus through thickness permeability,

$$\alpha = \frac{ko_{xx}H^2}{ko_{yy}L^2} \tag{4.12}$$

The ratio between injection pressure versus Young's modulus of the preform during phase 1 is determined as follows,

$$\delta_1 = \frac{P_{inj}}{E} \tag{4.13}$$

And the ratio between available stress versus Young's modulus of the preform during phase 2 and 3,

$$\delta_2 = \frac{P_{ap}}{E} = \frac{F}{AE} \tag{4.14}$$

Where A is area of the surface in contact with the tool. When the gap still exists the stress in the preform due to contact tool/preform equals zero, the top layer elements are then not deformed. Non dimensionalizing the vertical component of Eq. (2.16)

with respect to H_{gap} and substituting the characteristic time (4.8) or (4.7) depending on the phase, the gap equation becomes,

$$\left(\frac{\partial \hat{H}_g}{\partial \hat{t}}\right)_{\hat{x}} = \frac{H^2}{{H_{gap}}^2}\hat{K}_{yy}\left(\hat{x},\hat{y}=d\hat{l}\right)\left(\frac{\partial \hat{p}}{\partial \hat{y}}\right)_{\hat{x},\hat{y}=d\hat{l}} + \frac{{H_{gap}}^2 H^2}{12L^2 ko_{yy}}\frac{\partial}{\partial \hat{x}}\left(\hat{H}_g\left(\hat{x}\right)^3\left(\frac{\partial \hat{p}}{\partial \hat{x}}\right)_{\hat{x},\hat{y}=d\hat{l}}\right)_{\hat{x},\hat{y}=d\hat{l}} + \frac{ko_{xx}H^2}{ko_{yy}L^2}d\hat{l}\hat{K}_{xx}\left(\hat{x},\hat{y}=d\hat{l}\right)\left(\frac{\partial^2 \hat{p}}{\partial \hat{x}^2}\right)_{\hat{x},\hat{y}=d\hat{l}} \tag{4.15}$$

In Eq.(4.15), one can recast (4.12) and identify the ratio of the gap versus the through thickness permeability,

$$\beta = \frac{{H_{gap}}^2 H^2}{12L^2 ko_{yy}} \tag{4.16}$$

As well as the ratio between the gap and the preform thickness,

$$\gamma = \frac{H}{H_{gap}} \tag{4.17}$$

4.2 Flow front progression

The non dimensionalized form of the equation describing the evolution of the flow front in the gap (2.2) becomes,

$$\frac{\partial \hat{L}_g}{\partial \hat{t}} = -\frac{{H_{gap}}^2 H^2}{12L^2 ko_{yy}}\hat{H}_g\left(\hat{x}\right)^2\left(\frac{\partial \hat{p}}{\partial \hat{x}}\right)_x \tag{4.18}$$

Where one can identify α and β.

Similarly, the flow front progression through the thickness of the preform is written in its dimensionless form,

$$\left(\frac{\partial \hat{L}_p}{\partial \hat{t}}\right)_{\hat{x}} = -\frac{\hat{K}_{yy}\left(\hat{x},\hat{y}=\hat{L}_p\right)}{\phi\left(\hat{x},\hat{y}=\hat{L}_p\right)}\left(\frac{\partial \hat{p}}{\partial \hat{y}}\right)_{\hat{x},\hat{y}=\hat{L}_p} + \frac{ko_{xx}H^2}{ko_{yy}L^2}\frac{\hat{K}_{xx}\left(\hat{x},\hat{y}=\hat{L}_p\right)}{\phi\left(\hat{x},\hat{y}=\hat{L}_p\right)}\left(\frac{\partial \hat{L}_p}{\partial \hat{x}}\right)_{\hat{x},\hat{y}=\hat{L}_p}\left(\frac{\partial \hat{p}}{\partial \hat{x}}\right)_{\hat{x},\hat{y}=\hat{L}_p} \tag{4.19}$$

From the previous equations and the constitutive equations listed in chapter 2, one can identify 6 non dimensional parameters influencing the flow front progression and the compaction of the preform. They are listed in Table 4-2 along with their physical significance.

Table 4-2 Non dimensional parameters in the process

Non dimensional parameter	Physical significance
v_{f0}	Initial fiber volume fraction
$\alpha = \frac{ko_{xx}H^2}{ko_{yy}L^2}$	Ratio of in plane to through plane permeability
$\beta = \frac{H_{gap}{}^2H^2}{12L^2ko_{yy}}$	Ratio of gap to through plane permeability
$\gamma = \frac{H}{H_{gap}}$	Ratio of gap to preform thickness
$\delta_1 = \frac{P_{inj}}{E}$	Ratio of maximum stress to available stress to compact the preform during the first phase
$\delta_2 = \frac{F}{AE}$	Ratio of maximum stress and available stress to compact the preform during phase 2 and 3

Using Table 4-2, the governing equations can be expressed in their dimensionless form:

Flow front progression in the gap,

$$\frac{\partial \hat{L}_g}{\partial \hat{t}} = -\beta \hat{H}_g\left(\hat{x}\right)^2 \left(\frac{\partial \hat{p}}{\partial \hat{x}}\right)_{\hat{x}=\hat{L}_g} \tag{4.20}$$

Flow front progression in the preform,

$$\begin{aligned} \left(\frac{\partial \hat{L}_p}{\partial \hat{t}}\right)_{\hat{x},\hat{y}} = -\frac{\hat{K}_{yy}\left(\hat{x},\hat{y}=\hat{L}_p\right)}{\phi\left(\hat{x},\hat{y}=\hat{L}_p\right)}\left(\frac{\partial \hat{p}}{\partial \hat{y}}\right)_{\hat{x},\hat{y}=\hat{L}_p} + \\ \alpha\frac{\hat{K}_{xx}\left(\hat{x},\hat{y}=\hat{L}_p\right)}{\phi\left(\hat{x},\hat{y}=\hat{L}_p\right)}\left(\frac{\partial \hat{L}_p}{\partial \hat{x}}\right)_{\hat{x},\hat{y}=\hat{L}_p}\left(\frac{\partial \hat{p}}{\partial \hat{x}}\right)_{\hat{x},\hat{y}=\hat{L}_p} \end{aligned} \tag{4.21}$$

Pressure distribution in the gap,

$$\begin{aligned} \left(\frac{\partial \hat{H}_g}{\partial \hat{t}}\right)_{\hat{x}} = \gamma^2 \hat{K}_{yy}\left(\hat{x},\hat{y}=d\hat{l}\right)\left(\frac{\partial \hat{p}}{\partial \hat{y}}\right)_{\hat{x},\hat{y}=d\hat{l}} + \\ \beta\frac{\partial}{\partial \hat{x}}\left(\hat{H}_g\left(\hat{x}\right)^3\left(\frac{\partial \hat{p}}{\partial \hat{x}}\right)_{\hat{x},\hat{y}=d\hat{l}}\right)_{\hat{x},\hat{y}=d\hat{l}} + \alpha d\hat{l}\hat{K}_{xx}\left(\hat{x},\hat{y}=d\hat{l}\right)\left(\frac{\partial^2 \hat{p}}{\partial \hat{x}^2}\right)_{\hat{x},\hat{y}=d\hat{l}} \end{aligned} \tag{4.22}$$

Pressure distribution in the preform during phase 1,

$$\begin{aligned} \alpha\frac{\partial}{\partial \hat{x}}\left(d\hat{h}\left(\hat{x},\hat{y}\right)\hat{K}_{xx}\left(\hat{x},\hat{y}\right)\left(\frac{\partial \hat{p}}{\partial \hat{x}}\right)_{\hat{x},\hat{y}}\right)_{\hat{x},\hat{y}} + \\ d\hat{h}\left(\hat{x},\hat{y}\right)\frac{\partial}{\partial \hat{y}}\left(\hat{K}_{yy}\left(\hat{x},\hat{y}\right)\left(\frac{\partial \hat{p}}{\partial \hat{y}}\right)_{\hat{x},\hat{y}}\right)_{\hat{x},\hat{y}} = \\ d\hat{h}\left(\hat{x},\hat{y}\right)\left(\frac{d\hat{y}-d\hat{h}^t\left(\hat{x},\hat{y}\right)}{d\hat{h}^t\left(\hat{x},\hat{y}\right)d\hat{t}}\left(1-e^{-ct_c d\hat{t}}\right)\right) - \\ d\hat{h}\left(\hat{x},\hat{y}\right)\left(\frac{d\hat{y}}{d\hat{t}d\hat{h}^t\left(\hat{x},\hat{y}\right)}\delta_1\left(\hat{p}_{pref}\left(\hat{x},\hat{y}\right)-\hat{p}_{el}\left(\hat{x},\hat{y}\right)\right)\left(1-e^{-ct_c d\hat{t}}\right)\right) \end{aligned} \tag{4.23}$$

Pressure distribution in the preform during phase 2 and 3,

$$\begin{aligned}
&\alpha\frac{\partial}{\partial\hat{x}}\left(d\hat{h}(\hat{x},\hat{y})\hat{K}_{xx}(\hat{x},\hat{y})\left(\frac{\partial\hat{p}}{\partial\hat{x}}\right)_{\hat{x},\hat{y}}\right)_{\hat{x},\hat{y}}+\\
&d\hat{h}(\hat{x},\hat{y})\frac{\partial}{\partial\hat{y}}\left(\hat{K}_{yy}(\hat{x},\hat{y})\left(\frac{\partial\hat{p}}{\partial\hat{y}}\right)_{\hat{x},\hat{y}}\right)_{\hat{x},\hat{y}}=\\
&d\hat{h}(\hat{x},\hat{y})\left(\frac{d\hat{y}-d\hat{h}^{t}(\hat{x},\hat{y})}{d\hat{h}^{t}(\hat{x},\hat{y})d\hat{t}}\left(1-e^{-ct_{c}d\hat{t}}\right)\right)-\\
&d\hat{h}(\hat{x},\hat{y})\left(\frac{d\hat{y}}{d\hat{t}d\hat{h}^{t}(\hat{x},\hat{y})}\delta_{2}\left(\hat{p}_{pref}(\hat{x},\hat{y})-\hat{p}_{el}(\hat{x},\hat{y})\right)\left(1-e^{-ct_{c}d\hat{t}}\right)\right)
\end{aligned}\tag{4.24}$$

Chapter 5

NUMERICAL MODELING

From chapter 4 we determined the non dimensional equations that will govern the flow during the CRTM process. However, these partial differential equations cannot be solved analytically. A numerical technique is developed to cast the governing equations into a linear system of algebraic equation using finite difference method. The solution approach is presented for each phase of the process. The model is verified by comparing it with another established numerical simulation and results are also presented for a case study.

5.1 Numerical approach

5.1.1 Assumptions

In order to simplify the process model, several assumptions describing the compaction behavior have to be made.

5.1.1.1 Visco-elasticity

Due to the visco-elastic behavior of the dry preform and the high closing speeds involved, the dry part of the preform will be assumed to be stiff [23, 30]. Concerning the lubricated part of the preform, its visco-elasticity will be neglected (fiber volume fraction depends only on the applied stress).

5.1.1.2 Applied force

In the industry, the load is usually applied using a hydraulic press. Therefore, the press does not instantaneously set itself to the desired force. Moreover, numerically one cannot usually directly apply the full compaction force after the first phase. In our case, the shock wave that should be induced by the brutal transition is damped by the exponential term in the equation governing the preform compaction (Eq.(3.11)). However, we still include a ramping term that will insure a smooth transition between the loads applied in phase one and two. The load is linearly ramped at a certain rate. To model this progressive load, the following equation is used,

$$F(t) = F_0 + \frac{\left(F_{applied} - F_0\right)}{R} t \tag{5.1}$$

Where, F_0 is the averaged load exerted by the fluid on the preform at the end of the first phase, $F_{applied}$ is the target load, R is a ramping coefficient. R is chosen arbitrarily and will delay the full application of the force. A decrease of R will then speed the process but risk instability of the numerical solution. Once the targeted load is reached, the value of F becomes constant and equal to $F_{applied}$.

5.1.2 Discretization method

To model the flow during the CRTM process, one has to solve a system composed of the equations describing the flow as well as the compaction during the three phases (Eqs.(4.20), (4.21), (4.22), (4.23) and (4.24)) To do so, an implicit scheme regrouping all the primary unknowns (flow front positions, gap sizes, fluid pressures,…) is used [35]. The use of an implicit scheme allows us to have a stable solution for any value of time step. The secondary unknowns (permeabilities, deformation strains, fiber volume fractions) are then computed using the primary

unknowns. The unknown values and the criteria to end each phase are listed in Table 5-1,

Table 5-1 System unknowns and criteria to end each phase

	Primary unknowns	Secondary unknowns	End of phase criteria
Phase 1	L_g (flow front position in gap) L_p (flow front positions in preform) p (fluid pressure values)	K_{xx}, K_{yy} (permeabilities) H_g (gap size) v_f (fiber volume fraction) dh (deformed element thickness)	volume of resin in the system equal to volume of resin initially injected
Phase 2	L_g L_p p H_g Δ (distance between the two mold plates)	K_{xx}, K_{yy} v_f dh	When the tool touches the preform at any location.
Phase 3	L_g L_p p H_g p_{el} (compressive stress due to contact preform/tool) Δ	K_{xx}, K_{yy} v_f dh	Until every node is filled

Once all the primary unknowns are determined, the secondary unknowns are calculated by using the constitutive equations listed in chapter 3.

5.1.2.1 Mesh generation

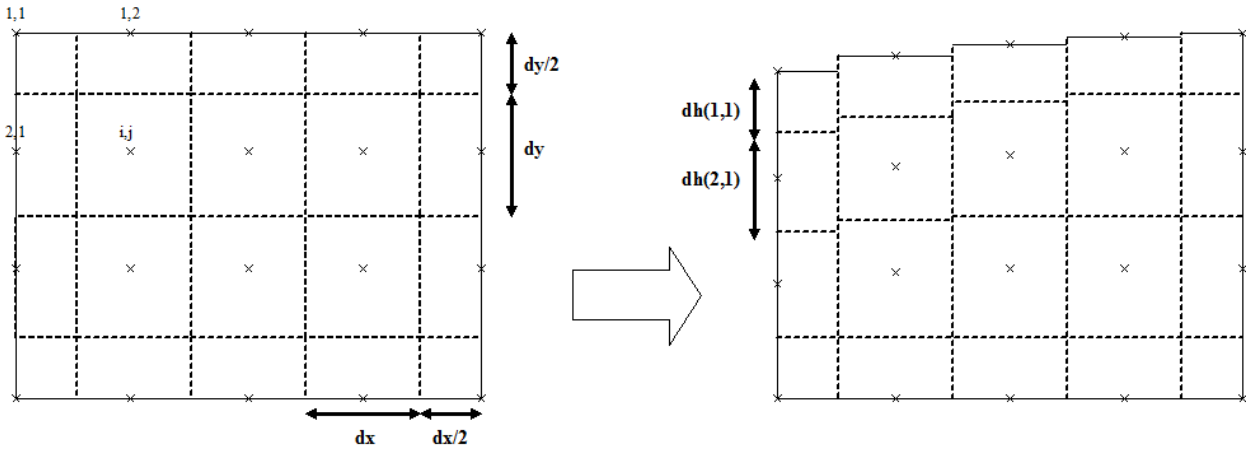

Figure 5-1 Two dimensional mesh used to solve the problem (before and after deformation)

The equations derived in chapter 4 are discretized according to a deformable mesh (Figure 5-1). A pressure is associated at each node in the mesh, whereas permeability of the fabric and the fiber volume fraction are assigned to each element. There are *m* nodes along the thickness and *n* nodes along the length of the part. During the CRTM process, the preform will deform. To solve the equations using a deformable mesh, one should use a transposition matrix to transform the deformable mesh into a fixed mesh in order to compute the derivatives properly [35, 36]. In our study, the nodes are displaced vertically only and a relatively stiff fabric has been used

for the simulation. The mesh is then only slightly deformed; hence the involved Jacobian matrix is close to identity. In order to simplify the derivative computations, a new variable is introduced to express the thickness of each element;

$$d\hat{h}_{i,j} = d\hat{y}(1+\varepsilon_{i,j}) \tag{5.2}$$

where $dh_{i,j}$ represents the deformed element thickness, $\varepsilon_{i,j}$ the strain of the element. The derivative will then be numerically expressed as a function of dh instead of dy and the mass balance for each element will be made over a stiff orthogonal mesh.

5.1.2.2 Finite differences and equation computation

In order to discretize the derivatives involved in the governing equations given by (Eqs.(4.20), (4.21), (4.22), (4.23) and (4.24)), the finite difference method will be used [35-37]. The equations associated to the boundaries of the domain will also be discretized and the method to solve the system of equations will be detailed.

5.1.2.2.1 Boundary condition

On the wall, the first derivative will be equal to zero. On the right and left sides of the wall,

$$\frac{\partial \hat{p}_{i,j}}{\partial \hat{x}} = 0 \tag{5.3}$$

And on the top and bottom of the mold,

$$\frac{\partial \hat{p}_{i,j}}{\partial \hat{y}} = 0 \tag{5.4}$$

To discretize the derivative at the domain walls, the mirror method is used. An imaginary node is created on the other side of the wall and its pressure value is the same than the node before the wall. Equation (5.3) is discretized as follows,

$$\hat{p}_{i,j+1} = \hat{p}_{i,j-1} \tag{5.5}$$

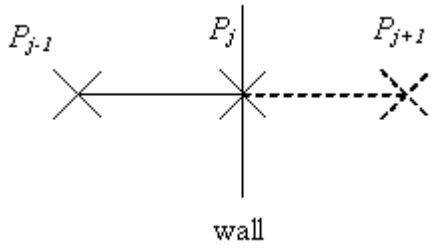

Figure 5-2 Mirror concept

Applying eq. (5.5) to the discretization of the second derivatives results in the following derivatives at the end of the mold (j=n),

$$\frac{\partial^2 \hat{p}_{i,j}}{\partial \hat{x}^2} = \frac{2\hat{p}^t_{i,j-1} - 2\hat{p}^t_{i,j}}{d\hat{x}^2} \tag{5.6}$$

At the symmetry axis (j=1), the second derivative is,

$$\frac{\partial^2 \hat{p}_{i,j}}{\partial \hat{x}^2} = \frac{2\hat{p}^t_{i,j+1} - 2\hat{p}^t_{i,j}}{d\hat{x}^2} \tag{5.7}$$

The injection gate being located in the middle, one can simplify the problem by applying a symmetry condition at the middle (see Figure 2-4). At j=1, one would apply Eq. (5.3) and (5.7).

5.1.2.2.2 Pressure interpolation

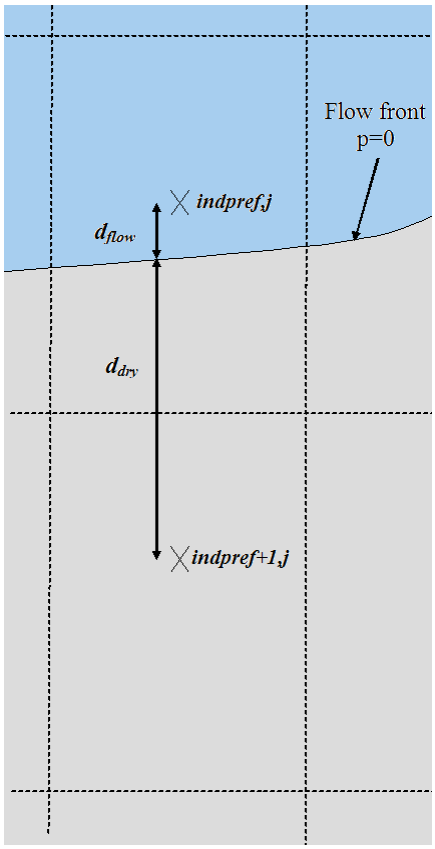

Figure 5-3 Schematic of interpolating pressure near the flow front

In order to locate the flow front between two nodes, an equation determining the pressure after the flow front is added. The pressure at the flow front is equal to zero, the pressure located after the flow front will then be negative. It will be

determined using a linear interpolation based on the fluid penetration between two vertical nodes (Figure 5-3),

$$\hat{p}_{flowfront} = 0 = \frac{\hat{p}_{indpref}\hat{d}_{dry}}{\hat{d}_{flow} + \hat{d}_{dry}} + \frac{\hat{p}_{indpref+1}\hat{d}_{flow}}{\hat{d}_{flow} + \hat{d}_{dry}} \tag{5.8}$$

Leading to,

$$\hat{d}_{dry}\hat{p}_{indpref,j} + \hat{d}_{flow}\hat{p}_{indpref+1,j} = 0 \tag{5.9}$$

Where d_{dry} and d_{flow} are the dry and wet lengths between two nodes, *indpref* is the vertical index of the last filled node. Similarly, the flow front in the gap is located by,

$$\hat{d}_{drygap}\hat{p}_{1,indgap} + \hat{d}_{flowgap}\hat{p}_{1,indgap+1} = 0 \tag{5.10}$$

Where d_{drygap} and $d_{flowgap}$ are the dry and wet lengths between two nodes, *indgap* is the horizontal gap index of the last filled node.

5.1.2.2.3 Finding the primary unknowns

At each time step, a system of equations is created from the discretization of the partial differential equations ((Eqs.(4.20), (4.21), (4.22), (4.23) and (4.24)) As an example Eq (4.20) can be discretized in the following way,

$$\hat{L}_g^{t+1} + \frac{\beta\hat{H}_{g_{indgap}}d\hat{t}}{d\hat{x}}\left(\hat{p}_{indgap}^{t+1} - \hat{p}_{indgap-1}^{t+1}\right) = \hat{L}_g^t \tag{5.11}$$

All the unknowns' coefficients are put in a matrix *G* that is multiplied by the unknowns vector *U*. This multiplication is equal to a forcing term *F*. The system has then the following structure,

$$[G].[U] = [F] \tag{5.12}$$

In Eq. (5.11), L_{gap}^{t+1} and p at t+1 form the unknown U vector and L_{gap}^{t} forms the force vector F whereas unity is the coefficient associated with the unknown L_{gap}^{t+1} and $\frac{\beta \hat{H}_{g_{indgap}} d\hat{t}}{d\hat{x}}$ is the coefficient associated with the unknown pressures in the matrix G. The unknown variables in the vector U can be calculated by solving the system of algebraic equations (5.12)

$$[U] = [G]^{-1}[F] \tag{5.13}$$

The vector U contains then every primary unknown required to compute the secondary unknowns stated in Table 5-1. As the primary unknowns change with each phase, the matrix structure will be described for each phase.

5.1.3 Application to the numerical method to the CRTM phases

In this section, the solution method will be applied to each phase of the CRTM process.

5.1.3.1 Calculation of the required volume of resin to inject

In order to saturate the preform without any voids one must compute the final porosity (volume that the resin can fill) as a function of the final geometry,

$$\phi_{final} = 1 - \frac{v_{f0}}{\hat{h}_{final}} \tag{5.14}$$

h_{final} is the final thickness, H is the initial thickness *and* v_{f0} is the initial fiber volume fraction. Once the final thickness is known, one can easily determine the required amount of resin needed to completely fill the part,

$$\hat{V}_{resin} = \hat{h}_{final} \hat{A} \phi_{final} \tag{5.15}$$

Where V_{resin} is the required amount of resin, A the area of the top surface of the mold.

Once the required amount of resin to inject is computed, the pressure at the node representing the injection gate is set equal to a constant value of 1.

5.1.3.2 Equations common to the three phases

The pressure distribution as well as the flow progression and the preform deformation will be governed by the discretized version of equations (4.20), (4.21), (4.22), (4.23) and (4.24). The flow front progression and pressure distribution in the preform equations are common to every phases of the process. However, the pressure distribution equation on the top layer as well as some boundary conditions will vary between the different phases. For each phase, they will be treated separately along with the matrix structure. Finally, once the primary unknowns are determined using the governing equations, the secondary unknowns can be computed. These computations are common to each phase.

5.1.3.2.1 Flow in the gap

The interpolated pressure is only a linear approximation; therefore it does not respect the conservation of mass in the element. The flow front progression in the gap is then computed using the pressures calculated from accurate relations. The derivative of the pressure with respect to x will then be approximated using a backward differentiation. The discretized version of Eq. (4.20) is,

$$\hat{L}_g^{t+1} + \frac{\beta \hat{H}_{g_{indgap}} d\hat{t}}{d\hat{x}} \left(\hat{p}_{indgap}^{t+1} - \hat{p}_{indgap-1}^{t+1} \right) = \hat{L}_g^t \tag{5.16}$$

5.1.3.2.2 Flow in the preform

To compute the vertical flow front position, the same reason than in the gap is used to choose the proper indices in order to compute the pressure derivatives.

The preform being compacted, the difference between depths of penetration has to be made from a vertical reference position. The y position of the top of the preform being not constant, the difference of L_p's will be calculated from the bottom of the mold as showed in Figure 5-4.

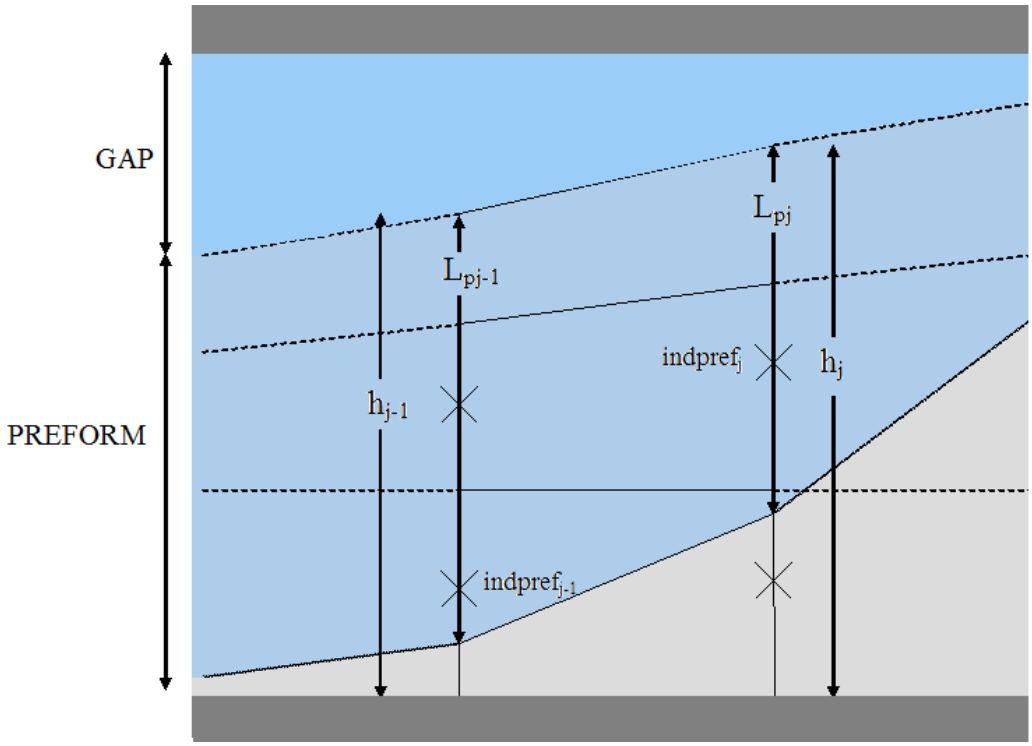

Figure 5-4 Schematic showing difference between two neighboring depths of penetration

The flow front progression in the preform can be expressed as follows,

$$\hat{L}_p^{t+1} - \frac{\alpha \hat{K}_{xx_{indpref+1,j}} d\hat{t}}{4d\hat{x}^2 \phi_{indpref+1,j}} \left(\left(\hat{h}_{j-1}^{t+1} - \hat{L}_{pj-1}^{t+1} \right) - \left(\hat{h}_j^{t+1} - \hat{L}_{pj}^{t+1} \right) \right) \left(\hat{p}_{indpref,j}^{t+1} - \hat{p}_{indpref,j-1}^{t+1} \right) + \frac{\hat{K}_{yy_{indpref+1,j}} d\hat{t}}{2d\hat{h}_{indpref,j} \phi_{indpref+1,j}} \left(\hat{p}_{indpref,j}^{t+1} - \hat{p}_{indpref-1,j}^{t+1} \right) = \hat{L}_p^t \quad (5.17)$$

Where *indpref* is the last vertical filled node of the column of nodes.

5.1.3.2.3 Pressure distribution in the preform

The equation describing the pressure in the preform is only applied to the rows below the first layer of nodes. The pressures in the first layer of nodes will be governed by the gap equation. To calculate the pressures in the preform, one has to determine the infinitesimal strain rate of deformation. It can be expressed as follows,

$$\left(\frac{\partial \varepsilon_{i,j}}{\partial \hat{t}} \right)^{t+1} = \frac{d\hat{h}_{i,j}^{t+1} - d\hat{h}_{i,j}^t}{d\hat{h}_{i,j}^t d\hat{t}} \quad (5.18)$$

The infinitesimal height of a control volume is computed by applying Eq. (3.11) to a control volume,

$$\hat{dh}_{t+1} = \hat{dh}_t + \left(\left(1 - \delta \hat{p}_{pref} - \delta \hat{p}_{el} \right) \hat{dy} - \hat{dh}_t \right) \left(1 - e^{-ct_c d\hat{t}} \right) \quad (5.19)$$

Substituting Eq. (5.19) into Eq.(5.18),

$$\left(\frac{\partial \varepsilon_{i,j}}{\partial \hat{t}} \right)^{t+1} = \frac{\left(1 - e^{-ct_c d\hat{t}} \right) \left(d\hat{y} - d\hat{h}_{i,j}^t \right)}{d\hat{h}_{i,j}^t d\hat{t}} - \frac{\delta d\hat{y} \left(1 - e^{-ct_c d\hat{t}} \right)}{d\hat{h}_{i,j}^t d\hat{t}} \left(\hat{p}_{1,j}^{t+1} - \hat{p}_{i,j}^{t+1} + \hat{p}_{elj}^{t+1} \right) \quad (5.20)$$

Discretizing Eq. (4.23) and substituting Eq. (5.20),

$$\hat{p}_{i,j}^{t+1}\left(-\frac{2\alpha\hat{K}_{xx_{i,j}}d\hat{h}_{i,j}^{t+1}}{d\hat{x}^2}-\frac{2\hat{K}_{yy_{i,j}}d\hat{h}_{i,j}^{t+1}}{d\hat{h}^2}-\frac{\delta d\hat{h}_{i,j}^{t+1}dy\left(1-e^{-ct_c d\hat{t}}\right)}{d\hat{h}_{i,j}^{t}d\hat{t}}\right)+$$
$$\hat{p}_{i,j-1}^{t+1}\left(-\frac{\alpha\Delta\hat{K}_{xx}d\hat{h}_{i,j}^{t+1}+\alpha\hat{K}_{xx_{i,j}}\Delta d\hat{h}}{4d\hat{x}^2}+\frac{\alpha\hat{K}_{xx_{i,j}}d\hat{h}_{i,j}^{t+1}}{d\hat{x}^2}\right)+$$
$$\hat{p}_{i,j+1}^{t+1}\left(\frac{\alpha\Delta\hat{K}_{xx}d\hat{h}_{i,j}^{t+1}+\alpha\hat{K}_{xx_{i,j}}\Delta d\hat{h}}{4d\hat{x}^2}+\frac{\alpha\hat{K}_{xx_{i,j}}d\hat{h}_{i,j}^{t+1}}{d\hat{x}^2}\right)+ \tag{5.21}$$
$$\hat{p}_{i-1,j}^{t+1}\left(-\frac{\Delta\hat{K}_{yy}d\hat{h}_{i,j}^{t+1}}{4\left(d\hat{h}_{i,j}^{t+1}\right)^2}+\frac{\hat{K}_{yy_{i,j}}d\hat{h}_{i,j}^{t+1}}{\left(d\hat{h}_{i,j}^{t+1}\right)^2}\right)+\hat{p}_{i+1,j}^{t+1}\left(\frac{\Delta\hat{K}_{yy}d\hat{h}_{i,j}^{t+1}}{4\left(d\hat{h}_{i,j}^{t+1}\right)^2}+\frac{\hat{K}_{yy_{i,j}}d\hat{h}_{i,j}^{t+1}}{\left(d\hat{h}_{i,j}^{t+1}\right)^2}\right)+$$
$$\hat{p}_{1,j}^{t+1}\left(\frac{\delta d\hat{h}_{i,j}^{t+1}dy\left(1-e^{-ct_c d\hat{t}}\right)}{d\hat{h}_{i,j}^{t}d\hat{t}}\right)+\hat{p}_{el_j}^{t+1}\left(\frac{\delta d\hat{h}_{i,j}^{t+1}dy\left(1-e^{-ct_c d\hat{t}}\right)}{d\hat{h}_{i,j}^{t}d\hat{t}}\right)=$$
$$\frac{d\hat{h}_{i,j}^{t+1}\left(1-e^{-ct_c d\hat{t}}\right)\left(dy-d\hat{h}_{i,j}^{t}\right)}{d\hat{h}_{i,j}^{t}d\hat{t}}$$

Where

$$\Delta\hat{K}_{xx}=\hat{K}_{xx_{i,j+1}}^{t+1}-\hat{K}_{xx_{i,j-1}}^{t+1} \tag{5.22}$$

$$\Delta\hat{K}_{yy}=\hat{K}_{yy_{i+1,j}}^{t+1}-\hat{K}_{yy_{i-1,j}}^{t+1} \tag{5.23}$$

$$\Delta d\hat{h}=d\hat{h}_{i,j+1}^{t+1}-d\hat{h}_{i,j-1}^{t+1} \tag{5.24}$$

And δ is δ_1 or δ_2 depending on the process phase. On the right wall of the mold, using the mirror method, Eq. (5.21) becomes,

$$\begin{aligned}
&\hat{p}_{i,j}^{t+1}\left(-\frac{2\alpha\hat{K}_{xx_{i,j}}d\hat{h}_{i,j}^{t+1}}{d\hat{x}^2}-\frac{2\hat{K}_{yy_{i,j}}d\hat{h}_{i,j}^{t+1}}{d\hat{h}^2}-\frac{\delta d\hat{h}_{i,j}^{t+1}dy\left(1-e^{-ct_c d\hat{t}}\right)}{d\hat{h}_{i,j}^{t}d\hat{t}}\right)+\\
&\hat{p}_{i,j-1}^{t+1}\left(\frac{2\alpha\hat{K}_{yy_{i,j}}d\hat{h}_{i,j}^{t+1}}{d\hat{x}^2}\right)+\hat{p}_{i-1,j}^{t+1}\left(-\frac{\Delta\hat{K}_{yy}d\hat{h}_{i,j}^{t+1}}{4\left(d\hat{h}_{i,j}^{t+1}\right)^2}+\frac{\hat{K}_{yy_{i,j}}d\hat{h}_{i,j}^{t+1}}{\left(d\hat{h}_{i,j}^{t+1}\right)^2}\right)\\
&+\hat{p}_{i+1,j}^{t+1}\left(\frac{\Delta\hat{K}_{yy}d\hat{h}_{i,j}^{t+1}}{4\left(d\hat{h}_{i,j}^{t+1}\right)^2}+\frac{\hat{K}_{yy_{i,j}}d\hat{h}_{i,j}^{t+1}}{\left(d\hat{h}_{i,j}^{t+1}\right)^2}\right)+\hat{p}_{1,j}^{t+1}\left(\frac{\delta d\hat{h}_{i,j}^{t+1}dy\left(1-e^{-cd\hat{t}}\right)}{d\hat{h}_{i,j}^{t}d\hat{t}}\right)\\
&+\hat{p}_{el_j}^{t+1}\left(\frac{\delta d\hat{h}_{i,j}^{t+1}dy\left(1-e^{-ct_c d\hat{t}}\right)}{d\hat{h}_{i,j}^{t}d\hat{t}}\right)=\frac{d\hat{h}_{i,j}^{t+1}\left(1-e^{-ct_c d\hat{t}}\right)\left(dy-d\hat{h}_{i,j}^{t}\right)}{d\hat{h}_{i,j}^{t}d\hat{t}}
\end{aligned}\tag{5.25}$$

Similarly on the left side, the pressure distribution on the wall is,

$$\begin{aligned}
&\hat{p}_{i,j}^{t+1}\left(-\frac{2\alpha\hat{K}_{xx_{i,j}}d\hat{h}_{i,j}^{t+1}}{d\hat{x}^2}-\frac{2\hat{K}_{yy_{i,j}}d\hat{h}_{i,j}^{t+1}}{d\hat{h}^2}-\frac{\delta d\hat{h}_{i,j}^{t+1}dy\left(1-e^{-ct_c d\hat{t}}\right)}{d\hat{h}_{i,j}^{t}d\hat{t}}\right)+\\
&\hat{p}_{i,j+1}^{t+1}\left(\frac{2\alpha\hat{K}_{xx_{i,j}}d\hat{h}_{i,j}^{t+1}}{d\hat{x}^2}\right)+\hat{p}_{i-1,j}^{t+1}\left(-\frac{\Delta\hat{K}_{yy}d\hat{h}_{i,j}^{t+1}}{4\left(d\hat{h}_{i,j}^{t+1}\right)^2}+\frac{\hat{K}_{yy_{i,j}}d\hat{h}_{i,j}^{t+1}}{\left(d\hat{h}_{i,j}^{t+1}\right)^2}\right)\\
&+\hat{p}_{i+1,j}^{t+1}\left(\frac{\Delta\hat{K}_{yy}d\hat{h}_{i,j}^{t+1}}{4\left(d\hat{h}_{i,j}^{t+1}\right)^2}+\frac{\hat{K}_{yy_{i,j}}d\hat{h}_{i,j}^{t+1}}{\left(d\hat{h}_{i,j}^{t+1}\right)^2}\right)+\hat{p}_{1,j}^{t+1}\left(\frac{\delta d\hat{h}_{i,j}^{t+1}dy\left(1-e^{-ct_c d\hat{t}}\right)}{d\hat{h}_{i,j}^{t}d\hat{t}}\right)\\
&+\hat{p}_{el_j}^{t+1}\left(\frac{\delta d\hat{h}_{i,j}^{t+1}dy\left(1-e^{-ct_c d\hat{t}}\right)}{d\hat{h}_{i,j}^{t}d\hat{t}}\right)=\frac{d\hat{h}_{i,j}^{t+1}\left(1-e^{-ct_c d\hat{t}}\right)\left(dy-d\hat{h}_{i,j}^{t}\right)}{d\hat{h}_{i,j}^{t}d\hat{t}}
\end{aligned}\tag{5.26}$$

On the bottom of the mold,

$$\hat{p}_{i,j}^{t+1}\left(-\frac{2\alpha\hat{K}_{xx_{i,j}}d\hat{h}_{i,j}^{t+1}}{d\hat{x}^2}-\frac{2\hat{K}_{yy_{i,j}}d\hat{h}_{i,j}^{t+1}}{d\hat{h}^2}-\frac{\delta d\hat{h}_{i,j}^{t+1}dy\left(1-e^{-ct_c d\hat{t}}\right)}{d\hat{h}_{i,j}^{t}d\hat{t}}\right)+$$
$$\hat{p}_{i,j-1}^{t+1}\left(-\frac{\alpha\Delta\hat{K}_{xx}d\hat{h}_{i,j}^{t+1}+\alpha\hat{K}_{xx_{i,j}}\Delta d\hat{h}}{4d\hat{x}^2}+\frac{\alpha\hat{K}_{xx_{i,j}}d\hat{h}_{i,j}^{t+1}}{d\hat{x}^2}\right)+$$
$$\hat{p}_{i,j+1}^{t+1}\left(\frac{\alpha\Delta\hat{K}_{xx}d\hat{h}_{i,j}^{t+1}+\alpha\hat{K}_{xx_{i,j}}\Delta d\hat{h}}{4d\hat{x}^2}+\frac{\alpha\hat{K}_{xx_{i,j}}d\hat{h}_{i,j}^{t+1}}{d\hat{x}^2}\right)+ \tag{5.27}$$
$$\hat{p}_{i-1,j}^{t+1}\left(\frac{2\hat{K}_{yy_{i,j}}d\hat{h}_{i,j}^{t+1}}{\left(d\hat{h}_{i,j}^{t+1}\right)^2}\right)+\hat{p}_{1,j}^{t+1}\left(\frac{\delta d\hat{h}_{i,j}^{t+1}dy\left(1-e^{-ct_c d\hat{t}}\right)}{d\hat{h}_{i,j}^{t}d\hat{t}}\right)$$
$$+\hat{p}_{el_j}^{t+1}\left(\frac{\delta d\hat{h}_{i,j}^{t+1}dy\left(1-e^{-ct_c d\hat{t}}\right)}{d\hat{h}_{i,j}^{t}d\hat{t}}\right)=\frac{d\hat{h}_{i,j}^{t+1}\left(1-e^{-ct_c d\hat{t}}\right)\left(dy-d\hat{h}_{i,j}^{t}\right)}{d\hat{h}_{i,j}^{t}d\hat{t}}$$

Finally on the bottom right and left of the mold, the vertical and horizontal mirrors are applied. The pressure equation on the bottom right of the mold is,

$$\hat{p}_{i,j}^{t+1}\left(-\frac{2\alpha\hat{K}_{xx_{i,j}}d\hat{h}_{i,j}^{t+1}}{d\hat{x}^2}-\frac{2\hat{K}_{yy_{i,j}}d\hat{h}_{i,j}^{t+1}}{d\hat{h}^2}-\frac{\delta d\hat{h}_{i,j}^{t+1}dy\left(1-e^{-ct_c d\hat{t}}\right)}{d\hat{h}_{i,j}^{t}d\hat{t}}\right)+$$
$$\hat{p}_{i,j-1}^{t+1}\left(\frac{2\alpha\hat{K}_{xx_{i,j}}d\hat{h}_{i,j}^{t+1}}{d\hat{x}^2}\right)+\hat{p}_{i-1,j}^{t+1}\left(\frac{2\hat{K}_{yy_{i,j}}d\hat{h}_{i,j}^{t+1}}{\left(d\hat{h}_{i,j}^{t+1}\right)^2}\right)+$$
$$\hat{p}_{1,j}^{t+1}\left(\frac{\delta d\hat{h}_{i,j}^{t+1}dy\left(1-e^{-ct_c d\hat{t}}\right)}{d\hat{h}_{i,j}^{t}d\hat{t}}\right) \tag{5.28}$$
$$+\hat{p}_{el_j}^{t+1}\left(\frac{\delta d\hat{h}_{i,j}^{t+1}dy\left(1-e^{-ct_c d\hat{t}}\right)}{d\hat{h}_{i,j}^{t}d\hat{t}}\right)=\frac{d\hat{h}_{i,j}^{t+1}\left(1-e^{-ct_c d\hat{t}}\right)\left(dy-d\hat{h}_{i,j}^{t}\right)}{d\hat{h}_{i,j}^{t}d\hat{t}}$$

In the first and second phase, there is no contact between the tool and the preform. The stress due to contact p_{el} will then be equal to zero. This equation is only valid inside the filled domain ($i \leq indpref$). For the node just beyond the flow front ($i=indpref+1$), the interpolation equation is solved. When the node position is beyond the interpolation line ($i>indpref+1$), the pressure at this node is set equal to zero.

5.1.3.2.4 Calculation of secondary unknowns

To find the secondary unknowns, one has to compute the new element thicknesses from the fluid pressures and the stresses due to the contact tool/preform (only present in the last phase).

According to Figure 5-5, to compute the total thickness, one has to sum all the elements over the thickness of the preform,

$$\hat{h}_j^{t+1} = \sum_{i=1}^{m} d\hat{h}_{i,j}^{t+1} \tag{5.29}$$

The thickness of the gap is then found by subtracting the preform thickness from the initial distance between the mold platens Δ,

$$\hat{H}_{g_j}^{t+1} = \hat{\Delta} - \hat{h}_j^{t+1} \tag{5.30}$$

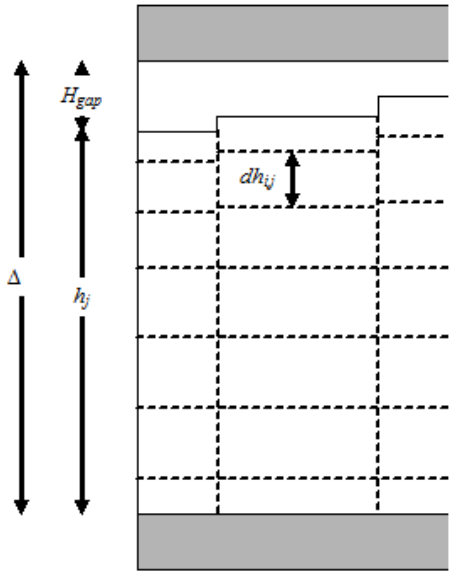

Figure 5-5 Schematic of the thickness chain of dimension

The fiber volume fraction of each element can be found by applying a mass conservation relation to the element,

$$v_{f_{i,j}}^{t+1} = \frac{v_{f0} d\hat{y}}{d\hat{h}_{i,j}^{t+1}} \tag{5.31}$$

Once the fiber fraction of the element is found, its permeability is computed using the Kozeny-Carman relation (3.12),

$$\hat{K}_{xx_{i,j}}^{t+1} = \frac{\left(1 - v_{f_{i,j}}^{t+1}\right)^3}{\left(v_{f_{i,j}}^{t+1}\right)^2} \tag{5.32}$$

$$\hat{K}_{yy_{i,j}}^{t+1} = \frac{\left(1 - v_{f_{i,j}}^{t+1}\right)^3}{\left(v_{f_{i,j}}^{t+1}\right)^2} \tag{5.33}$$

5.1.3.3 Specific equations and solving method related to phase 1

During the first phase, an injection gate is open and the resin is injected into the gap at a certain pressure. Due to the porosity of the preform, some of this fluid will also impregnate the fabric. The injection gate is modeled as a node characterized by a fixed constant pressure.

5.1.3.3.1 Pressure distribution in the gap

The pressure distribution in the gap will be calculated for all the nodes from j=2 to j=n. Indeed, at j=1 the pressure is fixed and equal to the injection pressure. In the gap, we have the following simplifications,

$$\hat{p}_{pref_{1,j}} = \hat{p}_{top} - \hat{p}_{1,j} = 0 \tag{5.34}$$

Involving,

$$\varepsilon_{1,j} = 0 \tag{5.35}$$

Therefore,

$$\frac{\partial \hat{K}_{xx_{1,j}}}{\partial \hat{x}} = 0 \tag{5.36}$$

The discretized form of equation (4.22) becomes,

$$\begin{aligned} \frac{\hat{H}_{g_j}^{t+1} - \hat{H}_{g_j}^{t}}{d\hat{t}} &= \frac{\gamma \hat{K}_{yy_{1,j}}}{d\hat{h}_{1,j}^{t+1}} \left(\hat{p}_{2,j}^{t+1} - \hat{p}_{1,j}^{t+1} \right) + \\ & \frac{3\beta \left(\hat{H}_{g_j}^{t+1} \right)^2}{12 d\hat{x}^2} \left(\hat{H}_{g_{j+1}}^{t+1} - \hat{H}_{g_{j-1}}^{t+1} \right) \left(\hat{p}_{1,j+1}^{t+1} - \hat{p}_{1,j-1}^{t+1} \right) + \\ & \left(\frac{\beta \left(\hat{H}_{g_j}^{t+1} \right)^3}{12 d\hat{x}^2} + \frac{\alpha \hat{K}_{xx_{1,j}}}{d\hat{x}^2} \right) \left(\hat{p}_{1,j+1}^{t+1} - 2\hat{p}_{1,j}^{t+1} + \hat{p}_{1,j-1}^{t+1} \right) \end{aligned} \tag{5.37}$$

On the right end of the gap, Eq. (5.37) becomes,

$$\frac{\hat{H}_{g_j}^{t+1}-\hat{H}_{g_j}^{t}}{d\hat{t}}=\frac{\gamma\hat{K}_{yy_{1,j}}}{d\hat{h}_{1,j}^{t+1}}\left(\hat{p}_{2,j}^{t+1}-\hat{p}_{1,j}^{t+1}\right)+\left(\frac{\beta\left(\hat{H}_{g_j}^{t+1}\right)^3}{12d\hat{x}^2}+\frac{\alpha\hat{K}_{xx_{1,j}}}{d\hat{x}^2}\right)\left(2\hat{p}_{1,j}^{t+1}+2\hat{p}_{1,j-1}^{t+1}\right) \quad (5.38)$$

All the values dependant on *p* in the brackets are secondary unknowns and taken from the previous iteration. At the very first iteration of each time step, the secondary values are taken from the last iteration of the last time step.

5.1.3.3.2 Matrix structure

All the discretized equations are now separated as explained in section 5.1.2.2. Every equation governing the flow and the pressures are arranged as a system of discretized equation in the matrix form in the following order (the numbers in bracket are the number of equations involved in the system, n is the total number of nodes in one line of the mesh),

$$\begin{bmatrix} Flow\ in\ gap(1) \\ Flow\ in\ preform(n) \\ \Pr essures\ in\ gap(n) \\ \Pr essures\ in\ preform\left(n*\left(\max\left(indpref\right)\right)\right) \end{bmatrix}\begin{bmatrix} \hat{L}_g \\ \hat{L}_p \\ \hat{p}_{top} \\ \hat{p} \end{bmatrix}=\begin{bmatrix} \hat{L}_g^{t-1} \\ \hat{L}_p^{t-1} \\ \dfrac{\hat{H}_{g_j}^{t+1}-\hat{H}_{g_j}^{t}}{d\hat{t}} \\ \dfrac{d\hat{h}_{i,j}^{t+1}\left(d\hat{y}-d\hat{h}_{i,j}^{t}\right)\left(1-e^{-ct_c d\hat{t}}\right)}{d\hat{h}_{i,j}^{t}\,d\hat{t}} \end{bmatrix}$$

5.1.3.3.3 Volume computation

The first phase of the process is stopped when the required amount of resin has been introduced in the system (preform+gap). The total volume of resin is computed by summing all the filled volumes over the preform and gap. In order to

simplify the volumes computation, it was approximated that a volume is considered completely filled if its associated node is filled. When the mesh is coarse, the volume computation will not be accurate but the error due to the volume computations will reduce as the mesh gets finer. The volume of each element at a given time step in the preform is computed as follows,

$$\hat{V}_{i,j}^{t+1} = d\hat{x}d\hat{h}_{i,j}^{t+1}\phi_{i,j}^{t+1} \tag{5.39}$$

Similarly, in the gap the volume of each element is computed as follows

$$\hat{V}_{gap_j}^{t+1} = d\hat{x}\hat{H}_{g_j}^{t+1} \tag{5.40}$$

Finally, the total volume of resin in the system is calculated by adding all the filled volumes,

$$\hat{V}ol^{t+1} = \sum_{j=1}^{indgap} \hat{V}_{gap_j}^{t+1} + \sum_{j=1}^{indgap} \sum_{i=1}^{indpref(j)} \hat{V}_{i,j}^{t+1} \tag{5.41}$$

5.1.3.4 Specific equation and solving method related to phase 2

From the first to the second phase, the injection gate is closed and a load is now applied to the fluid in the gap. Therefore, the force will be transferred and distributed to the fluid all over the preform surface. The forced pressure at the injection gate boundary condition will be replaced by an equation that insures the distribution of the load all over the filled region of the gap. The motion of the upper plate is driven by an applied force; an extra equation has to be added into the system of equations in order to compute this motion as a function of the fluid pressure.

5.1.3.4.1 Pressure distribution in the gap

The equation governing the distribution of the pressures in the gap (5.42) is still valid. However, from the first to the second phase, the gap size has been transferred from secondary unknown to primary unknown. Therefore, the coefficient associated the gap thickness at time t+1 has to be present into the *G* matrix. Equation (5.43) is recast as follows

$$
\begin{aligned}
-\frac{\hat{H}_{g_j}^{t}}{d\hat{t}} = &-\frac{\hat{H}_{g_j}^{t+1}}{d\hat{t}} + \frac{\gamma \hat{K}_{yy_{1,j}}}{d\hat{h}_{1,j}^{t+1}}\left(\hat{p}_{2,j}^{t+1} - \hat{p}_{1,j}^{t+1}\right) + \\
&\frac{3\beta\left(\hat{H}_{g_j}^{t+1}\right)^2}{12d\hat{x}^2}\left(\hat{H}_{g_{j+1}}^{t+1} - \hat{H}_{g_{j-1}}^{t+1}\right)\left(\hat{p}_{1,j+1}^{t+1} - \hat{p}_{1,j-1}^{t+1}\right) + \\
&\left(\frac{\beta\left(\hat{H}_{g_j}^{t+1}\right)^3}{12d\hat{x}^2} + \frac{\alpha \hat{K}_{xx_{i,j}}}{d\hat{x}^2}\right)\left(\hat{p}_{1,j+1}^{t+1} - 2\hat{p}_{1,j}^{t+1} + \hat{p}_{1,j-1}^{t+1}\right)
\end{aligned}
\tag{5.44}
$$

As previously explained the injection gate is closed and a force *F* is now applied (see Eq. (5.1)). An extra equation that integrates the fluid pressures over the surface of the preform to calculate the force, F experienced

$$
\hat{F} = \int_0^{\hat{L}_g} \hat{p}_{top}\left(\hat{x}\right) d\hat{x} \tag{5.45}
$$

Where p_{top} represents the pressure values on the surface of the preform. Eq (5.45) can be discretized as follows,

$$
\sum_{1}^{n} \hat{p}_{1,j}^{t+1} d\hat{x} = \hat{F} \tag{5.46}
$$

5.1.3.4.2 Motion of the mold

The motion of the mold is directly dependant on the value Δ representing the distance between the two plates. An extra equation is then introduced in the system

in order to calculate this value Δ. From Figure 5-5, Δ is a function of the total thickness of the preform and the gap size. Summing Eq. (5.19) over the thickness and relating it to the gap size and Δ results in the following relation

$$\hat{\Delta}_j^{t+1} - \hat{H}_{g_j}^{t+1} + \sum_{i=1}^{m} \delta\left(\hat{p}_{1,j}^{t+1} - \hat{p}_{i,j}^{t+1}\right) d\hat{y}\left(1 - e^{-cd\hat{t}}\right) = \sum_{i=1}^{m} d\hat{h}_{i,j}^{t} + \sum_{i=1}^{m}\left(d\hat{y} - d\hat{h}_{i,j}^{t}\right)\left(1 - e^{-ct_c d\hat{t}}\right) \tag{5.47}$$

Note that Δ has to be a constant value over the length of the preform as the mold is composed of two rigid plates translating vertically parallel to each other.

5.1.3.4.3 Matrix structure

The matrix structure associated to the solution for the second phase is shown as follows,

$$\begin{bmatrix} Flow\ in\ gap(1) \\ Flow\ in\ preform(n) \\ Average\ pressures\ on\ top(1) \\ Delta(n) \\ \Pr essures\ in\ gap(n) \\ \Pr essures\ in\ preform\left(n*\left(\max\left(indpref\right)\right)\right) \end{bmatrix} \begin{bmatrix} \hat{L}_{gap} \\ \hat{L}_p \\ \hat{\Delta} \\ \hat{H}_g \\ \hat{p}_{top} \\ \hat{p} \end{bmatrix} = \begin{bmatrix} \hat{L}_{gap}^{t-1} \\ \hat{L}_p^{t-1} \\ \hat{F} \\ \sum_{i=1}^{m} d\hat{h}_{i,j}^{t} + \sum_{i=1}^{m}\left(d\hat{y} - d\hat{h}_{i,j}^{t}\right)\left(1 - e^{-ct_c d\hat{t}}\right) \\ \hat{H}_g^{t-1} \\ \dfrac{d\hat{h}_{i,j}^{t+1}\left(d\hat{y} - d\hat{h}_{i,j}^{t}\right)\left(1 - e^{-ct_c d\hat{t}}\right)}{d\hat{h}_{i,j}^{t} d\hat{t}} \end{bmatrix}$$

5.1.3.5 Specific equation and solving method related to phase 3

During the last phase of CRTM, the upper platen continues to move downward until the final geometry of the part is achieved. This phase can be divided in two different stages: the first stage in which the gap progressively disappears (the

contact surface between tool and preform increases) and the second stage where the tool entirely touches and compacts the preform.

5.1.3.5.1 Pressure distribution on top of the preform

When the gap is still present in the system, the gap equation (5.44) is still valid. When the preform is in contact with the tool, the equation describing the pressures distribution in the preform (Eq.(5.21)) is used and the appropriate boundary conditions are applied. On the top layer of the preform, due to the contact preform/mold. Recalling Eq.(5.34), the stress due to the fluid gradient is equal to zero. The mirror method is used to compute the pressure distribution and Eq.(5.21) becomes,

$$\begin{aligned}
&\hat{p}_{i,j}^{t+1}\left(-\frac{2\alpha\hat{K}_{xx_{i,j}}d\hat{h}_{i,j}^{t+1}}{d\hat{x}^2}-\frac{2\hat{K}_{yy_{i,j}}d\hat{h}_{i,j}^{t+1}}{d\hat{h}^2}\right)+\\
&\hat{p}_{i,j-1}^{t+1}\left(-\frac{\alpha\Delta\hat{K}_{xx}d\hat{h}_{i,j}^{t+1}+\alpha\hat{K}_{xx}\Delta d\hat{h}}{4d\hat{x}^2}+\frac{\alpha\hat{K}_{xx_{i,j}}d\hat{h}_{i,j}^{t+1}}{d\hat{x}^2}\right)+\\
&\hat{p}_{i,j+1}^{t+1}\left(\frac{\alpha\Delta\hat{K}_{xx}d\hat{h}_{i,j}^{t+1}+\alpha\hat{K}_{xx}\Delta d\hat{h}}{4d\hat{x}^2}+\frac{\alpha\hat{K}_{xx_{i,j}}d\hat{h}_{i,j}^{t+1}}{d\hat{x}^2}\right)+\\
&\hat{p}_{i+1,j}^{t+1}\left(\frac{2\hat{K}_{yy_{i,j}}d\hat{h}_{i,j}^{t+1}}{\left(d\hat{h}_{i,j}^{t+1}\right)^2}\right)+\hat{p}_{el_j}^{t+1}\left(\frac{\delta d\hat{h}_{i,j}^{t+1}dy\left(1-e^{-ct_c d\hat{t}}\right)}{d\hat{h}_{i,j}^{t}d\hat{t}}\right)=\\
&\frac{d\hat{h}_{i,j}^{t+1}\left(1-e^{-ct_c d\hat{t}}\right)\left(dy-d\hat{h}_{i,j}^{t}\right)}{d\hat{h}_{i,j}^{t}d\hat{t}}
\end{aligned} \tag{5.48}$$

The pressure on the top right corner is also calculated,

$$\hat{p}_{i,j}^{t+1}\left(-\frac{2\alpha\hat{K}_{xx_{i,j}}d\hat{h}_{i,j}^{t+1}}{d\hat{x}^2}-\frac{2\hat{K}_{yy_{i,j}}d\hat{h}_{i,j}^{t+1}}{d\hat{h}^2}\right)+$$
$$\hat{p}_{i,j-1}^{t+1}\left(\frac{2\alpha\hat{K}_{xx_{i,j}}d\hat{h}_{i,j}^{t+1}}{d\hat{x}^2}\right)+\hat{p}_{i+1,j}^{t+1}\left(\frac{2\hat{K}_{yy_{i,j}}d\hat{h}_{i,j}^{t+1}}{\left(d\hat{h}_{i,j}^{t+1}\right)^2}\right)+ \tag{5.49}$$
$$\hat{p}_{el_j}^{t+1}\left(\frac{\delta d\hat{h}_{i,j}^{t+1}dy\left(1-e^{-ct_c d\hat{t}}\right)}{d\hat{h}_{i,j}^{t}d\hat{t}}\right)=$$
$$\frac{d\hat{h}_{i,j}^{t+1}\left(1-e^{-ct_c d\hat{t}}\right)\left(dy-d\hat{h}_{i,j}^{t}\right)}{d\hat{h}_{i,j}^{t}d\hat{t}}$$

An extra equation forcing the gap to be equal to zero is added.

5.1.3.5.2 Motion of the mold

The mold continues to travel toward the lower platen. When the gap remains, equation (5.47) is still valid. When the tool is in contact with the preform, the stress due to this contact is added into the expression of p_{pref}. and the unknown H_{gap} is replaced by p_{el} in the U vector. Equation (5.47) becomes,

$$\hat{\Delta}_j^{t+1}+\sum_{i=1}^{m}\delta\left(\hat{p}_{1,j}^{t+1}-\hat{p}_{i,j}^{t+1}+\hat{p}_{el_j}\right)d\hat{y}\left(1-e^{-ct_c d\hat{t}}\right)= \tag{5.50}$$
$$\sum_{i=1}^{m}d\hat{h}_{i,j}^{t}+\sum_{i=1}^{m}\left(d\hat{y}-d\hat{h}_{i,j}^{t}\right)\left(1-e^{-ct_c d\hat{t}}\right)$$

5.1.3.5.3 Matrix structure

The matrix structure associated with the solution for the third phase is shown as follows,

$$\begin{bmatrix} Position\ gap(1) \\ Position\ preform(n) \\ Average\ pressures\ top(1) \\ Delta(n) \\ Contact\ gap\ preform(\#\ of\ nodes\ in\ contact) \\ \Pr essures\ gap(n-\#\ of\ nodes\ in\ contact) \\ \Pr essures\ preform(\#\ of\ nodes\ in\ contact + n*(\max(indpref))) \end{bmatrix} \begin{bmatrix} \hat{L}_g \\ \hat{L}_p \\ \hat{\Delta} \\ \hat{H}_g, \hat{p}_{el} \\ \hat{H}_g \\ \hat{p}_{top} \\ \hat{p} \end{bmatrix} = \begin{bmatrix} \hat{L}_g^{t-1} \\ \hat{L}_p^{t-1} \\ \hat{F} \\ \sum_{i=1}^{m} d\hat{h}_{i,j}^{t} + \sum_{i=1}^{m} \left(d\hat{y} - d\hat{h}_{i,j}^{t} \right) \left(1 - e^{-ct_c d\hat{t}} \right) \\ 0 \\ \hat{H}_g^{t-1} \\ \dfrac{d\hat{h}_{i,j}^{t+1} \left(d\hat{y} - d\hat{h}_{i,j}^{t} \right) \left(1 - e^{-ct_c d\hat{t}} \right)}{d\hat{h}_{i,j}^{t}\, d\hat{t}} \end{bmatrix}$$

5.1.4 Solving scheme

At each time step, an iterative solution is computed and compared to the previous iteration. If the relative error between the two iterations is less or equal to a certain value, the time step is validated. The margin of error is described in the following equation,

$$\frac{\left\| U^k - U^{k-1} \right\|}{N} \leq err \tag{5.51}$$

Where $\left\| U^k - U^{k-1} \right\|$ is the Euclidean norm of the difference of the vector grouping all the primary unknowns, N is the length of this vector and err is an arbitrary chosen small value. For all numerical work conducted in this thesis the arbitrary err=1.10^{-5} has been chosen and verified. Only the lines of nodes associated with the filled elements are included in the equation system, this means that N will increase as time progresses as more and more elements are filled. If the results do not converge after a set number of iterations (in our case it was set to a maximum of 20 iterations), it is likely the flow is oscillating between two nodes varying the size of the vector U at each iteration. Hence, the margin of error generated at each iteration will oscillate

around a certain value and the solution will never converge. To overcome this issue, the time step is reduced by a factor of 10,

$$d\hat{t} = \frac{d\hat{t}}{10} \tag{5.52}$$

This decreases the rate of advancement of the flow and prevents the oscillation. The solution algorithm for each phase is described in Figure 5-6,

5.2 Validation

In order to investigate the validity of the simulation, two different verification tools will be used. As a similar modeling approach has not been done previously, it is very difficult to validate it using comparison with previous works. A first check will be conducted using the conservation of the resin through the process and the convergence of the solution for different mesh refinements. Another way to validate the process is to compare our model with previously established models for special cases in which the assumptions in our model are the same than in the finite element control volume numerical method.

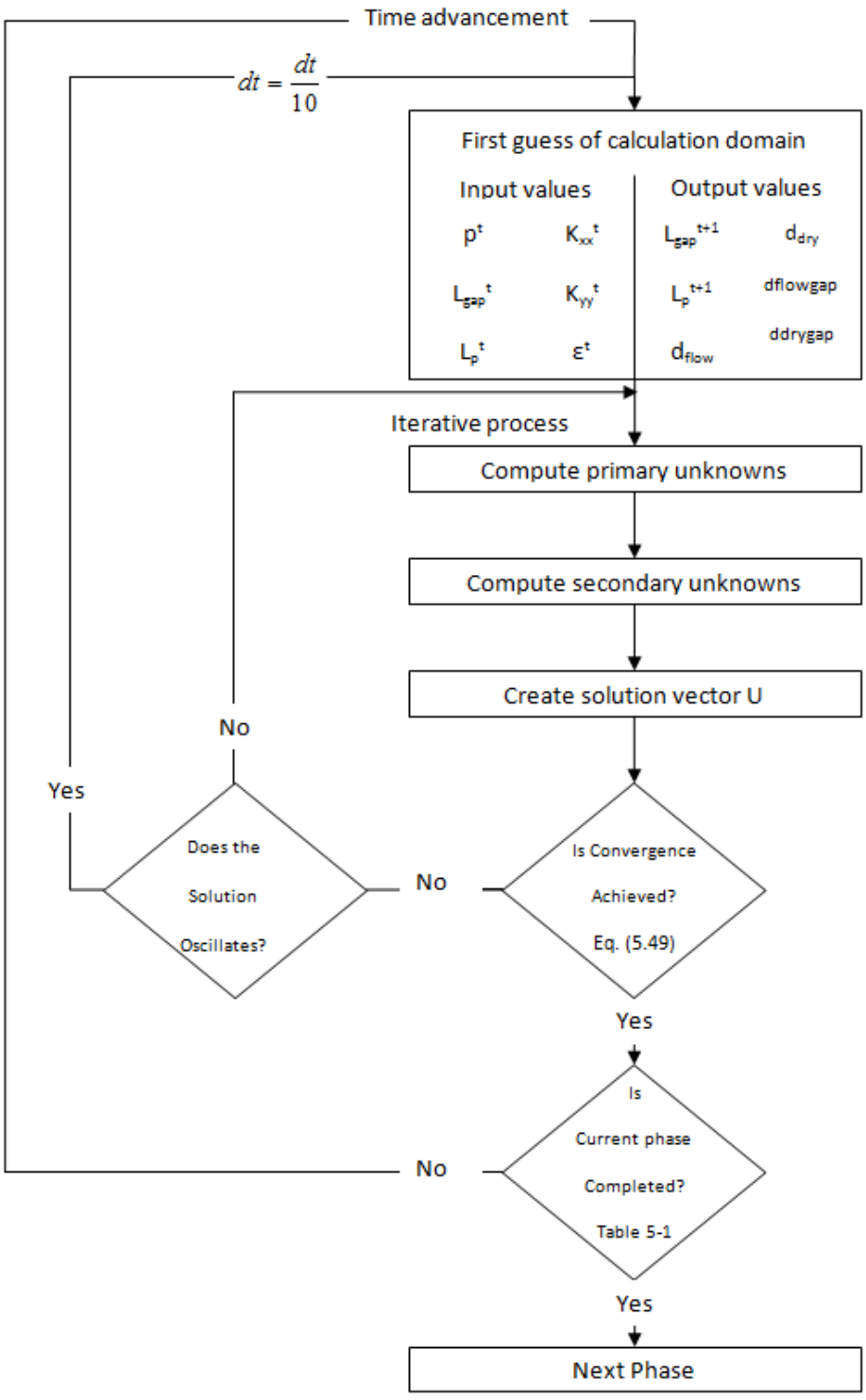

Figure 5-6 Numerical solution algorithm

5.2.1 Convergence of the solution

In order to verify the interpolations and discretization techniques, a convergence study is conducted by varying the number of elements in the mesh.

In finite differences, the error generated is mostly the truncation error due to the accuracy of the derivative discretization. A finer mesh reduces this error and it is a typical solution to increase the simulation accuracy. However, in our case, a more important number of nodes will result in a dramatic increase of matrix size and computation time to inverse it. Therefore, the convergence study will also help to determine the minimal mesh refinement to achieve reasonable accuracy.

The two dimensional model was used for this convergence study. The initial and target geometries are listed in Table 5-2. The element number was gradually increased from 200 to 6050 elements. A further increase could not be achieved due to the memory limitation of the computer. The aspect ratio of the elements was kept at 0.64. This ensures that the high aspect ratio of the element will not negatively influence the results in the study.

Table 5-2 Convergence study initial and final parameters

H_{gap}	H	P_{inj}	P_{ap}	v_{f0}	E	C	h_{target}	k_{oxx}	k_{oyy}
4 mm	1 cm	1.10^5 Pa	7.10^5 Pa	0.2	15.10^5 Pa	1	7 mm	2.10^{-10} m^2	2.10^{-12} m^2

It is expected that the achieved final thickness should converge as the number of elements increases. As the elements count increases, the variation in computed thicknesses decreases and the error related to mesh refinement can be considered as negligible. The final thickness converges to a value smaller than the target thickness. This loss of resin is due to the mesh approximation and can be neglected (error=2.86%).

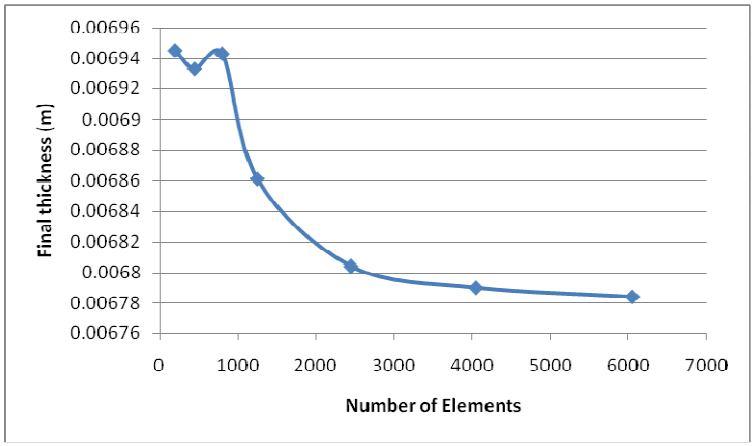

Figure 5-7 Study showing convergence of fiber volume fraction with increasing number of elements

The time required to fill the part is also recorded (Figure 5-8) and, as expected, it shows a convergent behavior similar to the final thickness curve (Figure 5-7).

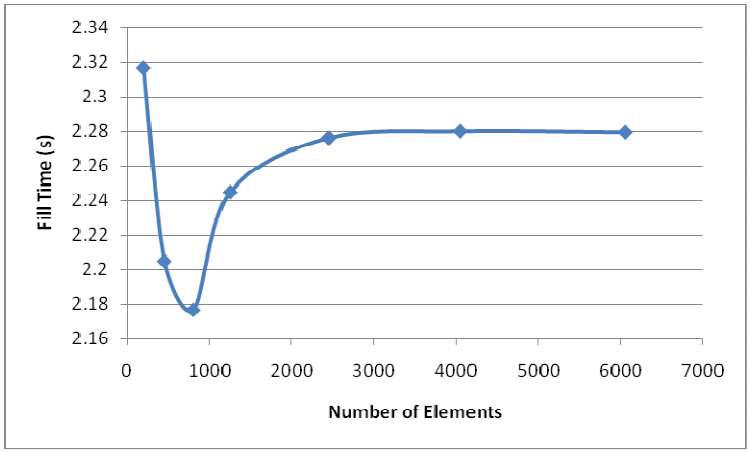

Figure 5-8 Study showing convergence of filling time with increasing number of elements

Due to the very high computing time (6 days) for relatively fine meshes (2450 elements), the followings studies will be conducted using a mesh involving 1250 elements. The results will not be very accurate but the general behavior or the system will be conserved and the computation can be completed in 12 hours.

5.2.2 Resin mass conservation

All the governing equations listed in chapter 4 are based on the principle of mass conservation. A good way to verify if the model is correct is to track the amount of resin present in the system during the process. During phase 1, resin is injected in the system; therefore the focus will be made on the two following phases as the injection is closed at the end of the first phase.

At the end of each time step, the amount of resin is computed using Eq.(5.41) and summing the calculated amount over all the elements. As explained in

section 5.1.3.3, the entire control volume is filled as soon as the associated node is assigned a positive pressure. The size of this control volume, however, will change during time as it gets compressed. As a result, one will notice an abrupt change in resin volume as soon as a node gets filled and a decrease of this volume until another node is filled. The accuracy of the resin computation will then increase as the mesh gets finer. Figure 5-9 and Figure 5-10 show the difference in volume accuracy through the entire CRTM process.

As mentioned in the previous section, the other source of resin loss can be attributed to the approximation in the derivative computation, leading to a flow front progressing slower than the reality.

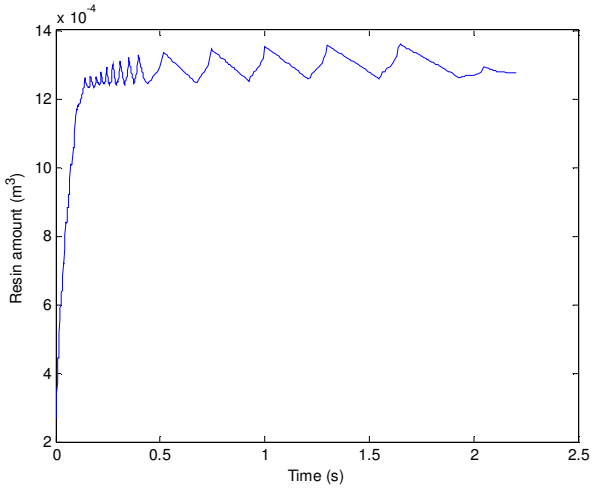

Figure 5-9 Amount of resin present in the system during the process (N_{el}=450 elements)

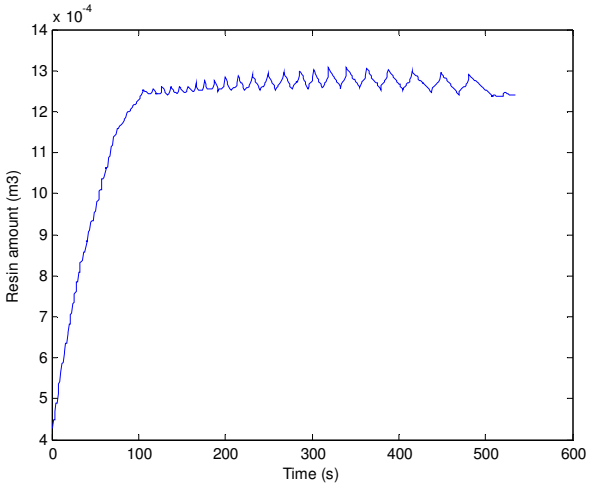

Figure 5-10 Amount of resin present in the system during the process (N_{el}=1250 elements)

5.2.3 Comparison using the software LIMS

LIMS (Liquid Injection Molding Simulation) is a software that simulates the filling stage of RTM and related processes by modeling the flow through a porous media using the finite element method [33, 38]. Previous work modeling the CRTM process has been done using this software [5, 6, 39]. The flow during the first phase of CRTM can be approximated as a VARTM flow using a highly permeable distribution media. This assumption will be used to validate our model by comparing our results to the results generated by LIMS. The fabric will be assumed to be rigid with a gap on top of it. A fixed amount of resin is injected into the system, the filling time and flow front position are recorded when all the resin has penetrated into the system (preform+gap). The input parameters are listed in Table 5-3 and the results are shown in Figure 5-11 and Figure 5-12. The final filling times were t_{fill}=3.18344 s for LIMS versus t_{fill}=3.1740s for our model.

Table 5-3 Input parameters in the first phase validation

H	L	H_{gap}	Vol
1 cm	25 cm	1 mm	0.001 m^3

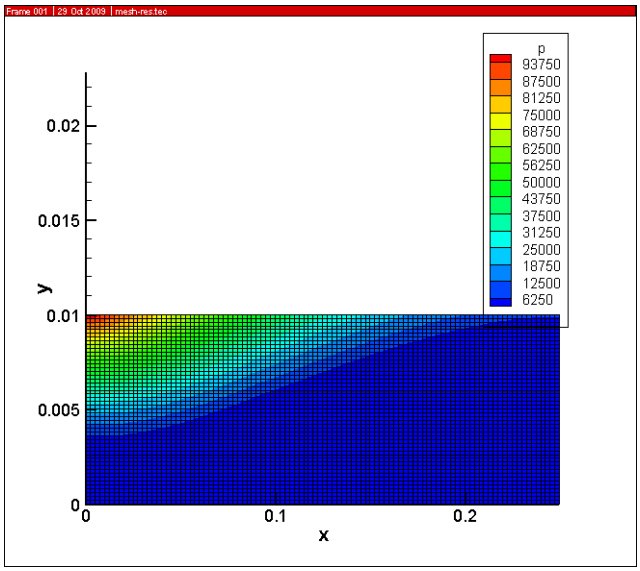

Figure 5-11 Pressure distribution computed with LIMS at the end of the first phase

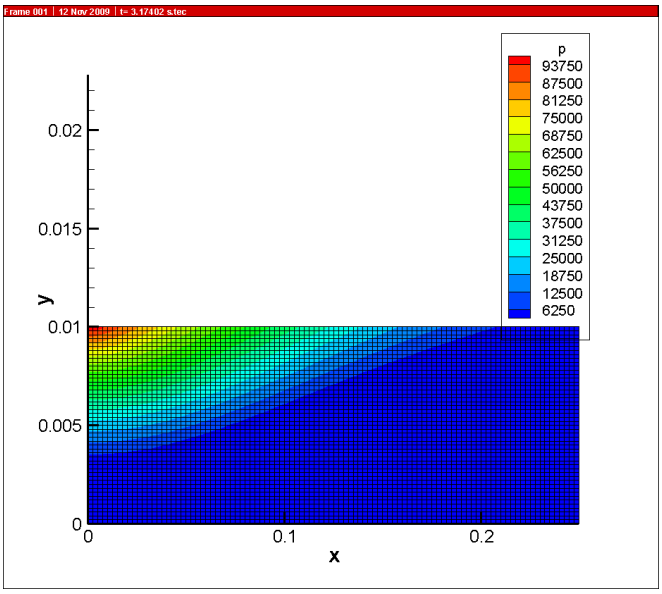

Figure 5-12 Pressure distribution computed with our model at the end of the first phase

5.3 Case study

The filling of an initial part of rectangular shape is modeled. The target dimensions of the part are known. The initial part will be submitted to the CRTM process model, the flow front position as well as the part thickness at the end of each phase will be recorded and is presented in Figure 5-13, Figure 5-14 and Figure 5-15 in their non dimensional form. Table 5-4 lists the input parameters for the model.

Table 5-4 Input parameters for the CRTM model

Preform initial properties	Initial thickness	1 cm
	Initial length	25 cm
	In plane permeability number	2.10^{-10} m^2
	through thickness permeability	2.10^{-12} m^2
	Young's modulus	15.10^5 Pa
	Initial fiber volume fraction	0.2
	Damping factor c	3
Preform final properties	Final thickness	7 mm
Process parameters	Gap size	3 mm
	Injection pressure	1.10^5 Pa
	Compaction force	$1.7.10^5$ N
	Ramping factor R	0.1
	Fluid viscosity	0.3 Pa.s

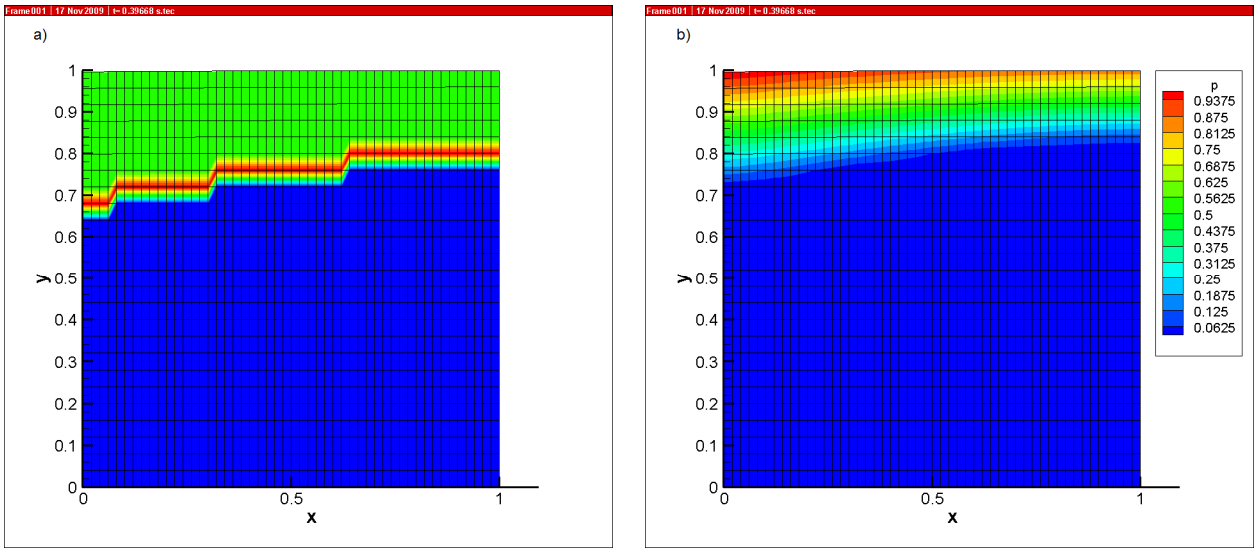

Figure 5-13 Flow front position a) and pressure distribution b) at the end of the first phase

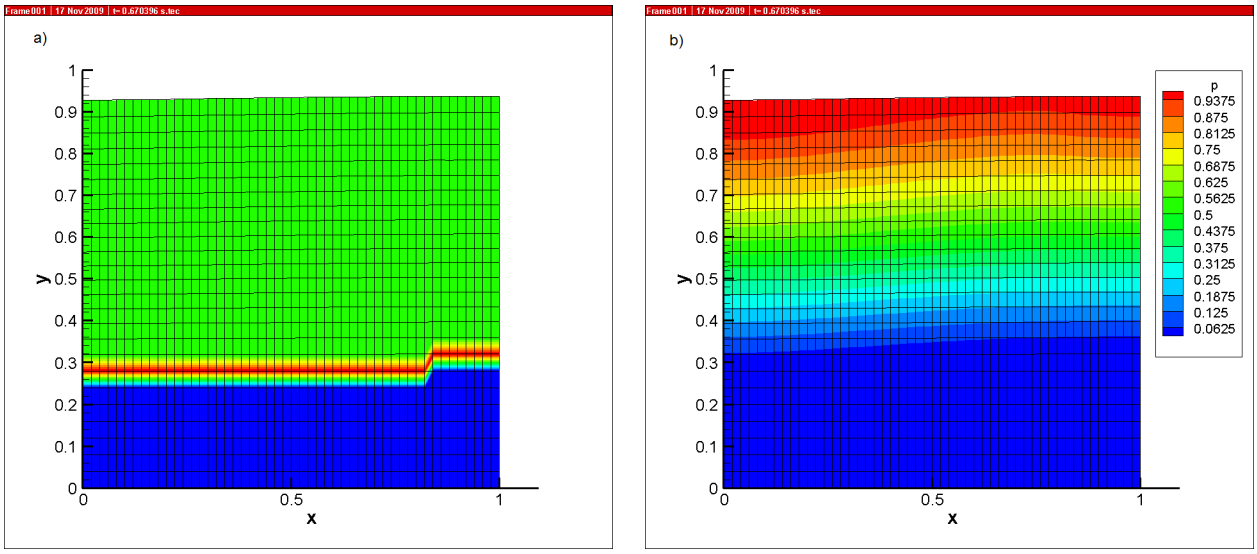

Figure 5-14 Flow front position a) and pressure distribution b) at the end of the second phase

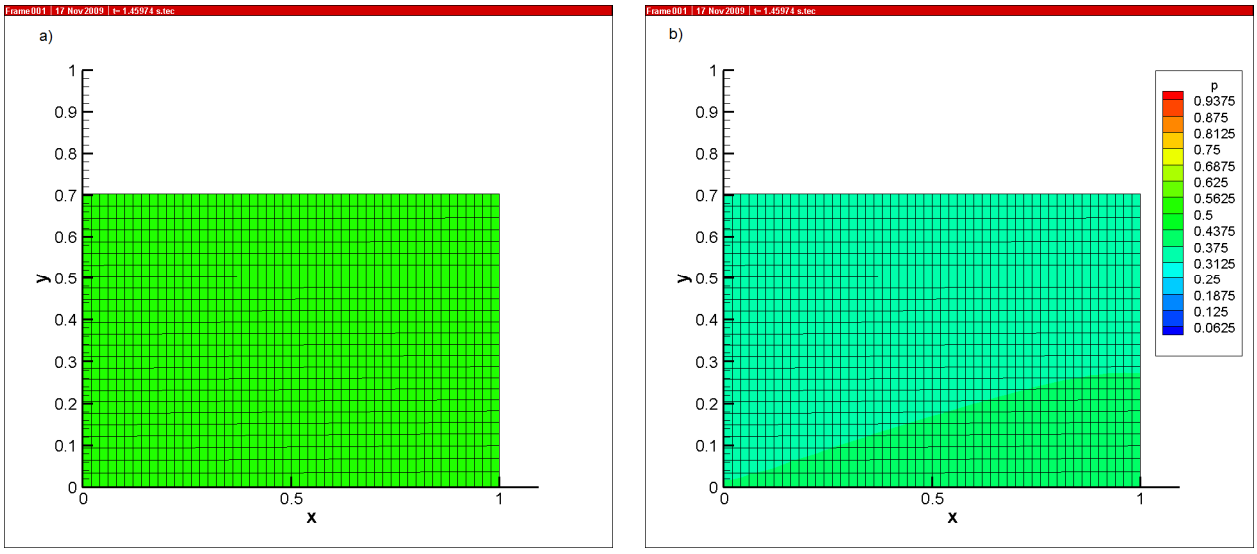

Figure 5-15 Flow front position a) and pressure distribution b) at the end of the third phase

Chapter 6

PARAMETRIC STUDY

The material properties and the final geometry are usually defined by the desired mechanical properties, hence only the influence of the parameters related to the injection pressure (δ_1), the applied force (δ_2) and the initial gap size (γ) is investigated.

6.1 Influence of initial gap size γ

In order to study the influence of γ on the flow front development and the preform compaction, several numerical experiments were conducted in which the value of γ was varied while the other two process parameters were held constant (δ_1=0.0667, δ_2=0.467) and so were the material parameters (v_{f0}=0.2 and α=0.04). However, the non dimensional number relating the gap permeability to the preform permeability β will change as γ changes. The preform permeability being unchanged, the characteristic time will stay the same. Figure 6-1 details the impact of the gap size on the time taken by the process to achieve the final dimension.

The gap size also influences the geometry of the flow. Indeed, the gap permeability is a function of the gap thickness. Therefore, the fluid will flow principally in the gap for large gaps and will flow more and more into the preform as the gap size reduces. Figure 6-2 shows the flow front geometry after the first phase of injection for different γ values.

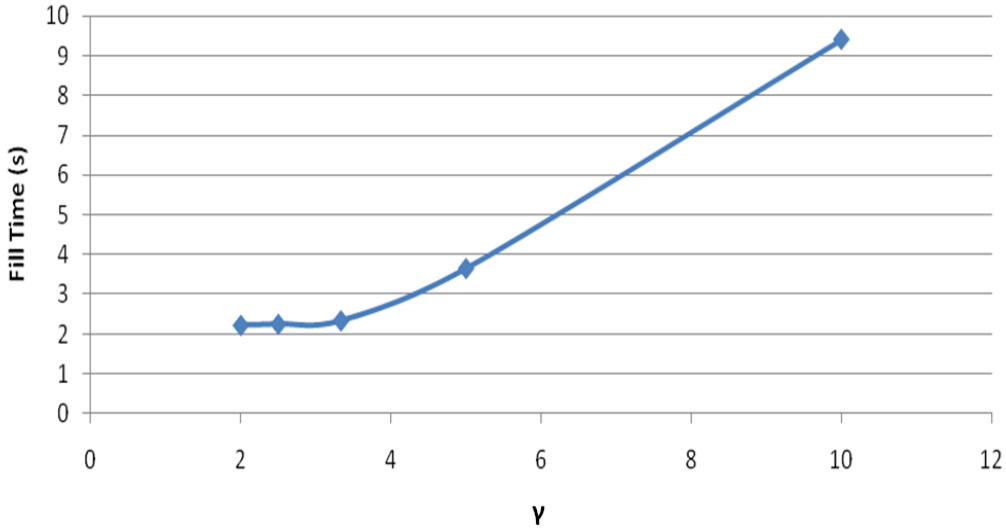

Figure 6-1 Influence of γ on the total filling time (δ_1=0.0667, δ_2=0.467)

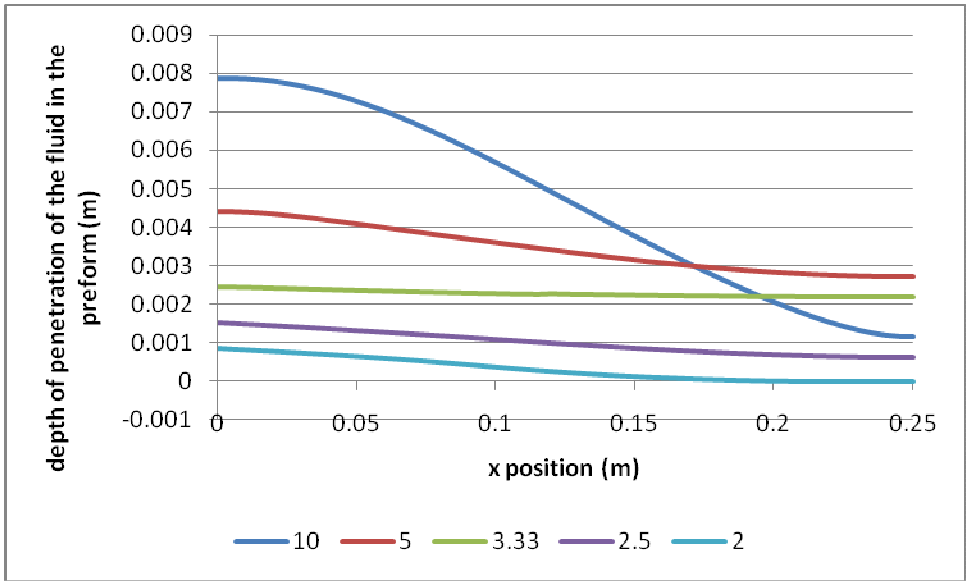

Figure 6-2 Flow front shape after the first phase for different values of γ (δ_1=0.0667), here x=0 is the symmetry plane

The increase of the gap size has a great impact on the filling time only if γ is relatively limited. For larger gap sizes values, an increase of γ will not improve the fill time by much.

To explain the improvement of the process time for limited gap sizes; one has to recall the geometry of the part. Indeed, the part is long and thin (H=1cm, L=25cm). If the gap is large (γ is small), the flow will be close to a one dimensional flow in the y direction (Figure 6-2). The part being thin, the fluid will fill the mold in a relatively short time. When the gap is small (large values of γ), the resin flow will quickly reach the bottom of the mold under the injection gate (Figure 6-2). The resin has then to impregnate the remaining preform region along the length to complete the filling. The time it takes to do this will be much larger than the time it takes to reach the bottom of the mold by travelling only vertically.

For large gap sizes ($\gamma \leq 2.5$), a decrease of γ will not have a great impact on the total filling time. For such large gaps, at the end of the first phase, the gap will not be entirely filled. When the phase two initiates, as the gap closes, the resin will be principally driven in the gap direction. When the resin reaches the end of the gap, a limited amount of resin will have penetrated the preform. This state is not that different than if one started with a smaller gap size. A larger gap size requires one to drive the resin to fill the gap. Hence although phase 1 time is reduced for large gaps, it will increase the phase two time.

6.2 Influence of applied load δ

The applied force or injection pressure has an impact on the compaction of the preform and therefore the permeability of the preform. An increase of the force (or injection pressure) will decrease the fill time; however, the improvement due to this

increase might not be worth the increase in tooling cost. To investigate this impact, the material parameters (v_{f0}=0.2 and α=0.04) were kept constant and γ was chosen such that the gap size provides a reasonable injection time. Figure 6-3 and Figure 6-4 detail the impact of the delta parameter on the fill time of phase one and the entire process respectively.

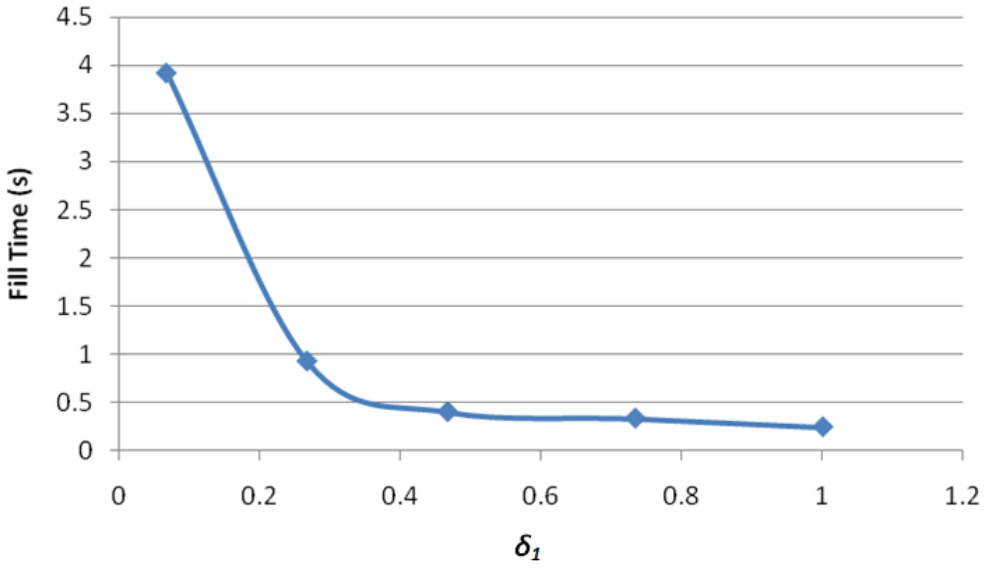

Figure 6-3 Influence of δ_1 on the phase 1 fill time (γ=10)

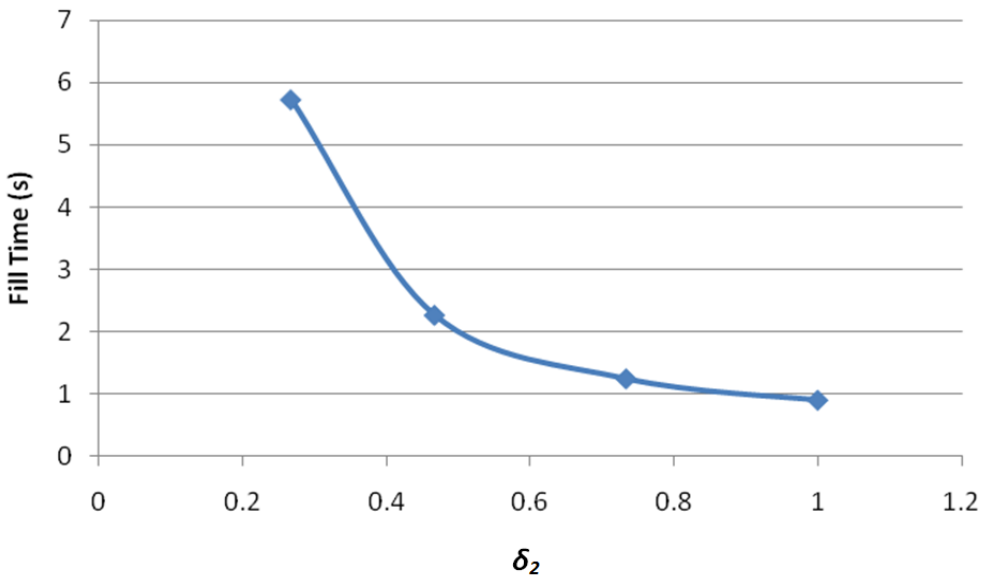

Figure 6-4 Influence of δ_2 on the process fill time (δ_1=0.0667 and γ=2.5)

The resulting overall behavior is the same for the variation of δ_1 and δ_2. The same analysis will be conducted for δ_1 and δ_2; a common number δ will then be used. Initially, increasing δ significantly lowers the fill time. However with further increase, its influence on the fill time improvement decreases relative to the increase of the force or pressure, and consequently, the tooling cost. As explained in section 7.2.5, one can define a $\delta_{optimal}$ value that will quantify the diminishing returns. In this study, $\delta_{optimal}$ can be set as the lowest value of δ satisfying,

$$\frac{t_{phase}\left(2\delta_{optimal}\right)}{t_{phase}\left(\delta_{optimal}\right)} \rangle 2 \qquad (6.1)$$

This means that doubling the applied force/injection pressure will half the phase time.

Chapter 7

LIMITING CASES

As seen in chapter 6, that the process parameters β which measures the influence of gap to through plane permeability and γ which is the ratio of the initial thickness to the initial gap can influence the geometry of the flow development. Higher value of β and lower value of γ will fill the gap preferentially before impregnating the preform. Once the entire gap is filled, the fluid will flow uniformly across the length in the thickness direction. Thus for this limiting case, the flow can be simplified to a unidirectional flow through the thickness of the preform as shown in Figure 7-1.

On the other hand, if the aspect ratio of the part α is significantly small ($\alpha<1.10^{-3}$) or if the ratio of the initial thickness to the initial gap thickness is limited ($\gamma\geq10$), the flow during phase 1 and 2 will be two dimensional until it reaches the bottom of the mold. Then, the flow front will start equalizing along the thickness of the preform and become vertical (Figure 7-2).

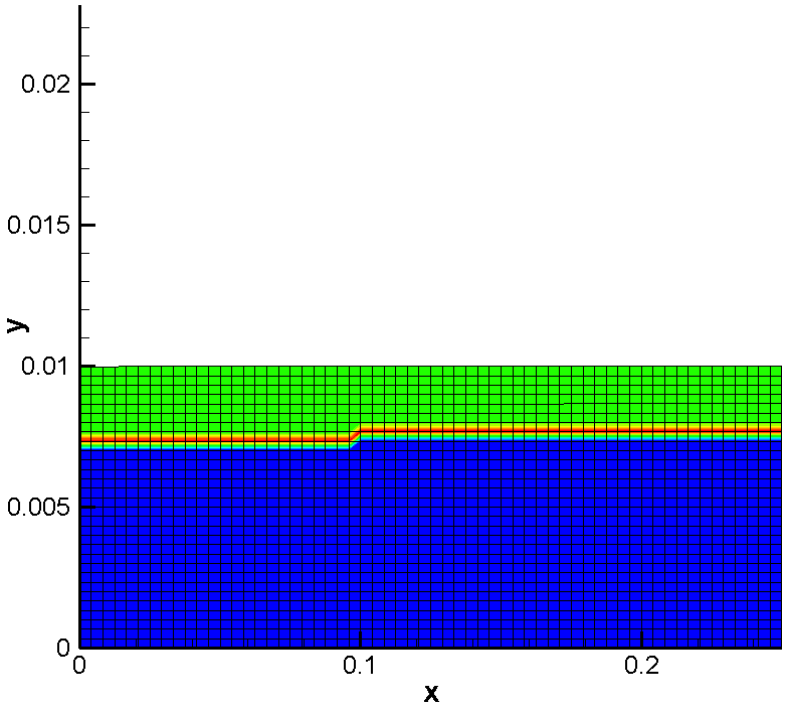

Figure 7-1 Uniform one dimensional flow through the thickness at the end of the first phase (β=*1070, γ=2.5*)

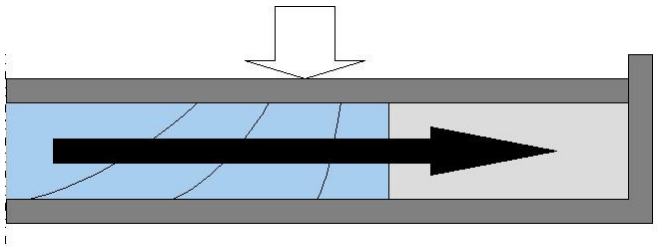

Figure 7-2 Flow front development during phase 1 and 2 for limited values of *β* and *α*

Therefore, the last phase can be approximated as a one dimensional flow front progression in the in plane direction. Figure 7-3 shows the flow development computed by the two dimensional model at the end of the second phase in such case.

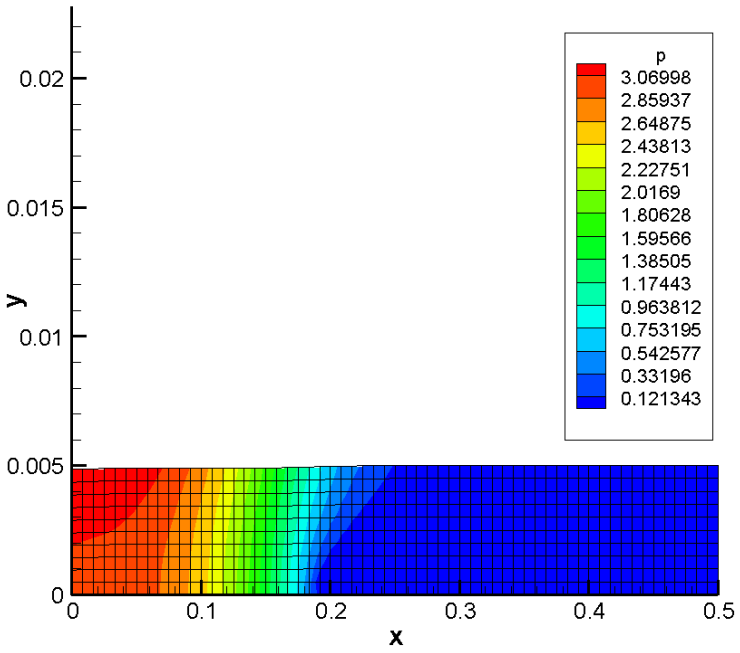

Figure 7-3 Result of the two dimensional flow model for α limited and γ large (H_{gap}=1mm)

In these two limiting cases, the two dimensional flow can be simplified into a dimensional flow. This will simplify the solution and allow one to study the

influence of various parameters. This chapter will detail the solution of these limiting cases, validate them with experiments and conduct parametric studies.

7.1 One dimensional flow through the thickness

7.1.1 Problem statement and assumptions

The goal of this section is to predict the compression of the fabric and the impregnation of the resin into the preform as the mold platen pushes the resin into the preform under a prescribed force (Figure 7-4). A parametric study will identify the role of the applied force on the resin impregnation dynamics.

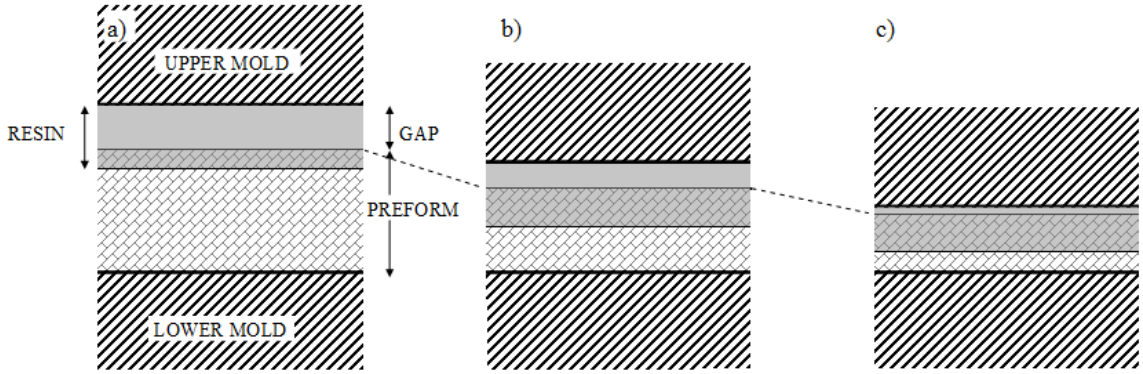

Figure 7-4 Schematic of the second phase of the CRTM process in which the resin impregnates the preform simultaneously compressing the preform even before the mold platen touches the preform.

If the injection pressure during phase one is limited, the pressure compacting the preform is small and one can neglect its deformation during phase one. It is also assumed that the gap permeability is significantly higher than the preform permeability which can be easily justified. This assumption ensures that the entire gap will be filled before any impregnation into the preform provided that the volume of resin injected is at least equal to the gap volume.

In phase one of the process, the gap volume is set slightly smaller than the injected resin volume. Thus, the gap will be fully filled and some resin will also impregnate the preform, as shown in Figure 7-4. We assume that a linear pressure gradient exists in the filled region of the preform before the initiation of phase two as the magnitude of this initial pressure is small and the depth of penetration is only a fraction of initial preform thickness. As the resin covers the entire surface of the preform uniformly in the first phase and the platen moves in the thickness direction when it closes the gap, one can assume a one dimensional flow through the thickness (see Figure 7-5).

Other assumptions are as follows:

(i) Due to the visco-elastic behavior of the dry preform and the high closing speeds involved, the dry part of the preform will be assumed to be stiff [23]. Concerning the lubricated part of the preform, its visco-elasticity will be neglected (fiber volume fraction depends only on the applied stress). This applies only to the preform deformation. The system will still behave visco-elastically as the necessary fluid transfer governed by Darcy law still dampens the deformation.

(ii) We assume that the flow follows Darcy's law and as the Reynold's number

is much less than one, we can assume it to be quasi-steady. This allows us to solve for the steady state problem at each time step.

7.1.2 Governing equations

To model the process, two "separate" equations governing the pressure distribution through the domain and the progression of the flow front need to be formulated.

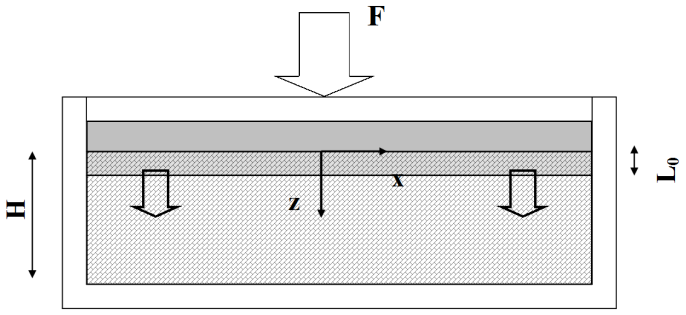

Figure 7-5 Schematic of the initial condition used in the model

The applied force is recast as applied pressure as the area on which the force acts does not change during the compression process. The two parameters are related in the following way,

$$P_{ap} = \frac{F}{A} \tag{7.1}$$

Where P_{ap} is the pressure resulting from the applied force F over the preform area A. The distribution of the fluid pressures p through the domain can be described using Darcy's law [19-21] coupled to the mass conservation due to the compaction of the elements by the fluid. At each time step, one finds

$$\nabla\left(-\frac{\mathbf{K}}{\eta}.\nabla p\right)=-\frac{\partial\varepsilon}{\partial t} \tag{7.2}$$

where ε is the strain. The rigorous evaluation of the deformation field requires a known stress-strain relation in both the wet and the dry fibrous preform. For modest deformations, one can use the infinitesimal strain which yields the following model to describe the rate of change of strain in the preform as

$$\frac{\partial\varepsilon}{\partial t}=-\frac{v_{f0}}{{v_f}^2}\frac{\partial v_f}{\partial t} \tag{7.3}$$

where v_{f0} is the initial fiber volume fraction of the fabric.

The derivative with respect to time of fiber volume fraction in Eq. (7.3) can be rewritten as function of compaction pressure p_{pref} (compaction stress experienced by the fiber preforms) as follows,

$$\frac{\partial v_f}{\partial t}=\frac{\partial v_f}{\partial p_{pref}}\frac{\partial p_{pref}}{\partial t} \tag{7.4}$$

which when substituted in eq. (7.3) results in,

$$\frac{\partial\varepsilon}{\partial t}=-\frac{v_{f0}}{{v_f}^2}\frac{\partial v_f}{\partial p_{pref}}\frac{\partial p_{pref}}{\partial t} \tag{7.5}$$

Similarly one can express the change in permeability of the preform in the through thickness direction, K_{zz} with respect to change in the thickness direction as follows

$$\frac{\partial K_{yy}}{\partial y} = \frac{\partial K_{yy}}{\partial v_f}\frac{\partial v_f}{\partial p_{pref}}\frac{\partial p_{pref}}{\partial y} \tag{7.6}$$

Using Eq. (7.2) to describe the resin flow in the z direction and substituting Eqs. (7.5) and (7.6) in Eq. (7.2) results in the following governing equation,

$$\frac{1}{\eta}\frac{\partial K_{yy}}{\partial v_f}\frac{\partial v_f}{\partial p_{pref}}\frac{\partial p_{pref}}{\partial y}\frac{\partial p}{\partial y} + \frac{K_{yy}}{\eta}\frac{\partial^2 p}{\partial y^2} = -\frac{v_{f0}}{{v_f}^2}\frac{\partial v_f}{\partial p_{pref}}\frac{\partial p_{pref}}{\partial t} \tag{7.7}$$

Equation (7.7) is a general expression which can incorporate any form of constitutive equations to describe (i) the change in fiber volume fraction v_f as a function of p_{pref} and (ii) change in preform permeability K_{yy} as a function of v_f.

To determine the flow front position, the flow front advancement is computed from the averaged velocity provided by the Darcy's law at the flow front position:

$$\frac{\partial L_p}{\partial t} = -\frac{K_{yy}\left(y = L_p\right)}{\eta\,\phi\left(y = L_p\right)}\left(\frac{\partial p}{\partial y}\right)_{y=L_p} \tag{7.8}$$

where L is the depth of penetration of the fluid into the preform relative to the upper surface of the preform and $\phi = (1 - v_f)$ is the porosity of the fabric.

7.1.3 Constitutive equations

One must consider the stress-strain relationship in lubricated preforms to develop the relationship between p_{pref} and v_f. A significant number of compaction models that propose various forms of such a constitutive equation have been published through the years [14, 24, 27, 29, 40-43]. As explained in chapter 3,we selected the following relationship between v_f and the applied stress p_{pref}, [31]

$$v_f = v_{f0} + \left(v_{fmax} - v_{f0}\right)\tanh^n\left(\frac{p_{pref}}{p_{pref\,max}\;m}\right) \tag{7.9}$$

One also needs a constitutive equation to describe the permeability as a function of the fabric fiber volume fraction v_f. One could use one of the many available in the literature, we selected the Kozeny-Carman [19, 20, 34] relation to describe this change. The Kozeny-Carman equation did provide a reasonable fit for the fiber volume fractions of our fabric with *ko*=2.7x10^{-12} m^2.

$$K_{yy}\left(v_f\right) = ko_{yy}\frac{\left(1-v_f\right)^3}{v_f^2} \tag{7.10}$$

7.1.4 Non dimensional analysis

In order to identify the key parameters, a non dimensional analysis was carried out where dependent and independent variables have been selected.

Using the non dimensionalization variables from Table 4-1, one can write the non dimensional form of Eq. (7.7) as,

$$\frac{ko_{yy}\,P_{ap}\,t_c}{v_{f0}\eta\,H^2}\quad v_f^2\left(-\frac{\partial\hat{K}_{yy}}{\partial v_f}\frac{\partial v_f}{\partial\hat{p}_{pref}}\left(\frac{\partial\hat{p}}{\partial\hat{y}}\right)^2+\hat{K}_{yy}\frac{\partial^2\hat{p}}{\partial\hat{y}^2}\right)=\frac{\partial\hat{p}}{\partial\hat{t}}\frac{\partial v_f}{\partial\hat{p}_{pref}} \tag{7.11}$$

One can choose the value of t_c in such a way as to make the value of the coefficient on the left hand side equal to unity, hence

$$t_c = \frac{v_{f0}\eta\,H^2}{ko_{yy}\,P_{ap}} \tag{7.12}$$

Interestingly, this value represents twice the time to fill a cavity between two plates separated by a distance *H*, filled by porous material of permeability *ko* with a fluid of viscosity η when injected with a constant injection pressure equal to P_{ap} with no preform deformation. As such, it provides a reasonable first order estimate of the filling time.

Substituting eq. (7.12) into eq. (7.11) and applying Terzaghi's relation [22] to express the deformation as function of fluid pressure,

$$v_f^2\left(-\hat{K}_{yy}{}'\left(\frac{\partial\hat{p}}{\partial\hat{y}}\right)^2+\frac{\hat{K}_{yy}}{v_f{}'}\frac{\partial^2\hat{p}}{\partial\hat{y}^2}\right)=\frac{\partial\hat{p}}{\partial\hat{t}} \tag{7.13}$$

where,

$$\hat{K}_{yy}{}'=\frac{\partial\hat{K}_{yy}}{\partial v_f}=\frac{-3\left(1-v_f\right)^2 v_f-2\left(1-v_f\right)^3}{v_f{}^3} \tag{7.14}$$

and

$$v_f{}'=\frac{\partial v_f}{\partial\hat{p}_{pref}}=\frac{\left(v_{f\max}-v_{f0}\right)nP_{ap}}{m\,P_{max}}\left(1+\tanh^2\left(\frac{\hat{p}_{pref}\;P_{ap}}{m\,P_{max}}\right)\right)\left(\tanh\left(\frac{\hat{p}_{pref}\;P_{ap}}{m\,P_{max}}\right)\right)^{n-1} \tag{7.15}$$

Using the non dimensionalization variables from Table 4-1 and substituting Eq. (7.12), the dimensionless version of Eq. (7.8) is,

$$\frac{\partial\hat{L}_p}{\partial\hat{t}}=-\frac{\hat{K}_{yy}\left(y=L_p\right)v_{f0}}{\phi\left(y=L_p\right)}\left(\frac{\partial\hat{p}}{\partial\hat{y}}\right)_{y=L_p} \tag{7.16}$$

Where the subscript $y=L_p$ represents the values at flow front position.

7.1.5 Numerical solution

As equation (7.13) is non linear, we will use a finite differences scheme with fluid pressure at each node as our primary variable for the calculations. As the resin progresses in the preform only in the transverse through thickness direction, one can increase the size of the domain at each time step to accommodate this moving resin boundary. The element size will increase as well.

To solve Eqs. (7.13) and (7.16), we use the finite differences scheme. The derivatives are discretized as follows,

$$\frac{\partial \hat{p}}{\partial \hat{y}} = \frac{\hat{p}_{i+1}^{t} - \hat{p}_{i-1}^{t}}{2\Delta \hat{y}} \tag{7.17}$$

$$\frac{\partial^2 \hat{p}}{\partial \hat{y}^2} = \frac{\hat{p}_{i+1}^{t+1} - 2\hat{p}_{i}^{t+1} + \hat{p}_{i-1}^{t+1}}{\Delta \hat{y}^2} \tag{7.18}$$

$$\frac{\partial \hat{p}}{\partial \hat{t}} = \frac{\hat{p}_{i}^{t+1} - \hat{p}_{i}^{t}}{\Delta \hat{t}} \tag{7.19}$$

The previous expressions are substituted into eq. (7.13) and its finite differences form becomes,

$$v_f^2 \left(-\hat{K}_{yy}{}' \left(\frac{\hat{p}_{i+1}^{t} - \hat{p}_{i-1}^{t}}{2\Delta \hat{y}} \right)^2 + \frac{\hat{K}_{zz}}{v_f{}'} \left(\frac{\hat{p}_{i+1}^{t+1} + \hat{p}_{i-1}^{t+1} - 2\,\hat{p}_{i}^{t+1}}{\Delta \hat{y}^2} \right) \right) = \frac{\hat{p}_{i}^{t+1} - \hat{p}_{i}^{t+1}}{\Delta \hat{t}} \tag{7.20}$$

The secondary unknowns (fiber volume fraction, permeability and their derivatives) are computed for $\hat{p}_i^t$. Note that the first order differentiation raised to square is expressed at the time t while the second derivative with respect to y is at t+1. The motivation of this choice is to restrict the solution technique to a semi-implicit scheme. The system should be more stable than the fully explicit one without dealing with the complex formulation and iteration difficulties encountered in fully implicit schemes.

By sorting the pressures at time t and t+1 and by grouping the coefficients by the individual nodal values one finds,

$$\frac{-\hat{K}_{yy}{}' v_f{}'}{4\hat{K}_{yy}} \left(\hat{p}_{i+1}^{t} - \hat{p}_{i-1}^{t} \right)^2 + \beta\, \hat{p}_{i}^{t} = \hat{p}_{i}^{t+1} \left(\beta + 2 \right) - \hat{p}_{i+1}^{t+1} - \hat{p}_{i-1}^{t+1} \tag{7.21}$$

where,

$$\beta = \frac{\Delta \hat{y}^2 v_f{}'}{\hat{K}_{yy} v_f^2\, \Delta \hat{t}} \tag{7.22}$$

This equation is valid for every internal node *i*. At boundaries *i=0* and $i=i_{L,}$ one apply the following boundary conditions,

$$p\left(\hat{y}=0\right)=1 \tag{7.23}$$

$$p\left(\hat{y}=\hat{L}_p\right)=0 \tag{7.24}$$

The best way to solve this system of equations is to express it as a matrix including every space step,

$$\begin{bmatrix} 1 & 0 & \cdots & \cdots & \cdots & \cdots & 0 \\ -1 & \beta_1+2 & -1 & 0 & 0 & \cdots & \vdots \\ 0 & -1 & \beta_2+2 & -1 & 0 & \ddots & \vdots \\ 0 & 0 & \ddots & \ddots & \ddots & \ddots & 0 \\ 0 & \ddots & \ddots & \ddots & \ddots & \ddots & 0 \\ \vdots & \ddots & \ddots & 0 & -1 & \beta_{N-1}+2 & -1 \\ 0 & \cdots & 0 & 0 & 0 & 0 & 1 \end{bmatrix} . \begin{bmatrix} p_0^{t+1} \\ p_1^{t+1} \\ p_2^{t+1} \\ \vdots \\ \vdots \\ p_{N-1}^{t+1} \\ p_N^{t+1} \end{bmatrix} = \begin{bmatrix} 1 \\ \beta_1 p_1^t - \dfrac{\hat{K}_{yy}{}' v_f{}'}{\hat{K}_{yy}} \left(p_2^t - p_0^t\right)^2 \\ \beta_2 p_2^t - \dfrac{\hat{K}_{yy}{}' v_f{}'}{\hat{K}_{yy}} \left(p_3^t - p_1^t\right)^2 \\ \vdots \\ \vdots \\ \beta_{\mathrm{N-1}} p_{\mathrm{N-1}}^t - \dfrac{\hat{K}_{yy}{}' v_f{}'}{\hat{K}_{yy}} \left(p_{\mathrm{N}}^t - p_{\mathrm{N-2}}^t\right)^2 \\ 0 \end{bmatrix} \tag{7.25}$$

For the initial pressure distribution, we assume that some fluid penetration has occurred during phase 1; it involves a linear pressure distribution over its length.

Substituting discretized derivatives into equation (7.16),

$$\frac{\hat{L}_{pi}^{t+1}-\hat{L}_{pi}^t}{\Delta\hat{t}} = \xi \frac{\hat{p}_{i+1}^t-\hat{p}_i^t}{\Delta\hat{y}} \tag{7.26}$$

where,

$$\xi = -\frac{\left(1-v_{fap}\right)^2}{v_{fap}^2}\frac{v_{f0}^3}{\left(1-v_{f0}\right)^3} \tag{7.27}$$

v_{fap} is the fiber volume fraction corresponding to a applied pressure of P_{ap} without any fluid pressure.

To solve the problem, the new domain is determined by solving eq. (7.26) at each time step. The new mesh over this domain is then generated and pressures are solved using equation (7.25).

In order to compute the deformation of the preform occurring during the process, the fluid pressure at each node is converted into a strain. To do so, Terzaghi's relation [22] is used to obtain the stress in the preform p_{pref} from the fluid pressure p. Once p_{pref} is known, the corresponding fiber volume fraction of each element is known by averaging the stresses at the two neighboring nodes and by applying Eq.(7.9). One needs then to integrate with respect to time the infinitesimal stress strain relation given by Eq.(7.3)

$$\varepsilon = \frac{v_{f0}}{v_f} - 1 \tag{7.28}$$

The strain is calculated for each element. The sum of all the infinitesimal deformations over the domain will give the global deformation.

7.1.6 Experimental validation

In order to validate the one dimensional solution, an experimental setup using constant applied pressure was developed. The setup consists of a semi-circular

cavity with a glass wall for the straight edge. This allows us to observe the evolution of the key components (flow front, preform top, molds) during the process of CRTM. A plate of similar shape is used as the top plate. The mold and plate form a male female combination. In this setup, the bottom mold moves vertically up and the upper plate is stationary. The movement of the mold is achieved by placing the mold on an inflatable rubber tube. This rubber tube is attached to a pressure bucket containing water. By injecting the water into the rubber tube at constant pressure, the lower part of the mold is pushed upwards with constant force (Figure 7-6).

Figure 7-6 One dimensional phase two experimental setup

A series of 5 experiments have been conducted with E-glass woven fabric 24 oz as a reference material due to its very small variability in its properties. The initial thickness as well as the initial weight, number of layers and resin viscosity were measured for each experiment. For each experiment, 15 layers of woven E-glass were placed into the mold. The gap was set to 4mm. Dyed corn syrup was injected using a syringe to cover the entire surface and fill the gap. Viscosity of the fluid was about 0.4Pa.s at room temperature. The final filling time and deformation were recorded until the preform came in contact with the tooling. The same parameters have been set as inputs in the simulation. The experimental results and the simulation outputs are compared (filling time (Figure 7-7) and final thickness (Figure 7-8)).

In Figure 7-7, the model errors bars represent the variability in filling time due to the variability of the measured permeability while the experiment errors bars represent the inaccuracy of the contact time determination. Similarly, in Figure 7-8, the model error bars represent the variability in deformation due to the compaction behavior while the experiment error bars represent the inaccuracy of the contact position measurement.

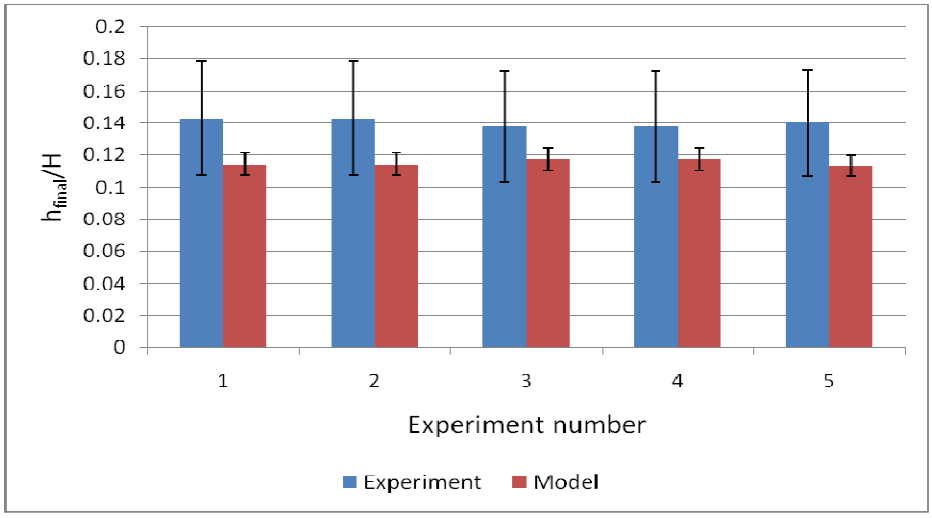

Figure 7-7 Prediction of normalized deformation (H=15mm) and its comparison with experimental results for 24 oz. E-glass fabric

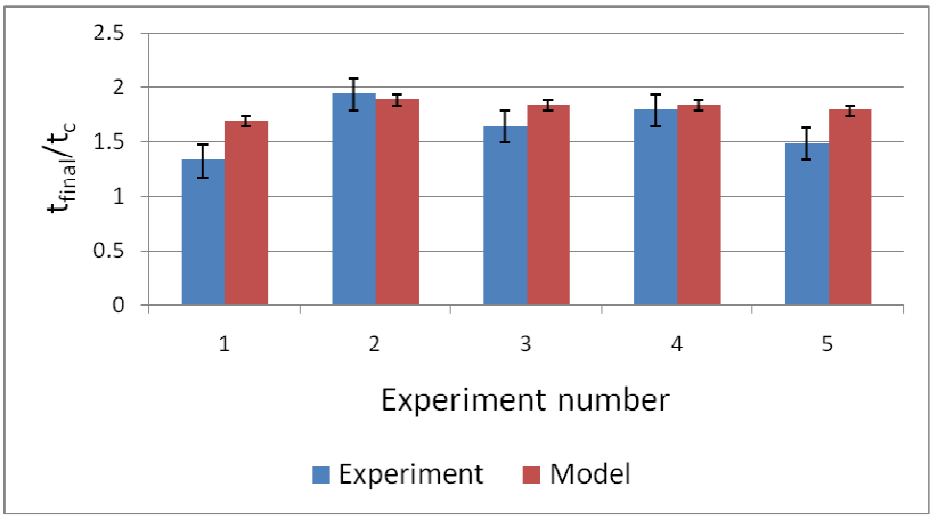

Figure 7-8 Prediction of normalized fill time (t_c=2.014s) and its comparison with experimental results for 24 oz. E-glass fabric

7.1.7 Parametric study

From Eq. (7.13) and (7.16), we can identify four parameters that do influence the flow front and the compaction of the preform. They are listed in Table 7-1 along with their physical significance.

Table 7-1 Non dimensional parameters in the one dimensional limiting phase 2 case

Non-dimensional parameter	Physical Significance
$\Omega = \frac{P_{ap}}{P_{\max}}$	Ratio of available stress and maximum stress to compact the preform
n, m	Parameters describing the preform compaction as a function of fiber volume fraction
v_{f0}	Initial fiber volume fraction
$\Gamma = v_{f\max} - v_{f0}$	Preform compliance

The material properties and the final geometry being usually fixed by the mechanical properties desired, only the influence of Ω will be studied.

In order to identify the role of Ω, several numerical experiments varying the applied force while maintaining the material properties (Γ=0.3, v_{f0}=0.3, n=0.45, m=0.86) constant were carried out. The impact of this variation on the two outputs: deformation and filling time is shown in Figure 7-9 and Figure 7-10. Final thickness, h_{final}, is non dimensionalized with respect to the initial thickness H. The fill time will not be non dimensionalized as the characteristic time is a function of the applied pressure. The gap size is fixed and different amounts of forces are applied on the resin

on top of the preform in order to squeeze it into the material. The filling time and final deformation are recorded when all the resin has penetrated the preform (calculated for v_{ffinal}=0.45 at the end of the process).

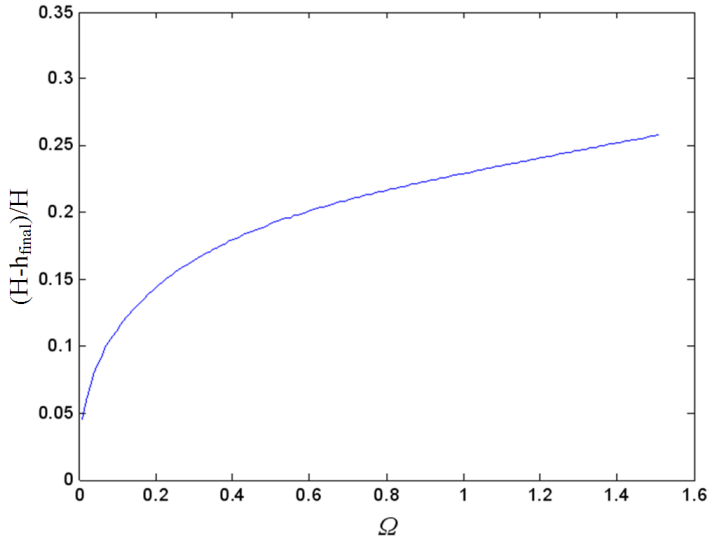

Figure 7-9 Influence of non-dimensional parameter Ω (ratio of available stress to maximum possible) on the final deformation

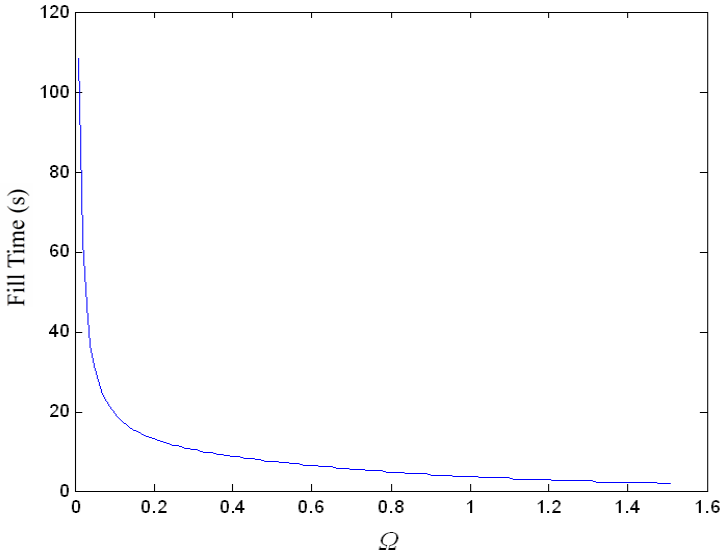

Figure 7-10 Influence of non-dimensional parameter Ω (ratio of available stress to maximum possible) on the filling time

Initially, increasing Ω increases the compaction of the fabric and more importantly significantly lowers the fill time. However with further increase, its influence on the fill time improvement decreases relative to the increase of the force, and consequently, the tooling cost. However, the overall improvement of the process will also depend on the last phase. This behavior has already been observed in CRTM when a prescribed force is applied to a saturated preform and pushes the fluid horizontally [31]. Therefore, there exists an optimal applied force that will improve significantly the process fill time without overly increasing the tooling cost. Beyond this point (which needs to be set on a case-by-case basis) further marginal improvement is still possible but it is not economical.

Another way to decrease the fill time of the second phase is to increase the initial depth of penetration of the fluid. This will decrease the gap size and therefore decrease the amount of resin to squeeze into the preform during phase two. As the final deformation is calculated using the final depth of penetration (which depends on the total volume of resin), the final thickness will be unchanged. However, the gain in time made in phase two will be offset by the increase in time required to complete phase one as one must inject the resin into the preform further in phase one under low pressure.

7.2 In plane one dimensional flow

Assuming that the part is long and thin and the permeability anisotropy is limited, it was demonstrated that the resin could saturate the preform through the thickness near the inlet once the platen comes in contact with the preform as shown in Figure 7-3 [18]. If this occurs, and as the mold platen compresses the preform, the flow front can only advance uniformly in the plane as shown in the schematic in Figure 7-11. The in-plane flow of resin during the compression of the partially impregnated preform is of utmost interest, as the resin moves slowest, or requires highest driving loads. To simplify the analysis, we assume that the part is long and slender ([1-3]) and thus the resin flows in x-direction only (see Figure 7-11). This limits the analysis to one dimensional flow and allows one to identify important process and material parameters. Previous work [13-15] has addressed this situation when the upper platen is compressing the preform with constant speed in which case the preform deformation is explicitly known. In this section, we will address the other important situation in which the preform is compressed under controlled force and

preform deformation needs to be evaluated along with the resin pressure to find the location of the flow front with time.

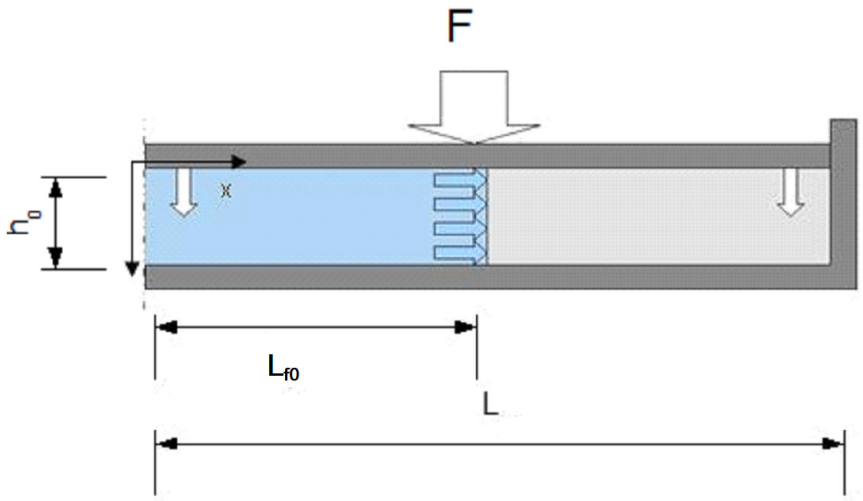

Figure 7-11 One dimensional flow of a partially impregnated preform (Due to symmetry only one half of the mold will be analyzed).

7.2.1 Problem statement and assumptions

In the following, we will simplify and model the final stage of the CRTM phase. The mold is in uniform contact with the preform, the initial location of the uniform flow front across the thickness in the partially impregnated preform is at L_0 as shown in Figure 7-11. As the initial thickness of the fabric when the mold makes contact, H, is known one can calculate the initial fiber volume fraction from the mass

and density of the preform material. The top mold platen under applied constant force compresses the preform which forces the resin to advance in the horizontal direction to saturate the dry preform. Due to the movement of the top platen, the preform thickness decreases, its fiber volume fraction increases and the compressive stress experienced by the fabric increases appropriately. The process is stopped when the flow front reaches the end of the mold and the preform is fully saturated. The resin will not entirely fill the preform if the applied force on the platen is smaller or equal to the force required to compact the fabric to the projected fiber volume fraction. In such situations, the force exhibited by the fabric will halt the movement of the upper mold platen prematurely. Otherwise, the flow front will progress until the entire preform is saturated. The goal of this study is to relate the transient flow progression with the known transient force applied on the mold. Practically, this will be used to determine the force required to ensure that the resin does reach the mold end within a certain amount of time as a function of the fabric compliance and the initial flow front position.

Other assumptions are made as follows:

(i) The mold is in direct contact with the wet and the dry parts of the fabric. When the fabric is compacted, we assume that the compaction behavior is the same in dry or wet preform. A different behavior for the dry part can however be easily added by separating the dry and wet areas during the stress integration.

(ii) We assume that the flow follows Darcy's law and the quasi-steady solution technique applies. This assumption is justified and validated.

7.2.2 Governing equations

The governing equation can be formulated by combining Darcy's law [19-21] in the x direction with the mass conservation due the movement of the upper platen at each time step as follows

$$\frac{K_{xx}\left(v_f\right)}{\eta}\frac{\partial^2 p\left(x,t\right)}{\partial x^2}=\frac{\dot{h}\left(t\right)}{h\left(t\right)} \tag{7.29}$$

where K_{xx} is the fabric permeability in the horizontal x- direction, η is the fluid viscosity, v_f is the fabric fiber volume fraction, p is the fluid pressure and h is the instantaneous preform thickness. Note that here the permeability of the fabric will reduce as the fiber volume fraction increases due to compression and that $\dot{h}(t)$ denotes $\partial h/\partial t$ and is not known *apriori* since the control is asserted over the applied force, not displacement. One can solve for the pressure field at a given instant in time inside the mold by applying the following two boundary conditions at the inlet (symmetry boundary condition) and at the flow front location (which is still unknown) $\left(\frac{\partial p}{\partial x}\right)_{x=0}=0$ and $p\left(x=L_f\left(t\right)\right)=0$

Thus, the resin pressure at a given time can be explicitly calculated as follows

$$p\left(x,t\right)=\frac{\eta}{2.K_{xx}\left(v_f\right)}\frac{\dot{h}\left(t\right)}{h\left(t\right)}\left(x^2-{L_f}^2\left(t\right)\right) \tag{7.30}$$

Now the total force, $F(t)$ per unit width at any time t acting on the platen is equal to the sum of the force exerted by the resin and the fabric according to Terzaghi's relation [22]. Thus,

$$F\left(t\right)=\int_0^{L_f(t)}p\left(x,t\right)dx+\int_0^{L_f(t)}p_{pref}\left(t\right)dx+\int_{L_f(t)}^{L}p_{pref\,dry}\left(t\right)dx \tag{7.31}$$

Here p_{pref} and $p_{pref\,dry}$ denote the compressive stress experienced by the saturated and dry parts of the fabric due to compression and must be separately characterized for each fabric as a function of deformation. To simplify the derivation, both dry and saturated fabrics are set to behave the same way under compression. In this case Equation (7.31) becomes,

$$F(t) = \int_0^{L_f(t)} p(x,t)\,dx + \int_0^{L} p_{pref}(t)\,dx \tag{7.32}$$

Substituting Eq. (7.30) in (7.32) and integrating the first term results in

$$F(t) = -\frac{\eta}{3\mathrm{K}_{xx}(v_f)}\frac{\dot{h}(t)}{h(t)}L_f{}^3(t) + \int_0^{L} p_{pref}(t)\,dx \tag{7.33}$$

Mathematically one can express the mass conservation inside the filled part of the preform as follows

$$\frac{\partial}{\partial t}\left(L_f h\phi\right) = 0 = \dot{L}_f h\phi + L_f h\dot{\phi} + L_f \dot{h}\phi \tag{7.34}$$

where ϕ is the porosity in the mold and the dot represents the derivative with respect to time. The volume conservation of the fabric inside the mold allows us to write the following equation

$$hv_f = h(1-\phi) = constant \tag{7.35}$$

Taking the time derivative and rearranging equation (7.35) allows one to find an expression for $\dot{\phi}$, which is

$$\dot{\phi} = \frac{\dot{h}(1-\phi)}{h} \tag{7.36}$$

Substituting Eq. (7.36) into Eq. (7.34) and rearranging leads to,

$$\frac{-\dot{h}(t)}{h(t)} = \frac{\dot{L}_f(t)}{L_f(t)}\phi(t) = \frac{\dot{L}_f(t)}{L_f(t)}\left(1-v_f(t)\right) \tag{7.37}$$

Rewriting Eq. (7.36) in terms of v_f results in

$$\frac{\partial}{\partial t}\left(v_f(t)h(t)\right) = \dot{v}_f(t)h(t) + v_f(t)\dot{h}(t) = 0 \tag{7.38}$$

which allows one to relate L_f to v_f by substituting equation (7.38) and (7.37) into equation (7.34),

$$\frac{\dot{v}_f}{v_f\left(1-v_f\right)} = \frac{\dot{L}_f}{L_f} \tag{7.39}$$

One can solve the ordinary differential equation (7.39) by applying the following boundary conditions,
$L_f(0) = L_{f_o}$ and $v_f(0) = v_{f_0}$

The result relates the current fiber volume fraction of the preform in the mold to the location of the flow front at that instant in time as follows

$$v_f(t) = \frac{L_f(t)v_{f_0}}{L_0\left(1-v_{f_0}\right) + L_f(t)v_{f_0}} \tag{7.40}$$

By substituting equation (7.40) in Eq. (7.30) and Eq. (7.33), we can eliminate the transient fiber volume fraction from the expressions for the resin pressure and the applied force per unit width at any instant in time

$$p(x,t) = \frac{\eta\left(L_{f_0}\left(1-v_{f_0}\right) + L_f(t)v_{f_0}\right)}{L_{f_0}K_{xx}\left(v_f\right)\left(1-v_{f_0}\right)}\frac{\dot{L}_f(t)}{L_f(t)}\left(L_f{}^2(t) - x^2\right) \tag{7.41}$$

and

$$F(t) = \frac{\eta\left(L_{f_0}\left(1-v_{f_0}\right) + L_f(t)v_{f_0}\right)}{3L_{f_0}K_{xx}\left(v_f\right)\left(1-v_{f_0}\right)}\dot{L}_f(t)L_f{}^2(t) + \int_0^L p_{pref}(t)\,dx \tag{7.42}$$

Equations (7.41) and (7.42) are general expressions which can incorporate any constitutive equation one selects to describe the change in fiber volume fraction v_f, and preform permeability, K_{xx}, as a function of p_{pref}. As explained in chapter 3, the hyperbolic tangent model (3.8) as well as the Kozeny Carman relation (3.12) will be used in this study.

By substituting the constitutive models (Eq. (3.12) for permeability and compaction Eq. (3.8)) in equation (7.42), the final governing equation that predicts the location of the flow front as a function of the applied force F per unit width is

$$\frac{\partial L_f(t)}{\partial t} = \frac{3ko_{xx}L_{f_0}^2\left(1-v_{f0}\right)^2}{v_{f_0}^2\eta L_f^{\,4}(t)}\left(F(t)+Lp_{pref\,max}m\tanh^{-1}\left(\left(\frac{L_f(t)v_{f0}-L_{f_0}v_{f0}\left(1-v_{f0}\right)-L_f(t)v_{f0}^2}{\left(L_{f_0}\left(1-v_{f0}\right)+L_f(t)v_{f0}\right)\left(v_{f\max}-v_{f0}\right)}\right)^{\frac{1}{n}}\right)\right) \quad (7.43)$$

The ODE (7.43) is not separable and an analytic solution for this ordinary differential equation is non-trivial. However, when F is constant, one can separate Eq.(7.43),

$$\int_{t_0}^{t} dt = \int_{L_{f_0}}^{L_f(t)} \frac{\xi^4}{\frac{3ko_{xx}L_{f_0}^2\left(1-v_{f0}\right)^2}{v_{f0}^2\eta}\left(\mathrm{F}+Lp_{pref\,max}m\tanh^{-1}\left(\left(\frac{v_{f0}\left(1-v_{f0}\right)\left(\xi-L_{f_0}\right)}{\left(L_{f_0}\left(1-v_{f0}\right)+\xi v_{f0}\right)\left(v_{fmax}-v_{f0}\right)}\right)^{\frac{1}{n}}\right)\right)} d\xi \quad (7.44)$$

Eq. (7.44) can be numerically integrated and one finds,

$$t_{fill} = t_0 + \int_{L_{f_0}}^{L} \frac{\xi^4}{\frac{3ko_{xx}L_{f_0}^2\left(1-v_{f0}\right)^2}{v_{f0}^2\eta}\left(\mathrm{F}+Lp_{pref\,max}m\tanh^{-1}\left(\left(\frac{v_{f0}\left(1-v_{f0}\right)\left(\xi-L_{f_0}\right)}{\left(L_{f_0}\left(1-v_{f0}\right)+\xi v_{f0}\right)\left(v_{fmax}-v_{f0}\right)}\right)^{\frac{1}{n}}\right)\right)} d\xi \quad (7.45)$$

If F is not constant, we use the finite difference explicit scheme to convert it to an algebraic form

$$\frac{3\Delta t k o_{xx} L_{f_0}^{\ 2}\left(1-v_{f_0}\right)^2}{v_{f_0}^2 \eta L_f^{\ t4}}\cdot$$

$$\left(F^t + Lp_{pref\,max} m \tanh^{-1}\left(\left(\frac{L_f^{\ t} v_{f0} - L_{f_0} v_{f_0}\left(1-v_{f_0}\right) - L_f^{\ t} v_{f_0}^2}{\left(L_{f_0}\left(1-v_{f_0}\right)+L_f^{\ t} v_{f_0}\right)\left(v_{f_{max}}-v_{f_0}\right)}\right)^{\frac{1}{n}}\right)\right) + L_f^{\ t} = L_f^{\ t+1} \tag{7.46}$$

As F is known (and constant in the following studies), Eq. (7.46) provides the value of L at time t+1, as all terms on the left hand side are known at time t and are functions of material parameters which stem from permeability and compaction characterization of the fabric and the viscosity of the resin injected.

To validate the numerical solution, F is set as constant and the two approaches are compared. The results are identical verifying the finite difference code.

Finally, the thickness obtained at the end of the process is calculated by relating the final flow front position with the final fiber volume fraction using equation (7.40). Final fiber volume fraction is then related to final thickness by the following relation,

$$h = \frac{H v_{f0}}{v_{ffinal}} \tag{7.47}$$

7.2.3 Non dimensional Analysis

Non-dimensional analysis was carried out to identify the important process and material parameters that influence the filling process. Independent and dependent variables in Equation (7.43) were non-dimensionalized as follows

$$\hat{L}_f = \frac{L_f}{L} \tag{7.48}$$

$$\hat{F} = \frac{F}{F_{\max}} \tag{7.49}$$

$$\hat{t} = \frac{t}{t_c} \tag{7.50}$$

Where L_{tot} is the total length of the preform to be impregnated, $F_{\max}$ is the maximum force per unit width available and t_c is the characteristic time, specified below. One can recast equation (7.43) in non-dimensional form as follows,

$$\frac{1}{\hat{L}_f^{\,4}(t)} + \frac{Lp_{pref\,max}m}{F_{\max}} \frac{1}{\hat{L}_f^{\,4}(t)} \tanh^{-1}\left(\left(\frac{1}{v_{f\max} - v_{f0}} \left(\frac{1}{1 + \frac{L_{f_0}(1-v_{f0})}{Lv_{f0}} \frac{1}{\hat{L}_f(t)}} \right) - \frac{v_{f0}}{v_{f\max} - v_{f0}} \right)^{\frac{1}{n}} \right) = \frac{\partial \hat{L}_f(t)}{\partial \hat{t}} \tag{7.51}$$

With the characteristic time t_c being equal to

$$t_c = \frac{v_{f0}^{\,2} \eta L^5}{3ko_{xx} L_{f_0}^{\,2} (1 - v_{f0})^2 F_{\max}} \tag{7.52}$$

The number L_{f0}/L is a function of the other non dimensional parameters. They are related in the following way,

$$\frac{L_{f_0}}{L} = \frac{v_{f0}(1 - v_{ffinal})}{1 - v_{f0}} \tag{7.53}$$

Where v_{ffinal} is the fiber volume fraction of the part obtained at the end of the process. Substituting eq. (3.8) in equation (7.53),

$$\frac{L_{f_0}}{L} = \frac{v_{f0}\left(1 - vf_0 - \left(v_{fmax} - v_{f0}\right)\tanh^n\left(\frac{\hat{F}F_{\max}}{Lp_{pref\max}\, m}\right)\right)}{1 - v_{f0}} \tag{7.54}$$

Reformulating eq.(7.51),

$$\frac{1}{\hat{L}_f^{\,4}(t)} + \frac{Lp_{pref\max} m}{F_{\max}} \frac{1}{\hat{L}_f^{\,4}(t)}$$

$$\tanh^{-1}\left(\left(\frac{1}{v_{f\max} - v_{f0}}\left(\frac{1}{1 + \left(1 - v_{f0} - \left(v_{fmax} - v_{f0}\right)\tanh^n\left(\frac{\hat{F}F_{\max}}{Lp_{pref\max}\, m}\right)\right)\frac{1}{\hat{L}_f(t)}}\right) - \frac{v_{f0}}{v_{f\max} - v_{f0}}\right)^{\frac{1}{n}}\right) = \frac{\partial \hat{L}_f(t)}{\partial \hat{t}} \tag{7.55}$$

7.2.4 Experimental validation

Before we non-dimensionalize the equation and conduct a parametric study to quantify the influence of the various parameters on the filling time, we carried out experiments to validate the one dimensional solution formulated above. The intent was to gage the validity of our assumptions in the model and to study the sensitivity of the material parameters on the results. An experimental setup which provides constant applied pressure which translates into constant applied force was developed. The setup consists of a rectangular cavity with a transparent wall on one side. This allows us to observe the evolution of the key components (flow front, preform compression, etc.) during the process. A plate of similar shape as the mold is used as the top plate. The mold and plate form a male female combination. In this setup, the bottom mold moves

vertically up and the upper plate is stationary. The movement of the mold is achieved by placing an air spring under the bottom platen. This air spring is attached to a pressurized air line. The complete setup is showed in Figure 7-12.

A total of 9 experiments were conducted using E-glass woven fabric 24 oz. The initial thickness as well as the initial weight, number of layer and resin viscosity were measured before initiating each experiment. For each experiment, dyed corn syrup was used as the resin and was injected under a pressure of 15 psi. A total of 10 layers of woven E-glass were placed in the mold. The initial length of penetration (L_0) of the resin was varied from 10 to 16 cm. Viscosity of the fluid varied between 0.08 and 0.17 Pa.s depending on the room temperature and the fluid. The applied force was 18kN. The final flow front position was measured along with the final thickness of the part. The same parameters were set as inputs in the simulation and the results were compared in Figure 7-13 and Figure 7-14. The characteristic times for each experiment are listed in Table 7-2.

Figure 7-12 Experimental setup used to compress the partially filled preform under constant applied force

Table 7-2 Characteristic times used in the normalization of the filling times

t_{c1}(s)	t_{c2}(s)	t_{c3}(s)	t_{c4}(s)	t_{c5}(s)	t_{c6}(s)	t_{c7}(s)	t_{c8}(s)	t_{c9}(s)
86.1	122	122	195.6	181.4	181.4	330.6	330.6	294

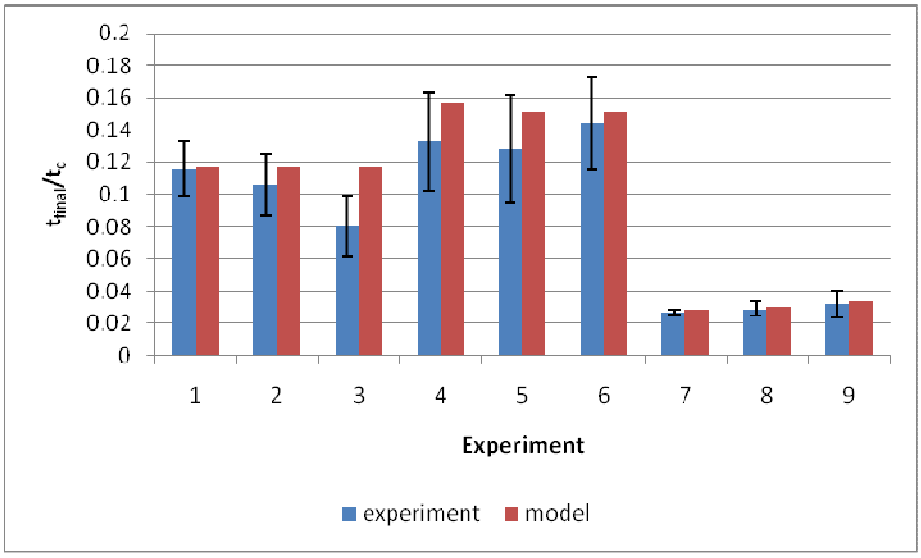

Figure 7-13 Prediction of normalized fill time and its comparison with experimental results for 24 oz. E-glass fabric

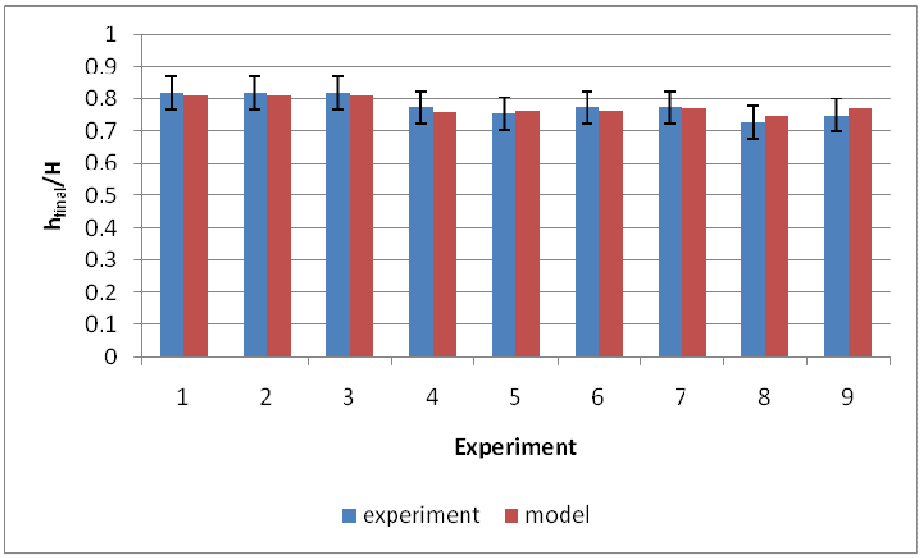

Figure 7-14 Prediction of normalized deformation (H=10mm) and its comparison with experimental results for 24 oz. E-glass fabric

From the above results, one can conclude that the model assumptions are reasonable. However, to reduce the error in the filling time, one will need a more accurate material characterization for permeability description.

7.2.5 Process feasibility and optimization

From equation (7.55) we can identify five parameters that influence the behavior of the flow front. They are listed in Table 7-3 along with their physical explanation.

Table 7-3 Non dimensional parameters in Eq. (7.55)

Non-dimensional parameter	Physical Significance
$\Omega = \frac{Lp_{pref\,max}}{F_{\max}}$	Ratio of maximum compressive force the preform can exert and and the available force to compact the preform
n, m	Shape parameters describing the preform compaction as a function of fiber volume fraction
v_{f0}	Initial fiber volume fraction
$\Gamma = v_{f\max} - v_{f0}$	Compliance of the preform

Equation (7.55) can be rewritten as follows,

$$\frac{1}{\hat{L}_f^{\,4}(t)}+\frac{\Omega \mathrm{m}}{\hat{L}_f^{\,4}(t)}\tanh^{-1}\left(\left(\frac{1}{\Gamma}\left(\frac{1}{1+\left(1-v_{f_0}-\Gamma\tanh^{n}\left(\frac{\hat{F}}{\Omega\, m}\right)\right)\frac{1}{\hat{L}_f(t)}}\right)-\frac{v_{f0}}{\Gamma}\right)^{\frac{1}{n}}\right)=\frac{\partial \hat{L}_f(t)}{\partial \hat{t}} \quad (7.56)$$

The simulation can be run to investigate the effect of the different parameters listed in Table 7-3. The material properties and the final geometry being usually fixed by the mechanical properties needed to reach the objectives, only the influence of Ω will be studied.

The study will focus on: (a) ensuring that the process is feasible and (b) finding the necessary applied force to accomplish the process in reasonable time. In the later case, compromise is sought between cost of slow compaction (low process cycle, reaction inhibitors) and the cost of applying force (press hardware, mold manufacturing).

The increase of the applied pressure has a great impact on the filling time only when Ω is relatively large (force smaller than the one used in conventional LCM processes). From equation (7.43), the applied stress on the platen is used to compact the fabric but also to push the fluid through it. According to Terzaghi's relation, for low Ω values, most of the stress is used to push the fluid while a limited part of it compacts the preform. This is the opposite for larger Ω where most of the force

compacts the preform. This phenomenon can be noticed in Figure 7-15 until Ω reaches $\Omega_{critical}$=7. The $\Omega_{critical}$ corresponds here to the minimal applied force to fill the mold.

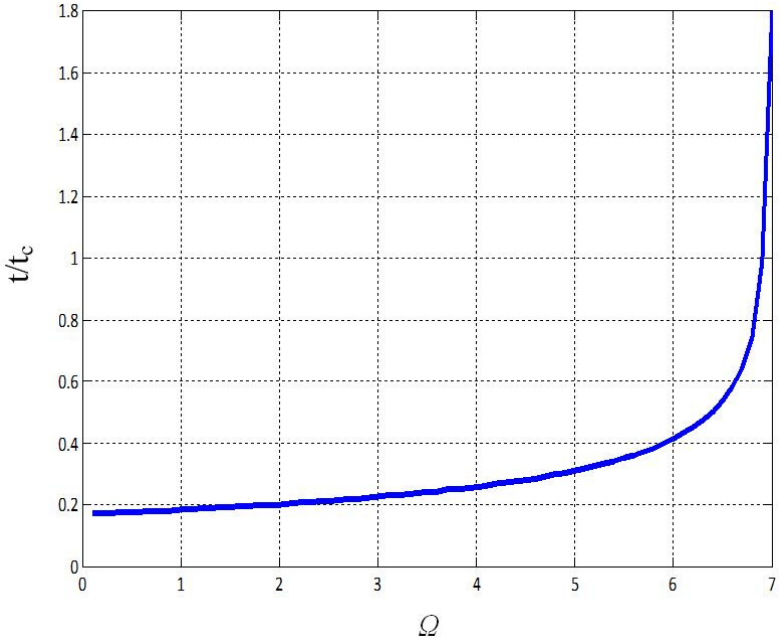

Figure 7-15 Influence of the applied force parameter on the non dimensional filling time (m=0.8, n=0.6, v_{f0}=0.3, Ψ=0.3)

Beyond $\Omega=\Omega_{critical}$, all the available stress cannot compress the fabric to the desirable fiber volume fraction. Consequently, the resin cannot flow forward and fill the mold.

For a given initial flow front position, one needs to apply at least a minimal force ($\Omega_{critical}$) to be able to fill the mold. Nevertheless, the fill time corresponding to Ω being superior or equal to $\Omega_{critical}$ is infinite. Decreasing Ω (increasing force) lowers the fill time. However as one continues to decrease Ω, the fill time improvement is disproportionally small compared to the increase of the force, and consequently, the tooling cost. Hence one can define a $\Omega_{optimal}$ value that will quantify the diminishing returns. In this paper, $\Omega_{optimal}$ is the lowest value of Ω satisfying,

$$\frac{t_{fill}\left(2\Omega_{optimal}\right)}{t_{fill}\left(\Omega_{optimal}\right)} \rangle 2 \tag{7.57}$$

This means that doubling the applied force will half the time to fill the part. Here, t_{fill} is the non dimensional fill time. Contour plots are generated in Figure 7-16 and Figure 7-17 which show the values of $\Omega_{critical}$ and $\Omega_{optimal}$ respectively for each combination of v_{f0} and Γ. v_{f0} and Γ influence the compaction behavior and hence the applied force. If Ω is smaller than the values of Figure 7-17, the benefit from decreasing the fill time does not justify the additional cost in terms of higher force (which is lowering of Ω). The optimal applied force is mostly dependent on the compliance of the preform. The ratio $\Omega_{critical}/\Omega_{optimal}$ is usually the same as the general shape of the curve $t_{fill}=f(\Omega)$ is the same.

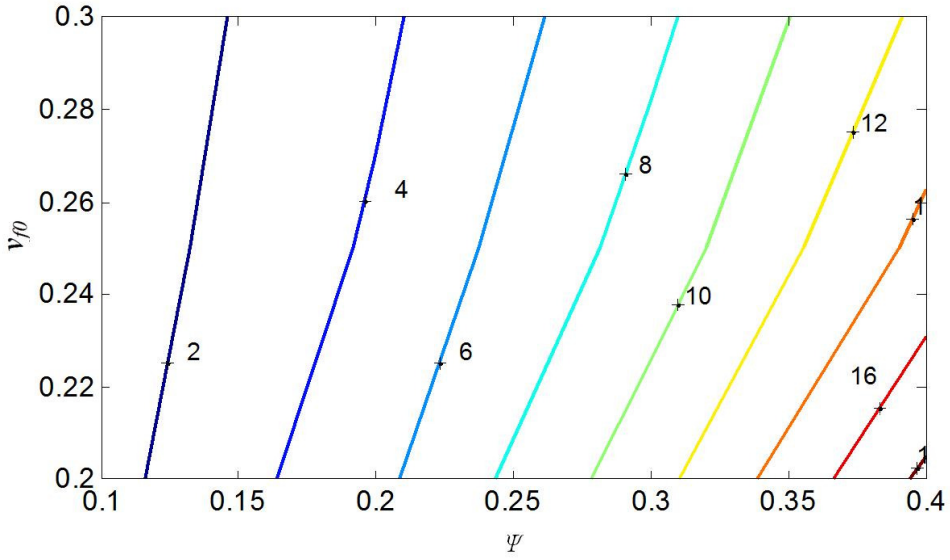

Figure 7-16 Values of $\Omega_{critical}$ for different preform properties

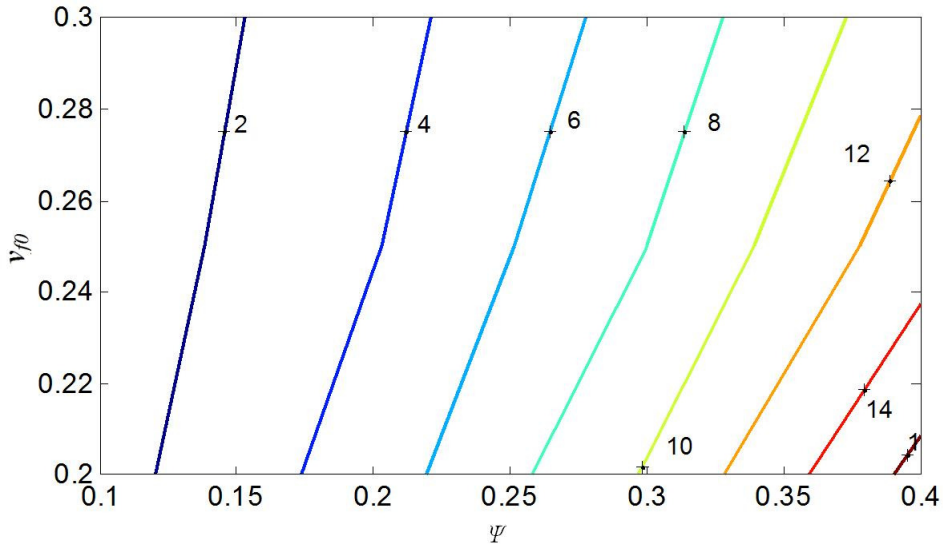

Figure 7-17 Values of $\Omega_{optimal}$ for different preform properties

Through these two limiting cases of this chapter, it has been shown that the flow through the preform can be simplified into a one dimensional problem. The problem being much simpler, the computation time will be significantly reduced (from 12 hours to less than one hour). The two problems have been experimentally verified and the model's predictions are accurate enough considering the variability in material permeability. Through a parametric study, it was shown that the applied force parameter has an important influence on the process; an increase of this force can significantly improve the time to fill for this phase. However, this improvement decreases with a further increase of the compression force.

Chapter 8

CONCLUSION AND FUTURE WORK

In this work, a previous assumption stating that the fabric does not deform under a load created by the fluid pressure was found to be not justifiable when the preform deformation was measured for a simple case. Therefore, a two dimensional flow and compaction model describing the flow during the CRTM process allowing the preform to non uniformly deform through the thickness under fluid pressure has been formulated and numerically implemented. The resin is injected into the gap using constant pressure and the motion of the mold is driven by a prescribed constant force. The problem solution predicts the progression of the flow front as well as the part thickness during the three phases of the process (injection, gap closing and preform compaction). Through a parametric study, an optimal injection pressure, compaction pressure and gap size has been highlighted. It was also demonstrated that the gap size had an important influence on the flow front development and therefore the filling time. Finally, the problem was simplified and two particular one dimensional cases reducing the computation time have been formulated. They highlight the behavior of the flow front progression in the horizontal direction and in the vertical direction when the preform is compacted under prescribed force. Their solution has been validated using experiments and it has been shown that the solutions are accurate enough considering the variability in material properties. Non dimensional parameters have been identified that play an important role in this process.

Additional work needs to be done to further advance the analysis of the process. An experimental validation of the two dimensional model needs to be conducted to verify the assumptions and quantify the improvement compared to the previous CRTM simulations. The two terms damping the application of the force (R) as well as the preform compaction (C) have to be studied to investigate the stability of the system and the impact on the fill time. Moreover, some work remains to make this simulation suitable for more complex part manufacturing. The assumption that the dry preform can be considered as rigid due to its visco-elastic behavior will have to be investigated further. One cannot model this problem as a two dimensional flow if the fluid does not cover the entire surface of the preform. Indeed, if the tool is in direct contact with the dry preform, the process will stop, the preform being considered as undeformable. An adequate compaction model has to be found and implemented into the general model. Furthermore, when the part is long and thin, it has been demonstrated that the gap closes before reaching the end of the mold, dramatically increasing the fill time. To manufacture these parts, a multiple injection gates system can be envisioned to improve the filling time and hence the cycle time of the process. Hence it is also useful to study the flow when the fluid is injected from multiple injection points. Finally, to make the model suitable for complex parts, the governing equations will have to be solved using the finite elements method instead of finite differences.

REFERENCES

1.Seeman, W., Unitary vacuum bag for forming fiber reinforced composite articles. 1991.

2.Seeman, W., Plastic transfer molding apparatus for the production of fiber reinforced plastic structures. 1991.

3.Seeman, W., Plastic transfer molding techniques for the production of fiber reinforced plastic structures. 1990.

4.Kerang H, Jun N., Toth J, Lee LJ, Analysis of an injection/compression liquid composite molding process. Polymer Compos 1998. 19: p. 487-496.

5.Bhat, P., Simulation and validation of mold filling during compression resin transfer molding (CRTM) process, in Mechanical Engineering. 2007, University of Delaware: Newark.

6.Bhat P, S.P., Advani SG, Process analysis of compression resin transfer molding. Composites: Part A 2009. 40: p. 431-441.

7.Kang MK, L.W., Analysis of resin transfer/compression molding process. Polymer compos 1999. 20: p. 293-304.

8.Pillai KM, T.I.C., Phelan Jr FR, Numerical simulation of injection/compression liquid composite molding. Part 2. Preform compression. . Composites: Part A, 2001. 32(2): p. 207-220.

9.Pillai KM, T.C., Phelan FR, Numerical simulation of injection/compression liquid composite molding. Part 1. Mesh generation. Composites: Part A, 2000. 31: p. 87–94.

10.Shojaei, A., Numerical simulation of three-dimensional flow and analysis of filling process in compression resin transfer moulding. Composites part A, 2006. 37: p. 1434-50.

11.Shojaei, A., A numerical study of filling process through multilayer performs in resin injection/compression molding. Compos Sci Technol 2006. 66: p. 1546–57.

12.Shojaei, A., A numerical study of filling process through multilayer preforms in resin injection/compression molding. Composites Science and Technology, 2006. 66: p. 1546–1557.

13.Buntain MJ, B.S., Modeling forces generated within rigid liquid composite molding tools. Part A: Experimental study. Composites: Part A, 2007. 38: p. 1729–1741.

14.Buntain MJ, B.S., Modeling forces generated within rigid liquid composite molding tools. Part B: Numerical analysis. Composites: Part A, 2007. 38: p. 1742–1754.

15.Pham XT, T.F., Gauvin R, Simulation of compression resin transfer molding with displacement control. J Reinf Plast Compos 1998. 17: p. 1525-56.

16.Bickerton S, A.M., Modeling and evaluation of the filling stage of injection/compression moulding. Compos Sci Technol, 2003. 63: p. 1359-75.

17.Bickerton S, B.M., Somashekar AA, The viscoelastic compression behaviour of liquid composite molding preforms. Composites Part A 2003. 34: p. 431-44.

18.Simacek P, A.S., Iobst SA, Modeling flow in compression resin transfer molding for manufacturing of complex lightweight high-performance automotive parts. J Compos Mater, 2008. 42: p. 2523–45.

19.Advani SG, S.E., Process modeling in composites manufacturing. 2002, New York: Marcel Dekker.

20.Astroem B, P.R., Advani S On flow through aligned fiber beds and its application to composites processing. J Compos Mater, 1992. 26(9): p. 1351-73.

21.Darcy, H., Les fontaines publiques de le ville de Dijon. Paris:Dalmont, 1856.

22.Terzaghi K, P.R., Soil Mechanics in Engineering Practice. 2 ed. 1967, New York: John Wiley & Sons.

23.Robitaille FR, G.R., Compaction of Textile Reinforcements for Composites Manufacturing. I: Review of Experimental Results. Polym Comp, 1998. 19: p. 198-216.

24.Robitaille FR, G.R., Compaction of Textile Reinforcements for Composites Manufacturing. II: Compaction and Relaxation of Dry and H,O-Saturated Woven Reinforcements. Polym Comp, 1998. 19: p. 543-57.

25.Trevino L, R.K., Young WB, Analysis of resin injection molding in molds with replaced fiber mats I: Permeability and compressibility measurements. Polym Comp, 1991. 12: p. 20-29.

26.Rudd CD, B.L., Morris DJ, Compaction and in-plane permeability characteristics of quasi-unidirectional and continuous random reinforcements. Mater Sci Tech, 1996. 12: p. 436-44.

27.Comas-Cardona S, L.g.P., Binetruy C, Krawczak P, Unidirectional compression of fiber reinforcements. Part 1: A non linear elastic-plastic behaviour. Composites science and technology, 2007. 67: p. 507-514.

28.Comas-Cardona S, B.C., Krawczak P, Unidirectional compression of fibre reinforcements. Part 2: A continuous permeability tensor measurement. Composites Science and Technology, 2007. 67: p. 638–645.

29.Kelly PA, U.R., Bickerton S, Viscoelastic response of dry and wet fibrous materials during infusion processes. Composites Part A 2006. 37: p. 868-873.

30.Gokce A, C.M., Advani S.G., Walsh S.M., Permeability estimation algorithm to simultaneously characterize the distribution media and the fabric preform in vacuum assisted resin transfer molding process. Composites Science and Technology, 2005. 65: p. 2129–2139.

31.Simacek P, A.S., Binetruy C, LIMS, A Comprehensive tool. Proceedings of JEC-Composites, 2004: p. 146-146.

32.Merotte J, Simacek P., Advani S.G., Resin Flow Analysis with Fiber Preform Deformation in through thickness direction during Compression Resin Transfer Molding. Submiteted to Composites Part A, 2009.

33.Carman, P., Trans. Inst. Chem. Eng., 1937. 15: p. 150-166.

34.Fletcher, C.A.J., Computational techniques for fluid dynamics 2ed. Springer Series in Computational Physics. Vol. 1. 2006: Springer-Verlag.

35.Fletcher, C.A.J., Computational techniques for fluid dynamics. 2 ed. Springer Series in Computational Physics. Vol. 2. 2006: Springer-Verlag.

36.D'Acunto, B., Computational methods for PDE in mechanics. Advances in mathematics for applied science, Vol. 67. 2004, Singapore: World scientific.

37.Simacek P, A.S., Desirable Features in Mold Filling Simulations for Liquid Composite Molding Processes. Polymer compos, 2004. 25(4): p. 355-367.

38.Deleglise M, B.C., Krawczak P, Simulation of LCM processes involving induced or forced deformations. Composites Part A, 2006. 37: p. 874-880.

39.Gutowski TG, K.J., Boucher D, Experiment in composite consolidation: fiber deformation. Antec, 1986: p. 1316-20.

40.Batch GL, C.S., Macoskow, Compaction of Fiber Reinforcements. Polym. Comp., 2002. 23(3): p. 307-18.

41.Lekakou C, J.M., Bader MG, Compressibility and flow permeability of two-dimensional woven reinforcements in the processing of composites. Polym Comp 1996. 17(5): p. 666–72.

42.Saunders RA, L.C., Bader MG Compression in the processing of polymer composites 2. Modelling of the viscoelastic compression of resin-impregnated fibre networks. Composites science and technology, 1999. 59: p. 1483-94.

43.Merotte J, Simacek P., Advani SG, Flow Analysis during Compression of Partially Impregnated Fiber Preform under Controlled Force. Submitted to Composite Science and technology, 2009.

Appendix A

P4 FABRIC CHARACTERIZATION

The model describing the unidirectional flow through the thickness of the preform has also been validated using the P4 fabric. The P4 fabric is manufactured by Owens Corning Fiber Glass Co. and the term P4 stands for Programmable Powdered Preforming Process. It was introduced for automotive industry to form net shapes of a composite skeleton at a very high rate of production. The P4 material is made of chopped glass fibers binded with a small amount of melted thermoplastic powder. The fibers are uniformly distributed using a programmable robot and the whole preform is vacuumed into a mold that will give the final shape. We obtained this fabric from Oak Ridge National Laboratories [5, 6]. Figure A-1 shows the material surface.

Figure A-1 P4 preform

To conduct the validation of the unidirectional flow through the thickness of the preform, one has to characterize the compaction behavior as well as the permeability of the preform.

A.1 Compaction behavior

The response of the fabric to an applied stress has been measured using the experimental setup detailed in chapter 3 by Mr. Timo Gebauer from the Center for Composite Materials [5]. The experiment was repeated 16 times. The compaction response of the fabric is shown in Figure A-2,

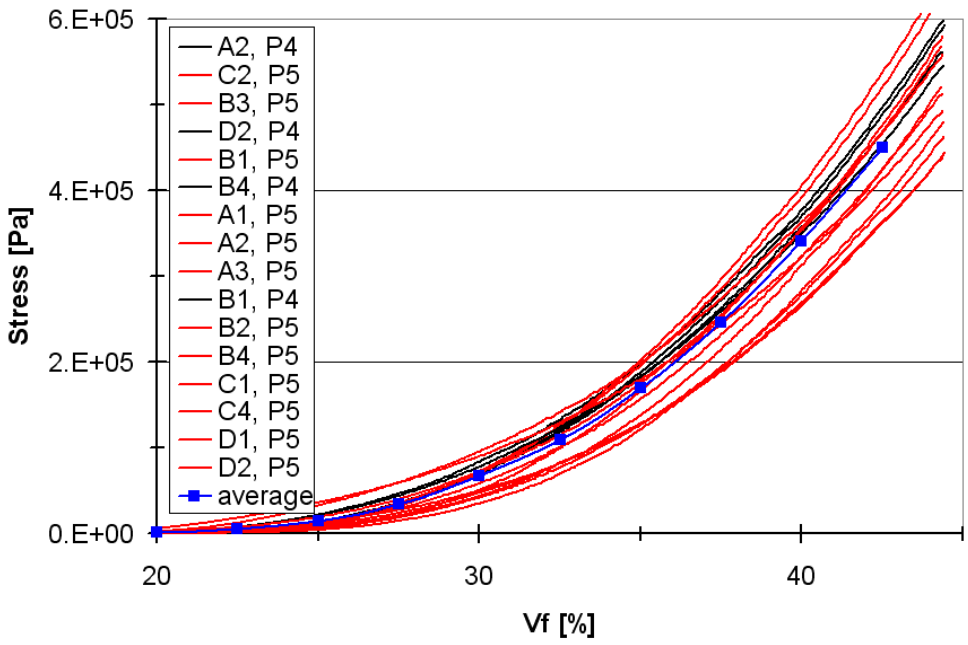

Figure A-2 Compaction behavior of the lubricated P4 fabric

The letters A,B,C,D represent the location of the sample on a panel of P4 fabric while the letter P followed by a number represents the fabric panel. The P4 fabric reveals an important variability in properties (up to 5% of fiber volume fraction variation for a given compressive stress). This important variability can be due to the distribution of the chopped fibers and binder over the panel. The model will have to take into account these changes in behavior. Table A-1 shows the values of the compaction parameters used in the model (3.8),

Table A-1 Compaction model parameters for compaction model of P4 357D-3120

P4 fabric 305D-3120			
	Low compliance	Average	High compliance
n	66	50	40
m	76	80	97
v_{fmax}	0.43	0.43	0.43
v_{f0}	0.2	0.2	0.2
$p_{prefmax}$	4.5.105 Pa	4.5.105 Pa	4.5.105 Pa

A.2 Permeability

The permeability of the P4 fabric has been measured using the experimental setup described in section 3.2. Due to the limited amount of fabric available, the experiment has been realized only one time for five different fiber volume fractions. The permeability as a function of fiber volume fraction is shown in Figure A-3.

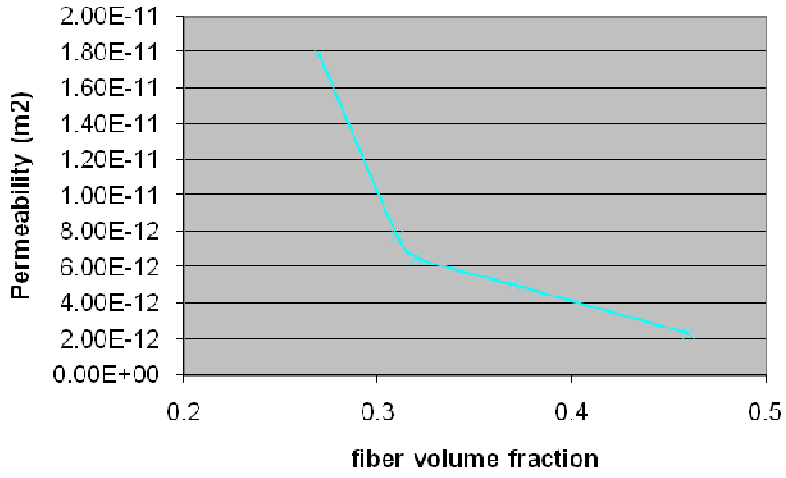

Figure A-3 permeability values of P4 fabric (357D-3120) at different fiber volume fractions

A curve fit with the Kozeny-Carman relation (3.12) has revealed a value of ko_{yy}=2.73.10^{-12} m^2. According to the previous measurement, the limited number of experiments and the usual variability in permeability measurement for a single material, two extreme permeabilities have been introduced. They will be 25% higher or lower than the measured permeability. Table A-2 shows the values of the permeability parameter used in the validation.

Table A-2 Permeability parameter P4 357D-3120

P4 fabric 305D-3120			
	Low permeability	Measured permeability	High permeability
ko_{yy} (m^2)	2.15.10-12	2.87.10-12	3.59.10-1240

Appendix B

VALIDATION OF THE UNIDIRECTIONAL FLOW THROUGH THE THICKNESS MODEL USING P4 FABRIC

The experimental setup used to validate the model with P4 fabric is detailed in section 7.1.6. 10 experiments were conducted, the initial thickness as well as the initial weight, number of layers and resin viscosity were measured for each experiment. For each experiment, 3 layers of P4 fabric were placed into the mold. The final filling time as well as the deformation at the end of phase two were recorded. The same parameters have been set as inputs in the simulation (fluid viscosity, gap size, initial fluid penetration). The experimental results and the simulation outputs are compared for filling time (Figure B-1) and for the final thickness (Figure B-2).

In the graphs, the errors bars for the experiment correspond to a reading error of about half a millimeter above and half a millimeter below the read value. This is due to the fact that we only look at a specific and relatively small location of the entire setup. The error bars in the simulation are due to the variability in permeability (Figure B-1) and compaction behavior (Figure B-2).

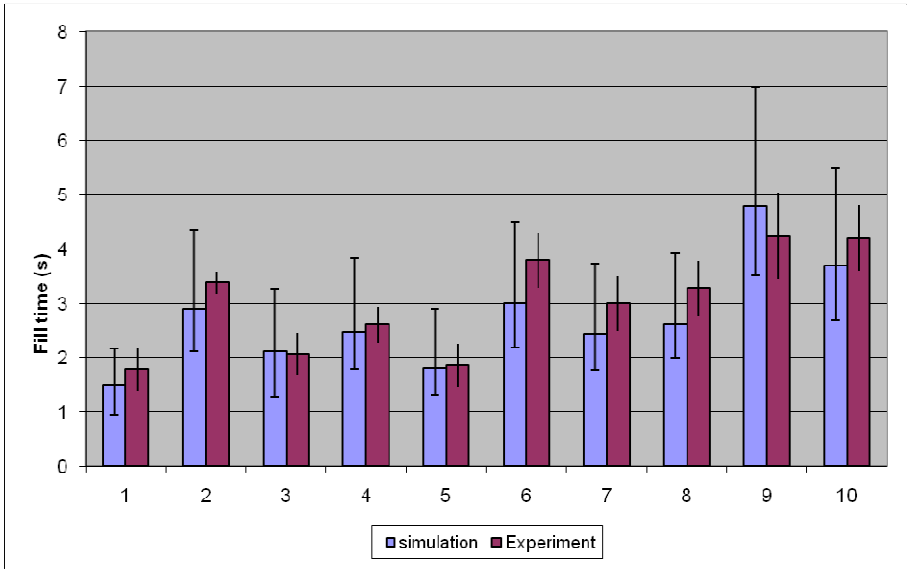

Figure B-1 Prediction of fill time and its comparison with experimental results for P4 357D-3120 fabric

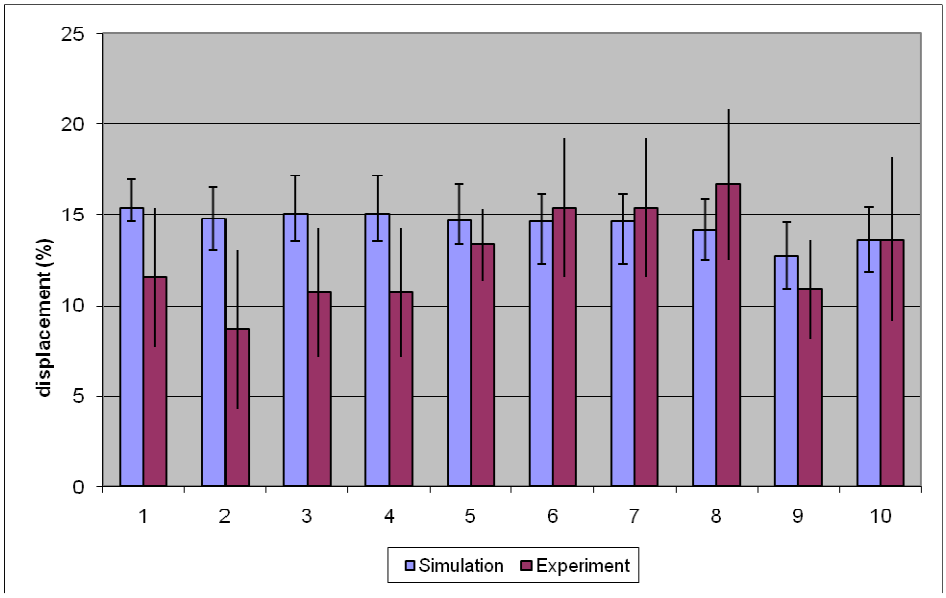

Figure B-2 Prediction of normalized deformation (H=15mm) and its comparison with experimental results for P4 357D-3120 fabric

Appendix C

RADIAL FORMULATION FOR IN PLANE FLOW

As an alternative problem to the one formulated in section 7.2, one can think of a setup using radial injection. The problem can be reduced to a two dimensional problem, the resin being at the same position through the thickness and assuming that the preform has isotropic properties. As well as the previous section, this problem has been solved for pressures kinematically driven [14]. Using polar coordinates, one finds that the pressure will not vary with the theta direction (Figure C-1). The problem can then be reduced to a one dimensional polar problem.

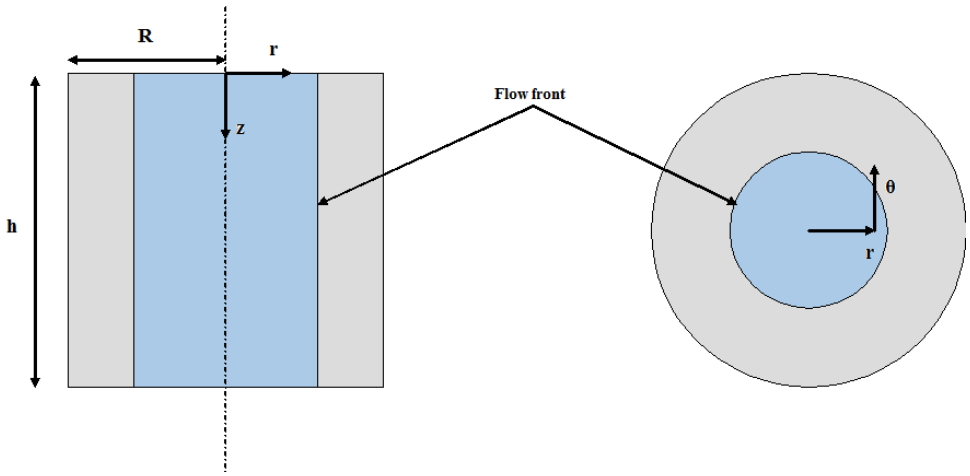

Figure C-1 Schematic of phase three radial flow

Adapting equation (7.29) to this situation, one finds,

$$\frac{K_r\left(v_f\right)}{\eta}\frac{1}{r}\frac{\partial}{\partial r}\left(r\left(\frac{\partial p}{\partial r}\right)_{r,t}\right)_{r,t}=\frac{\dot{h}(t)}{h(t)} \tag{C.1}$$

where K_r is the fabric permeability in the radial direction and η is the fluid viscosity. At the flow front $r=r_f$ one can use the following boundary conditions $p\left(r_f\left(t\right),t\right)=0$ and $\left(\frac{\partial p}{\partial r}\right)_{r=0,t}=0$ at the center of the part. The conservation of resin volume during the process,

$$\frac{\partial}{\partial t}\left(\pi {r_f}^2 h\phi\right)_r=0\Leftrightarrow 2\frac{\dot{r}_f}{r_f}\phi=-\frac{\dot{h}}{h} \tag{C.2}$$

One finds,

$$p\left(r,t\right)=\frac{\eta\phi(t)}{2\mathrm{K_r}}\frac{\dot{r}_f(t)}{r_f\left(t\right)}\left(r_f^2\left(t\right)-r^2\left(t\right)\right) \tag{C.3}$$

and

$$F\left(t\right)=\frac{\pi\eta\phi(t)}{2K_r}r_f\left(t\right)r_f^3\left(t\right)+\pi R^2 p_{pref}\left(t\right) \tag{C.4}$$

Applying equation (7.40) to equation (C.2), one obtains the followings relationship,

$$\phi(t)=1-\frac{r_f^2\left(t\right)v_{f0}}{r_{f0}^2\left(1-v_{f0}\right)+r_f^2\left(t\right)v_{f0}} \tag{C.5}$$

The equations describing p and F are then,

$$p\left(r,t\right)=\frac{\eta {r_{f0}}^2\left(1-v_{f0}\right)}{2K_r\left(r_{f0}^2\left(1-v_{f0}\right)+r_f^2\left(t\right)v_{f0}\right)}\frac{\dot{r}_f\left(t\right)}{r_f\left(t\right)}\left(r_f^2\left(t\right)-r^2\left(t\right)\right) \tag{C.6}$$

$$F\left(r,t\right)=\frac{\pi\eta {r_{f0}}^2\left(1-v_{f0}\right)}{2K\left(r_{f0}^2\left(1-v_{f0}\right)+r_f^2\left(t\right)v_{f0}\right)}\dot{r}_f\left(t\right)r_f^3\left(t\right)+\pi R^2 p_{pref}\left(t\right) \tag{C.7}$$

The final governing equation for the radial flow is obtained by plugging the permeability and compaction models,

$$\dot{r}_f = \frac{2ko_r F(t)\left(1-v_{f0}\right)^2 r_{f0}^4}{\pi\eta v_{f0}^2 r_f^7(t)} - \frac{2\mathrm{R}^2 p_{pref}(t) ko_r \left(1-v_{f0}\right)^2 r_{f0}^4}{\eta v_{f0}^2 r_f^7(t)} \qquad \text{(C.8)}$$

Where $k_{or}=k_{oxx}$ in this study. Using the following boundary conditions:
$\left(\frac{\partial p}{\partial x}\right)_{r=0} = 0$ and $p_{r=r_f(t)} = 0$

As explained in section 7.2.2, if F is constant, a close form solution can be found. If F varies with time, the solution is determined using the finite differences explicit scheme,

$$r_f^{\,t+1} = r_f^{\,t} + \frac{2\Delta t ko_r F(t)\left(1-v_{f0}\right)^2 r_{f0}^4}{\pi\eta v_{f0}^2 \left(r_f^t\right)^7} - \frac{2\Delta t \mathrm{R}^2 p_{pref}(t) ko_r \left(1-v_{f0}\right)^2 r_{f0}^4}{\eta v_{f0}^2 \left(r_f^t\right)^7} \qquad \text{(C.9)}$$

The radial resin flow, during the compaction of a circular part will then be analyzed. A circular part of radius R is injected with resin until an initial radial depth of penetration r0. A force F is applied on top of the preform. Table C-1 represents the dimensions and properties of the fabric used as well as the force applied and the fluid viscosity.

Table C-1 Input parameters for the simulation of the flow through as circular porous media

Radius of the part	R	0.1m
Initial radius of penetration	r_0	0.06m
Initial part thickness	H	0.0113m
Initial fiber volume fraction	v_{f0}	0.3
Compaction parameters	n	0.45
	m	0.86
Maximal fiber volume fraction	v_{fmax}	0.6
Maximal applied stress	$p_{prefmax}$	$4.5.10^5$Pa
Permeability number	ko_r	2.10^{-10}Pa
Applied force	F	2.10^5Pa
Fluid viscosity	η	0.3

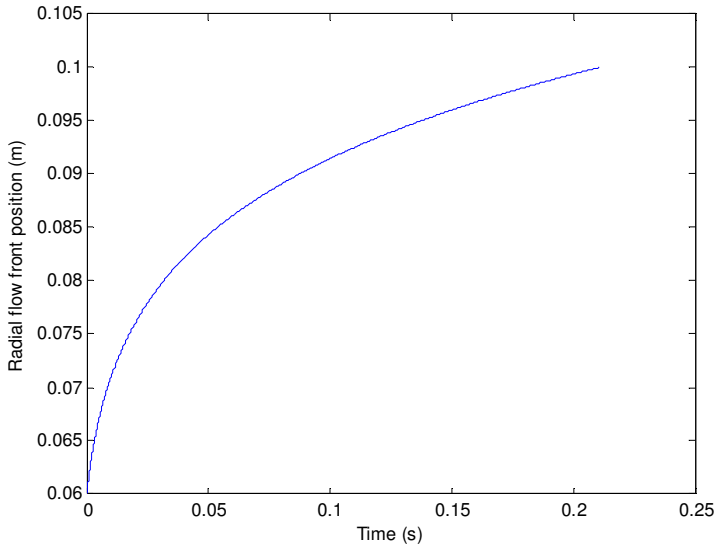

Figure C-2 Flow front position during the compaction of the preform

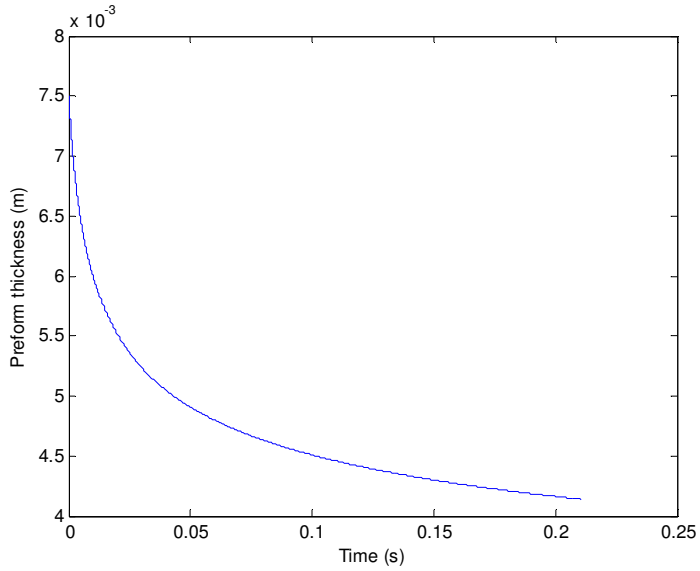

Figure C-3 Thickness of the preform during compaction

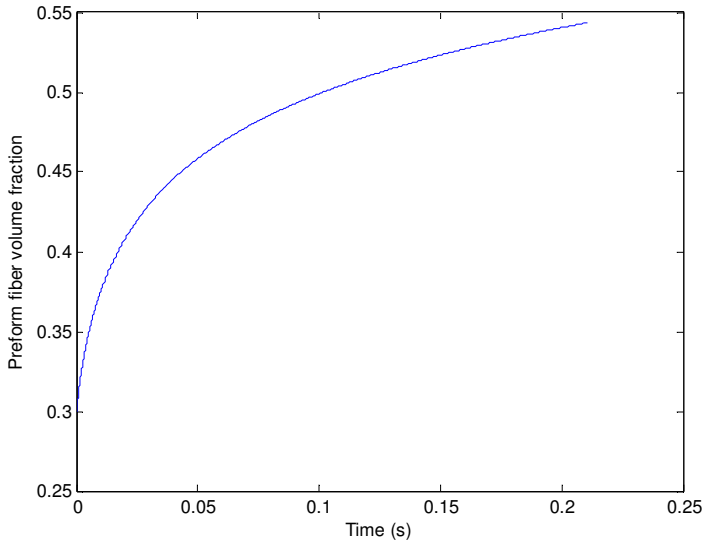

Figure C-4 Fiber volume fraction during the compaction of the preform